THE REMOVAL OF DISSOLVED ORGANIC MATTER (DOM) FROM WATER USING PHOTOCATALYSIS COUPLED WITH COAGULATION

---

by

LERATO MOSS

DISSERTATION IN FULFILMENT OF THE REQUIREMENT FOR THE DEGREE

MASTERS

in

CHEMISTRY

in the

COLLEGE OF SCIENCE, ENGINEERING AND TECHNOLOGY

of the

UNIVERSITY OF SOUTH AFRICA

Supervisor : PROF. THABO TINKAMBULE

Co-supervisors : DR. GCINA MAMBA

PROF. PETER JARVIS

DECLARATION

Name: Lerato Moss

Student number: 65103599

Degree: Masters in Chemistry

Exact wording of the title of the dissertation or thesis as appearing on the copies submitted for examination:

THE REMOVAL OF DISSOLVED ORGANIC MATTER (DOM) FROM WATER USING PHOTOCATALYSIS COUPLED WITH COAGULATION

I declare that the above dissertation is my own work and that all the sources that I have used or quoted have been indicated and acknowledged by means of complete references.

_____

SIGNATURE AND DATE

DEDICATION

I would like to dedicate my work to the Lord Almighty, who has provided me with the ability and will to finish this degree. Moreover, I would like to thank my family and relatives for their constant support and ensuring that I was physically and mentally fit. They contributed greatly to my wellbeing. To the love of my life, thank you for your moral support.

PUBLICATIONS AND PRESENTATIONS

Peer-reviewed Publications:

- Lerato Moss, Gcina Mamba, Peter Jarvis, Irene Carra, Pascal Finkbeiner, Thabo T.I. Nkambule, *Activated coagulation processes for removal of micropollutant and bulk contaminants* (**In preparation**).
- Lerato Moss, Gcina Mamba, Peter Jarvis,Thabo TI Nkambule**,** *The removal of humic acid by a photocatalytic-coagulation hybrid system under visible light* (**In preparation**).

ACKNOWLEDGEMENTS

I would like to acknowledge the following institutions and individuals for their contribution to this work

- The University of South Africa (UNISA) and the Institute for Nanotechnology and Water Sustainability (iNanoWS) for funding this project.
- My supervisors Prof. Thabo T.I. Nkambule and co-supervisor Dr. Gcina Mamba for their academic guidance, constructive criticism and support throughout the execution of this work.
- Cranfield University and the Water Science Institute for the collaboration on the work we have done.
- Prof. Peter Jarvis and Dr. Pascal Fienkbeiner (Cranfield University, UK) for their guidance and academic support throughout the execution of this project.
- Mr Alexander John (Cranfield University, UK) for his assistance in the execution of several experiments.
- Laboratory technicians, Mr Roderigo (Cranfield University, UK) for his help and guidance with the TOC and Mrs Monika (Cranfield University, UK) for her help and training with the LCMS.
- Laboratory technicians: Prof. Nyoni and Mr Mokalane (UNISA, iNanoWS) for their guidance and assistance with the lab work.
- Council for Scientific and Industrial Research (CSIR) for providing access to their instruments (SEM, TEM and XRD).
- Dr Tshepo Malefetse, Principal Research Editor, TheEditingDoctor$^{(Pty)Ltd}$, for proof-editing this work.

- iNanoWS administration, staff and friends.

ABSTRACT

Dissolved organic matter (DOM) comprises of both synthetic and natural organic compounds such as pharmaceuticals, pesticides, natural organic matter (NOM), found in the environment. Most of the DOM pollute drinking water sources, which inevitably end up in water distributed to communities for consumption. There are several methods that are currently employed in water treatment plants to eliminate DOM from drinking water, but the removal efficiencies are not of required standard. The existence of NOM in drinking water is undesirable because it decreases the aesthetic merit of water. Moreover, NOM can result in the generation of disinfection by-products (DBPs) when it reacts with chlorine-based disinfectants. Pesticides are also a major concern as they contribute to drinking water pollution. Water pollution resulting from organic materials such as pesticides have been linked to several adversative effects on the environment and human health.

This work is divided into two parts, with both aimed to evaluate a photocatalysis-coagulation integrated process for the removal of DOM in water. The first part of the study focussed on the photocatalytic-coagulation of a herbicide, mecoprop using titanium dioxide (TiO_2) as a photocatalyst and ferric sulphate ($Fe_2(SO_4)_3$) as a coagulant, under Ultraviolet-C (UVC) irradiation. The aim was to facilitate simultaneous removal of mecoprop, background organic matter and turbidity, as well as the removal and recovery of TiO_2 nanoparticles (NPs) from surface water. Jar tests were performed to optimize the coagulation conditions ([$Fe_2(SO_4)_3$] and pH). Subsequently, oxidative degradation experiments were conducted with UVC radiation in a bench scale collimated beam system. Control tests were performed, where removal of mecoprop was evaluated under photolysis, catalysis and coagulation, respectively. Furthermore, the combination of UV-coagulation, UV-TiO_2, TiO_2-coagulation were employed for the removal of mecoprop from surface water samples. Up to 88% removal of mecoprop was achieved by direct photolysis at a maximum UV fluence of 8000 $cm^2.mJ^{-1}$. Comparatively, photocatalysis with TiO_2, displayed complete degradation of mecoprop at UV fluence of 4500 $cm^2.mJ^{-1}$and TiO_2 concentration of 100 mg/L. However, when

photocatalysis (UV-TiO_2) and coagulation (Fe^{3+}) were combined, a maximum degradation rate constant of 0.0034 $cm^2.mJ^{-1}$ was obtained. This was followed by the UV-Fe^{3+} process, with a rate constant of 0.0031 $cm^2.mJ^{-1}$. The improved mecoprop removal in the photocatalysis-coagulation was due to the synergy between a Fenton-like process (UV/Fe^{3+}) and photolysis (UV), which overall lead to an improved production of hydroxyl radicals. However, the addition of TiO_2 into the system improved the degradation rate by 0.0003 $cm^2.mJ^{-1}$, which is negligible. Therefore, the degradation of mecoprop could be performed without the photocatalysis, but with the UV/Fe^{3+} system alone.

The second part of the study entailed the photocatalytic-coagulation removal of humic acid as a model NOM pollutant at a concentration of 10 mg/L, which is the concentration that is usually recorded in natural water. Titanium dioxide was modified by co-doping with varying concentrations of nitrogen and sulphur (1 g, 2 g, 4 g of thiourea, denoted as 1NS-TiO_2, 2NS-TiO_2, 4NS-TiO_2) to achieve a visible light active catalyst. Coagulation experiments were performed using ferric chloride ($FeCl_3$) to evaluate the recovery of NS-TiO_2 nanoparticles and background organic matter. Subsequently, coagulation and photocatalysis processes were performed individually as controls and to optimize parameters such as coagulant dose, pH and photocatalyst dose. The photocatalysis-coagulation process was conducted under the optimized conditions ([$FeCl_3$]= 30 mg/L, pH= 6, [2NS-TiO_2]= 150 mg/L) under visible light irradiation (250 W). Optical differences were observed between the doped and undoped TiO_2. Consequently, the pristine TiO_2 (3.19 eV) band gap decreased when doped with nitrogen and sulphur and continued to decrease further with an increase in dopant (1NS-TiO_2 = 3.18 eV, 2NS-TiO_2 = 2.55 eV and 4NS-TiO_2 = 2.41 eV). The results demonstrate that the combined photocatalysis-coagulation treatment process has a higher humic acid removal rate than the photocatalysis, coagulation individual processes (photocatalysis-coagulation k_1 = 0.0143 min^{-1}, photocatalysis k_1 = 0.0066 min^{-1}, coagulation k_1 = 0.0074 min^{-1}). In this case, both processes have been conclusively demonstrated to work synergistically to degrade and remove humic acid.

TABLE OF CONTENTS

Section ***Page***

TABLE OF CONTENTS

Chapter ***Description*** ***Page***

LIST OF FIGURES

LIST OF TABLES

LIST OF ABBREVIATIONS

AOP(s)	Advanced Oxidation Process(es)
BET	Brunauer-Emmett-Teller
DBP(s)	Disinfection by-product(s)
DNA	Deoxyribonucleic Acid
DOC	Dissolved Organic Carbon
DOM	Dissolved Organic Matter
EDC(s)	Endocrine Disrupting Chemical(s)
FE-SEM	Field Emission Scanning Electron Microscopy
FTIR	Fourier Transform Infrared
GAC	Granular Activated Carbon
GQD	Graphene Quantum Dots
HA	Humic Acid
HAA	Haloacetic Acids
HRTEM	High Resolution Transmission Electron Microscopy
IE	Ion Exchange
LC-MS	Liquid Chromatography Mass Spectroscopy
MCPP	Mecoprop or 2-(2-methyl-4-chlorophenoxy)-propionic
MW	Molecular Weight
NPOC	Non-purgeable Organic Carbon
NF	Nanofiltration

NOM	Natural Organic Matter
NP(s)	Nanoparticle(s)
OFE	Ofloxacin
OM	Organic Matter
OP	Organic pollutants
PACl	Polyaluminium Chloride
PFS	Polyferric Sulphate
POP(s)	Persistent Organic Pollutants
QD	Quantum Dots
RNA	Ribonucleic Acid
THM(s)	Trihalomethane(s)
TOC	Total Organic Carbon
UV	Ultra-Violet
WWTP	Wastewater Treatment Plant
XRD	X-ray Diffraction

CHAPTER 1:
INTRODUCTION

1.1. Background

Over the past decades, governmental and non-governmental organisations have shown significant interest in the detection and control of environmental agents such as herbicides, pesticides and other organic and inorganic substances that endanger human health and environmental sustainability [1]. This interest is driven mainly by a rapid increase in the amounts of chemical substances released into freshwater systems such as streams, dams, rivers and lakes. In addition to being suspected chronic disease-causing agents, many of these water pollutants and/or their degradation by-products have adverse effects on terrestrial and aquatic environments [2]. Generally, water pollutants can be categorised into three main groups, namely: microbial, inorganic, and organic pollutants. Organic pollutants are the most common pollutants found in drinking water and are linked to multiple health problems such as reproductive disorders, cancer, alteration of the immune system, deterioration of neurobehavior, endocrine disturbance, genotoxicity, and increased birth defects [3].

In natural soil and surface water, dissolved organic matter (DOM) is referred to as natural organic matter (NOM) or synthetic organic matter [3]. The presence of natural organic materials in drinking water during the disinfection stage has been linked to the production of disinfection by-products (DBPs) [4]. Consequently, the occurrence of DBPs in drinking water is associated with various negative health impacts such as cancer of the bladder, spontaneous abortions, and birth defects [5]. However, NOM provides nutrition for microbial species, making it beneficial in selected environments. Other organic pollutants that form part of DOM include synthetic organic pollutants such as pesticides, pharmaceuticals, herbicides, and paints [1]. Both pesticides and herbicides have been discovered in various water sources including ground and surface water. The transportation of these organics to areas outside their intended application zone results in the accumulation of these substances in the environment where they are linked to various harmful effects [2].

1.2. Problem statement

NOM reacts with disinfectants during the disinfection step of the drinking water treatment process to form DBPs [6]. DBPs have been found to be carcinogenic and mutagenic. Additionally, similar organic compounds of pharmaceutical and pesticide origin also contribute to drinking water pollution. Pesticides and their by-products, in particular, pass into the atmosphere, soil and water, allowing harmful compounds to accumulate and endanger human health and the environment [3]. Furthermore, cumulative pesticides lead to biodiversity loss. The pesticides remain in the soil and pollute land and surface water as most pesticides are barely degradable. Additionally, numerous pesticides have been reported as endocrine disrupting chemicals (EDCs), suggesting their ability to alter the normal functioning of both animal and human endocrine systems [1]. EDCs increase the occurrence of breast cancer, growth pattern irregularities, childhood neurodevelopment delays, and fluctuations in immune function [2,3].

Conventional water treatment processes (mainly coagulation and flocculation) have, to a limited extent, been effectively applied in the removal of NOM from water. In addition, several reports have confirmed the poor removal of pesticides by coagulation-flocculation processes [7]. Current water treatment regimes do not effectively remove NOM and herbicides in drinking water sources. Therefore, a need exists to develop more effective and advanced water treatment technologies targeted at improving the quality of drinking water.

An advanced oxidation process (AOP) namely, photocatalysis has been extensively explored in the degradation of a varied range of organic, inorganic and microbial pollutants in water. Despite its ability to completely mineralise organic pollutants, incomplete degradation is a common concept that could generate potentially toxic by-products [8]. AOPs can and have been coupled to achieve complete mineralisation or eventual removal of organic pollutants. One of the most often utilised semiconductors for photocatalytic degradation of organic molecules is titanium dioxide. However, owing to its band gap of 3.2 eV, activation can only be *via* UV irradiation [9]. Modifications such as nonmetal doping can ensure activation in the visible light range [10]. Moreover, most of the photocatalysts are employed in

the form of a powder, thus making their recovery, and recycling problematic and ultimately leading and contributing to secondary pollution. The removal of a powdery photocatalyst product after treatment of water can be achieved by centrifugation; however, such a process can be impractical, tedious and time consuming.

It is envisaged that the coupling of photocatalysis to the coagulation step could improve the overall removal of organic pollutants. Such a hybrid process would involve initial degradation of NOM by NS-TiO_2 and herbicides (mecoprop) by commercial TiO_2, into less complex and easily removable by-products. Subsequently, the degradation by-products could be removed by coagulation. This work focussed on doping TiO_2 nanoparticles (NPs) with nitrogen and sulphur to adjust the band gap and thus developed a material that is active under visible light illumination. Once the NPs were doped, photocatalysis was coupled with coagulation to determine its efficiency in the removal of humic acid as well as the recovery of NS-TiO_2 in surface water. Additionally, in another part of the study, the removal of a herbicide, mecoprop *via* a photocatalysis-coagulation system using commercial TiO_2 was explored. The photocatalysis-coagulation hybrid system offered numerous advantages such as enhanced properties for the elimination of organic pollutants, the resultant by-products and recovery of the photocatalyst nanoparticles.

1.3. Justification

The study covered the removal of NOM and a herbicide (mecoprop) *via* a photocatalytic-coagulation hybrid water treatment process, and the benefits of the hybrid system are discussed in the sections to follow:

1.3.1 Degradation of NOM and herbicides using photocatalysis

The efficiency of the degradation of a broad range of organic matter has been demonstrated utilising heterogeneous photocatalysis by titanium dioxide. Titanium dioxide has been widely studied for its excellent oxidative strength, good photo durability, environmental friendliness, chemical inertness and relatively low cost [12]. Rodriguez and colleagues reported on the successful elimination of ofloxacin (OFX) from water by TiO_2 photocatalysis [13]. Additionally, different studies on the

degradation of organic compounds by TiO_2 have been undertaken [8]. In the recent past, anion doping has proved to be efficient for band gap reduction and good visible light photocatalytic activity has been observed over the resultant doped materials [14]. For this reason, consideration has been afforded to new preparation methods for anion doped TiO_2 and to understand the factors that are responsible for visible light activity. Anion doping includes incorporation of elements such as nitrogen (N), sulphur (S), fluorine (F), boron (B), and carbon (C) [15]. Yalçın *et al.,* [16] examined the function of nonmetal (N, S, C) doping in TiO_2 photocatalysis and concluded that the reduction of the band gap arose from the influence of orbitals N 2p, C 2p, O 2p, and S 3p to the Ti 3d states in TiO_2 valence band (VB), as well as the occurrence of midgap states induced by C and S in the band gap states. Sathish and associates explored the degradation of methylene blue by NS-TiO_2, compared to the photodegradation performance of commercial TiO_2, with NS-TiO_2 showing higher activity in the visible region as paralleled with commercial TiO_2 [10]. Since TiO_2 photocatalysis has proven to be an efficient method for the removal of DOM in water, it would be beneficial to explore anion doping to improve the visible light activity of the TiO_2. As a result, this work focused on exploring the efficiency of commercial TiO_2 and NS-TiO_2 in the removal of organic compounds such as pesticides and NOM under UVC and visible light irradiation, respectively.

1.3.2 Photocatalysis-coagulation for water treatment

Coagulation-flocculation is a versatile method for eliminating a varied range of pollutants from water, such as colloidal particles (organic and metal oxides) and dissolved organic compounds [17]. This is achieved by destabilizing suspended particles. However, organic pollutants are not completely removed from the water bodies by coagulation. Combining photocatalysis and coagulation is an alternative treatment regime that has a number of advantages. Combining the two methods in the purification of drinking water has several advantages and these include: (i) Removal of particle with simultaneous degradation of organic pollutants; (ii) retrofitting of coagulation-based water treatment facilities; and (iii) design of a compact facility for hazardous material emergency response [16]. The use of nanoparticles for photocatalysis in water treatment may contribute to secondary pollution. The difficulty in separating TiO_2 NPs from aqueous suspensions by

sedimentation, particularly in crystalline anatase form, is owing to the existence of powerful repulsive forces that exist amongst the photocatalyst particles [18]. Although TiO_2 NPs have been found to aggregate rapidly in water without electrolytes, it should be noted that the aggregation of TiO_2 NPs is affected by other factors [19]. For example, NOM could hinder the aggregation of TiO_2 NPs through the formation of TiO_2 NP-NOM complexes *via* repulsive interactions and electrostatic attraction as well as van der Waals and steric interactions [18]. About 80% of commercial nanoparticles have been reported to have been successfully removed by alum-based coagulation [20]. Several studies have reported successful removal of TiO_2 NPs by coagulation-flocculation processes [3,4,20].

Coagulation-flocculation has been applied and studied for the removal of TiO_2 NPs. Kagaya *et al.,* [17] attained the separation of TiO_2 from 100 mL of suspension by adding aluminium chloride solution. They achieved sedimentation of at least 100 mg of titanium dioxide in 100 mL of the suspensions. Wang *et al.,* [19] investigated the elimination of TiO_2 nanoparticles from water by four types of coagulants: alum ($Al_2(SO_4)_3$), ferric chloride ($FeCl_3$), polyferric sulfate (PFS) ,and polyaluminium chloride (PACl) The researchers concluded that PFS could achieve high removal (~84%) of TiO_2 NPs with pH reduction. These studies serve as proof that coagulation is a viable method for the removal/separation of NPs in water.

The intention is to explore a treatment method that will remove DOM from water and further recover TiO_2 NPs from water post treatment. Coagulation and photocatalysis have both proven to be efficient in the removal of DOM and coagulation can be explored for the recovery of TiO_2 NPs. Combining the two treatment processes will simultaneously remove DOM and recover the TiO_2.

1.4. Aim of the study

The aim of this study was to investigate the efficiency of a photocatalysis-coagulation integrated water treatment process for the degradation and removal of NOM and mecoprop using TiO_2-P25 and NS-TiO_2, respectively.

1.5. Research Objectives

Objectives of this research study are as follows:

- Prepare and characterize TiO_2 and NS-TiO_2 nanoparticles.
- Evaluate the performance of NS-TiO_2 in the photocatalytic-coagulation hybrid system for the degradation/removal of NOM over visible-light irradiation.
- Assess the performance of commercial TiO_2 (P25) in a photocatalytic-coagulation hybrid system in the degradation of mecoprop under UVC irradiation
- Investigate the effects of pH, photocatalyst concentration, and irradiation dose on the degradation kinetics of NOM and mecoprop.
- Optimize the amount of coagulant required to successfully flocculate NS-TiO_2 and commercial TiO_2.

1.6. Dissertation outline

The balance of the dissertation is arranged as follows:

Chapter 2: This chapter is dedicated to an inclusive assessment of literature, relating to water pollution by organic pollutants, conventional water treatment methods and advanced oxidation processes (AOPs), and their implementation in drinking water treatment. The literature review includes the removal of organic pollutants by photocatalysis as well as the two-in-one photocatalysis-coagulation system.

Chapter 3: Chapter 3 presents experimental procedures that provide details on the preparation of photocatalysts and describes the experiments followed for the photocatalytic-coagulation removal of NOM and mecoprop under UV/visible-LED irradiation. A detailed description of instrument techniques, process of assessment and experimental set-up implemented for the execution of the research study is also undertaken.

Chapter 4: The chapter focuses on evaluating the degradation and removal of mecoprop and/or its degradation by-products by a photocatalysis-coagulation integrated system under UVC irradiation. Furthermore, this chapter discusses the recovery of TiO_2 NPs from water with ferric sulphate using coagulation process.

Chapter 5: Chapter 5, covers the characterization and analysis of NS-TiO_2. Furthermore, the efficiency of the photocatalytic-coagulation hybrid system is evaluated in the degradation of NOM in water under visible light. The recovery efficiencies of NS-TiO_2 by coagulation are also discussed.

Chapter 6: This chapter presents some concluding remarks on the key findings of this research. Lastly, recommendations for future work are also presented.

References

[1] N. Vela, G. Pérez-Lucas, J. Fenoll, and S. Navarro, “Recent overview on the abatement of pesticide residues in water by photocatalytic treatment using TiO_2 Nuria”, *Applications of titanium dioxide. Intech, Croatia,* pp. 148-177, 2017

[2] S. Benfeito, T. Silva, J. Garrido, P. B. Andrade, M. J. Sottomayor, F. Borges, and E. M. Garrido, “Effects of chlorophenoxy herbicides and their main transformation products on DNA damage and acetylcholinesterase activity”, *BioMed research international*, vol. 2014, 2014.

[3] K. M. G. Mostofa, C. Liu, M. A. Mottaleb, and G. Wan, “Dissolved organic matter in natural waters”, *Photobiogeochemistry of organic matter*, Springer, Berlin, Heidelberg, pp. 1-137, 2013.

[4] G. Wang, S. T. Hsieh, and C. S Hong, “Destruction of humic acid in water by UV light - catalyzed oxidation with hydrogen peroxide”, *Water research*, vol. 34, pp. 3882–3887, 2000.

[5] A. Matilainen, and M. Sillanpää, “Removal of natural organic matter from drinking water by advanced oxidation processes”, *Chemosphere*, vol. 80, pp.351-365, 2010.

[6] M. R. Teixeira, S. M. Rosa, and V. Sousa, “Natural organic matter and disinfection by-products formation potential in water treatment”, *Water resources management*, vol. 25, pp. 3005–3015, 2011.

[7] T. P. Shabee , A. Saha, V. T. Gajbhiye, S. Gupta, K. M. Manjaiah, and E. Varghese, “Simultaneous removal of multiple pesticides from water: Effect of organically modified clays as coagulant aid and adsorbent in coagulation – flocculation process”, *Environmental technology*, vol. *35*, pp.2619-2627, 2014.

[8] M. Sillanpää, M. C. Ncibi, and A. Matilainen, “Advanced oxidation processes for the removal of natural organic matter from drinking water sources: A

comprehensive review", *Journal of environmental management*, vol. 208, pp. 56–76, 2018.

[9] M. Sheydaei, H. Reza, K. Shiadeh, B. Ayoubi-feiz, and R. Ezzati, "Preparation of nano N-TiO_2 / graphene oxide / titan grid sheets for visible light assisted photocatalytic ozonation of cefixime", *Chemical engineering journal*, vol. 353, pp. 138–146, 2018.

[10] X. Sun, J. Xing, and J. Qiu, "Preparation and photocatalytic activity of nonmetal co-doped titanium dioxide photocatalyst", *Russian journal of physical chemistry A*, vol. 90, pp. 1151–1156, 2016.

[11] Z. Cai and M. M. Benjamin, "NOM fractionation and fouling of low-pressure membranes in microgranular adsorptive filtration", *Environmental science and technology*, vol. 45, pp. 8935–8940, 2011.

[12] P. Hu, S. Zhang, H. Wang, D. A. Pan, J. Tian, Z. Tang, and A. A. Volinsky, "Heat treatment effects on Fe_3O_4 nanoparticles structure and magnetic properties prepared by carbothermal reduction", *Journal of alloys and compounds*, vol. 509, pp. 2316–2319, 2011.

[13] H. Z. Huang, A. Yan, "Influences of doping on photocatalytic properties of TiO_2 photocatalyst", *Semiconductor photocatalysis—materials, mechanisms and applications*; *Cao, W.*, Ed., pp.31-80, 2016

[14] Y. Yalçın, M. Kılıç, and Z. Cinar, "The Role of non-metal doping in TiO_2 photocatalysis the role of non-metal doping in TiO_2 photocatalysis", *Journal of advanced oxidation technologies*, vol. 13, pp.281-296, 2010.

[15] T. Mano, S. Nishimoto, Y. Kameshima, and M. Miyake, "Investigation of photocatalytic ozonation treatment of water over WO_3 under visible light irradiation", *Ceramic society of japan*, vol.119, pp. 822-827, 2011.

[16] L. Ki-Chang, and C. Kwang-Ho, "Hybridization of TiO_2 photocatalysis with coagulation and flocculation for 1,4-dioxane removal in drinking water treatment", *Chemical engineering journal*, vol. 231, pp. 227–235, 2013.

[17] J. M. Santos, J. P.S Valente, S. M. A. Jorge, P. M. Padilha, M. J. Saeki, G. R. Castro and A.O. Florentino, "Coagulation-flocculation of TiO_2 in suspension used in heterogeneous photocatalysis", *The electronic journal of chemistry*, vol. 231, pp. 227–235, 2013.

[18] R. Li, T. Li, and Q. Zhou, "Impact of titanium dioxide (TiO_2) modification on its application to pollution treatment—a review", *Catalysts*, vol. 10, pp. 804, 2020.

[19] M. M. Fan, Y. Wang, N. Xue, Y. Zhao, Z. Wang, M. Wang, and Yi. Zhao,B. Gao, "Technology coagulation of TiO_2 nanoparticles-natural organic matter composite contaminants in various aquatic media : Fluorescence characteristics , flocs properties and membrane fouling abilities", *Separation and purification technology*, vol. 205, pp. 113–120, 2018.

[20] H. T. Wang, Y. Y. Ye, J. Qi, F. T. Li, and Y. L. Tang, "Removal of titanium dioxide nanoparticles by coagulation: Effects of coagulants, typical ions, alkalinity and natural organic matters", *Water science and technology*, vol. 68, pp. 1137–1143, 2013.

[21] A. Asadi, R. Akbarzadeh, A. Eslami, T. C. Jen, and P. O. Oviroh, "Effect of synthesis method on NS-TiO_2 photocatalytic performance", *Energy procedia*, vol. 158, pp.4542-4547, 2019.

[22] G. Mamba, M. A. Mamo, X. Y. Mbianda, and A. K. Mishra, "Nd, N, S-TiO_2 decorated on reduced graphene oxide for a visible light active photocatalyst for dye degradation: Comparison to its MWCNT/Nd, N, S-TiO_2 analogue", *Industrial & engineering chemistry research*, vol. *53*, pp.14329-14338, 2014.

[23] A. H.Mahvi, A. Maleki, R. Rezaei, and M. Safari, "Reduction of humic substances in water by application of ultrasound waves and ultraviolet irradiation, pp. 233-240, 2009.

CHAPTER 2:
LITERATURE REVIEW

2.1 Introduction

Water treatment plants utilise a series of processes to ensure adequate water quality in compliance with the standards set by the government. It is important that drinking water is safe for consumption by humans and animals, and for use in various activities such as agriculture and manufacturing processes. Viruses and bacteria are a few of many microorganisms that cause illnesses such a cholera, polio, infectious hepatitis, typhoid, dysentery, which have led to death [1]. Agricultural runoff, which contains pesticides, herbicides, and a substantial concentration of nutrients such as nitrogen and phosphorus, accelerates the rate of eutrophication in receiving waters. The most noticeable impact of eutrophication is the development of algal and phytoplankton blooms that decrease water clarity and quality. Algal blooms restrict light penetration, which cause plant deaths in coastal areas; they also decrease the success rate of predators, which sometimes rely on light to pursue and capture prey [2]. Furthermore, the microbial decomposition of algal blooms when they die significantly deplete dissolved oxygen thus producing an anoxic environment that is unable to sustain most organisms [3]. However, organic pollutants (OP) are of greater concern in drinking water treatment since they are linked to the formation of health threatening by-products.

2.2 The presence of organic matter in surface water

Organic matter in natural water sources can be categorised into dissolved, suspended, and particulate matter [4,5]. The dissolved organic matter (DOM) is a combination of autochthonous (i.e., organic materials in the water column derived from biological processes), allochthonous (i.e., vegetation and animal debris carried into water bodies by runoff) and manmade or synthetic organic compounds originating from industrial or agricultural activities such as pharmaceuticals, pesticides, and cosmetics [6]. Particulate or dissolved matter are found in water or wastewater such as dissolution of minerals, soil erosion, decomposition of vegetation or industrial and domestic discharge, which may be found suspended in

water in numerous forms such as bacteria, algae, viruses, and detritus [7,8]. Moreover, there are variations in the size of the particulate and dissolved organic species, which has an effect on the degree of their dispersion in water. DOM found in surface waters is referred to as natural organic matter (NOM), and it originates from the decay of dead plants and animals in water bodies. NOM consists mainly of humic substances of terrestrial origin such as fulvic acids of algal and/or phytoplankton origin, carbohydrates, sugars, lipids, amino acids, proteins, phenols, organic acids, alcohols and acetylated amino sugars constitute the rest of NOM [9].

Water pollution by synthetic organic compounds of agricultural origin is common to an extent that pesticides are often detected in drinking water and wastewater. Due to their widespread use as plant growth regulators, chlorophenoxy herbicides have gained special attention. Mecoprop, which is an authorised British Standard Institution (BSI) chlorophenoxy herbicide with a tradename (R, S) 2-(2-methyl-4-chlorophenoxy)-propionic acid) (also called MCPP), is commonly used to manage leafy weeds in cereal fields, ornaments such as lawns (both in residential and commercial formulations) and sports fields [10]. Owing to their solubility and polar nature, chlorophenoxy herbicides like MCPP can effortlessly be transferred to surface and ground waterways [11]. Furthermore, their toxicity is recognized, and high-level exposure in animal studies has revealed their hepatotoxicity and nephrotoxicity. Chlorophenoxy herbicides may cause human soft tissue sarcoma, chronic liver injury, malignant lymphoma and non-Hodgkin's lymphoma [12].

Conventional water treatment methods such as coagulation-flocculation are usually used to remove NOM or pesticides found in wastewater or drinking water. However, the removal rates are not impressive. Elimination of dissolved organic matter is most often achieved by improving coagulation-flocculation methods or by adding processes such as filtration and nanofiltration (NF) or granular activated carbon [13]. Besides the dissolved organic matter passing through sewage and industrial waste into the water body, great concentrations of inorganic pollutants and heavy metals contaminate the water. These inorganic pollutants include non-biodegradable compounds such as mineral acids, inorganic salts, and trace metals. Radioactive materials occurring as isotopes, which originate from mining and ore processing,

are some of the major culprits comprising inorganic pollutants [2]. However, this chapter only focuses on methods designed for the treatment of organic pollutants, and these are explored in more detail in **Section 2. 3**.

2.3 Water Treatment

Treatment of drinking water usually includes the removal of suspended colloidal materials, contaminants such as bacteria, algae, fungi, viruses, minerals such as iron and manganese and organic contaminants [14]. All these contaminants are a concern, as they pose serious risks to human health. Several of the treatment processes are designed to target specific contaminants, hence a series of them are applied to treat drinking water in order to obtain safe water for distribution to the communities. Raw water treated for drinking purposes can be abstracted from ground or surface water. Different sources of raw water have different characteristics and the adoption of a particular treatment regime is greatly influenced by the type of source water involved [15]. To this end, the conventional treatment process flow sheet has been modified over the years as more contaminants are identified and their effect on public health are established. This has also resulted in the redesign of some water treatment plants to enable the elimination of these new and emerging contaminants [16]. Although plant redesign remains an option, it is important to investigate the conditions of the site (for design purposes), including the chemical and microbial nature of the water to be treated. Compilation of a detailed risk assessment is key, as well as a report that contains detailed laboratory or pilot scale results to measure the efficiency of the procedure, and to optimize chemical doses [17]. The conventional treatment flowsheet illustrated in **Figure 2.1** provides a framework for a water treatment plant.

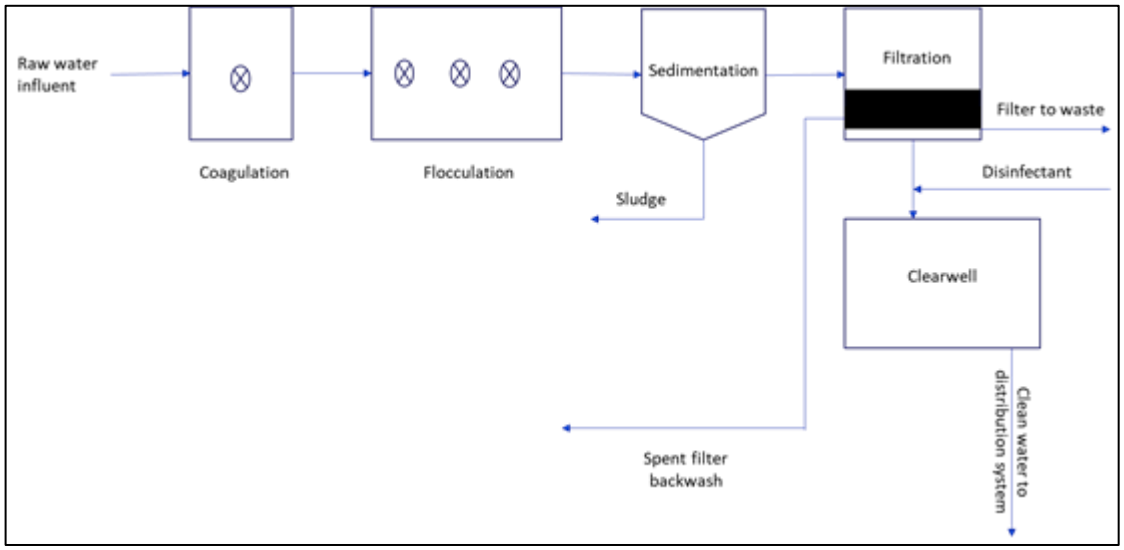

Figure 2. 1: Conventional water treatment systems [18].

Other treatment processes (e.g., membrane filtration, ion exchange, adsorption on activated carbon and advanced oxidation processes) that are regarded as conventional methods are however not shown in **Figure 2. 1**. Typical conventional water treatment flowsheet is designed to remove microbial contamination and some colloidal particles to lower the turbidity of the water [18]. Suspended particles prevent effective disinfection and lower the aesthetic merit of the water. Coagulation and flocculation are always included in water treatment to remove any suspended particles before disinfection [19]. In recent water treatment practices, coagulation and flocculation are still as important, and even more so as the removal of particulate matter and organics has become increasingly important. The United States treat water to a turbidity of 0.3 NTU today, down from 1.0 NTU in 1989. Similar amendments have been adopted by many other developed countries [20]. Coagulation and flocculation procedures are usually followed by the sedimentation/clarification step.

Coagulation and flocculation play key roles in cheese making, biochemistry, and rubber manufacturing [20]. In water treatment, the stability of a particle describes the capability to remain as a distinct entity, or to avoid aggregation with other particles in the aquatic environment [21]. Aggregation avoidance remains a challenge in water treatment, and coagulation offers the most effective option for

destabilising suspended particles in water. The process of coagulation is one of destabilising suspended particles in water. This process is always coupled with flocculation, which involves the aggregation of destabilised particles to form flocs [20]. Interactions between the colloids in the raw water and products of the chemical coagulation should occur before flocculation to destabilise particles [15].

Colloid particles fall into two general classes, lipophilic and lyophilic, which are described as hydrophobic and hydrophilic, respectively, in the field of water treatment. However, a particle can be comprised of both classes, and there may be an interchange of these states by a colloidal particle as it goes through different treatment processes [21]. With respect to the suspended colloidal particles, the main aim of the water treatment is to destabilise the charges of the suspended particles to overcome the repulsive forces existing amongst the particles. If only particle destabilisation is considered, the two main mechanisms of coagulation, which are based on the concentration of the coagulant and pH, are: (i) neutralization of charged particles by adsorption of positively charged parts of the coagulants; and (ii) and the enmeshment of colloidal particles in $Al(OH)_3$ solids if alum is used as a coagulant [20]. Aluminium or iron-based coagulants are the most often utilised coagulants [8]. Destabilisation is achieved when a positively charged metal hydroxyl precipitate adheres on sites on the surface of a suspended particle, rather than attaching in a uniform manner as indicated in **Figure 2. 2** [15].

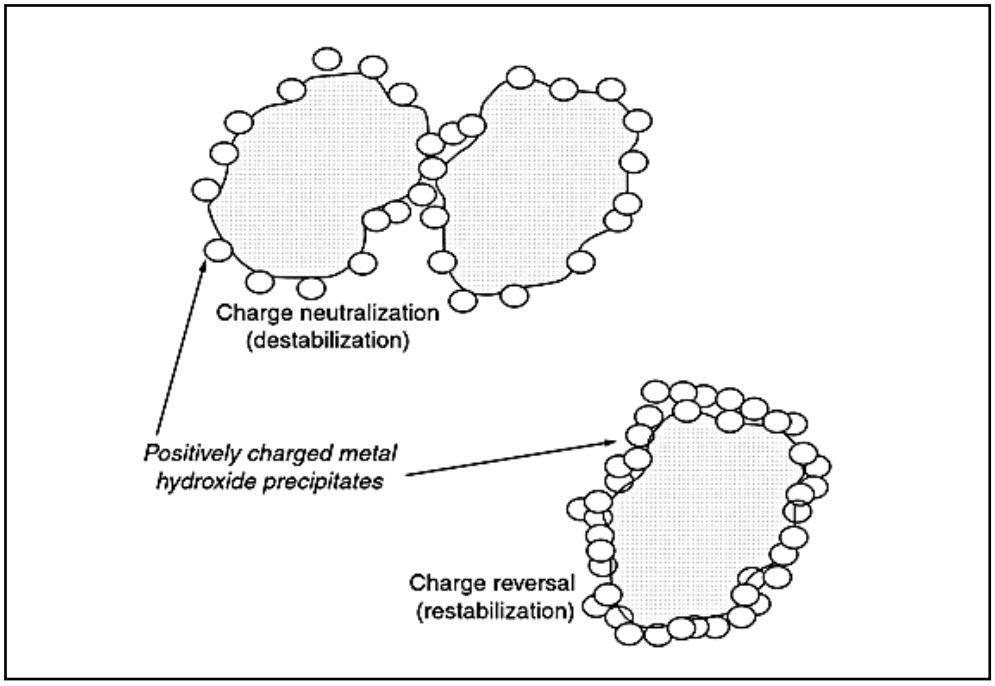

Figure 2. 1: Schematic of destabilization by metal hydroxyl precipitate [22].

Coagulant chemicals are either organic or inorganic substances that promote particle instability when the correct dose is added. When dissolved in water, most coagulants are cationic, and include substances like lime, ferric salts, alum, and cationic organic polymers [20]. Aggregation of colloids and small particles to form filterable (flocs) or settleable particles is called flocculation [12]. Flocculation occurs after the suspended particles destabilise in the zone of decaying mixing energy subsequent to rapid mixing, or consequent to conveying flow turbulence [23]. In some cases, this unintentional flocculation may be a passable flocculation process. To improve interaction between destabilised particles and generate floc particles of optimal density, size, and strength, a separate flocculation step is frequently incorporated in the treatment train. The flocs that are formed will increase in weight and be drawn down by force of gravity, and this is where sedimentation is introduced.

Sedimentation can be described as a process whereby sludge or suspended particles settle (due to force of gravity) out of water in a settling tank during treatment. Sedimentation is one of several prefiltration application techniques; dissolved air flotation is also another technique. Procedures of separation between solids and liquids are similarly referred to as clarification [24, 25]. Sedimentation

provides some degree of purification; hence it is applied in most water treatment works around the world. After the solids have settled, they are separated from the water through filtration.

Solids are removed *via* filtration from surface water or wastewater after coagulation and sedimentation [2]. In some cases, it may be required to use a softening process when filtration is used, since filtration alone may not effectively remove dissolved solids. For instance, anthracite filtration is employed in softening precipitation to eliminate residual salts that persist after clarification, which results in the filtration of a portion of the clarified water. An effective sand filtration system can reduce turbidity levels in clarified water from 10 NTU to 1.0 NTU [26]. At this point, the majority of the dissolved organic matter has been removed and disinfection can be introduced to remove microorganisms before distribution.

The main aim of the disinfection process is to deactivate all harmful microorganisms present in the water. The disinfection process does not kill microorganisms in the water, it hinders their growth and reproduction rate. Several illnesses have been linked to the presence of microorganisms in water, hence the importance of the disinfection process. Sterilization is interrelated to disinfection; however, sterilization destroys both harmful and non-harmful microorganisms. For this reason, disinfection is more appropriate for water treatment [27].

In water treatment, several disinfection techniques are used. Chlorine disinfection is most commonly used for huge quantities of water; however, its use in smaller quantities is less prevalent. Ultraviolet irradiation and ozone are the most common disinfection methods used in private supplies [28]. Chlorine gas is usually used as both primary and secondary disinfection. The advantages of using chlorine gas for disinfection is that it is cheaper than ultraviolet (UV) or ozone disinfection treatment methods and it is highly effective in deactivating a wide range of pathogens. Moreover, residual chlorine serves as a long-lasting disinfectant even after distribution [18]. Ozone disinfects by destroying the cell walls of pathogenic microorganisms present in the water, and this results in the disintegration and destruction of the microorganism [2]. UV causes disinfection by changing the

genetic make-up of a microorganism by breaking bonds in the deoxyribonucleic acid (DNA), ribonucleic acid (RNA) or proteins [10, 29].

2.4 Removal of NOM and pesticides by coagulation and flocculation

In the treatment of wastewater and drinking water, coagulation is a commonly used conventional method. The use of coagulation in the elimination of NOM from drinking water sources has gained significant consideration from scientists around the world due to its ability to minimise the development of disinfection by-products (DBPs). Nevertheless, increased variation of NOM in water (in terms of both concentration and composition) has led to a significant decline in the performance of traditional coagulation methods. The coagulation process is substantially more effective at eliminating high molecular weight organics than it is at removing lower molecular weight fractions. The inconstant composition of NOM poses significant challenges to the conventional techniques. A higher charge density is usually observed for the hydrophobic portion of NOM, than the hydrophilic portion, making it easier to coagulate [30]. As a result, there is a need to improve coagulation processes by increasing operating conditions (coagulant dose and pH), generating more effective inorganic or organic coagulants, and integrating coagulation with other processes [20].

Besides the coagulation-flocculation processes, other procedures such as membrane filtration, advanced oxidation processes (AOPs), and biological and ion exchange (IE) processes were explored for the removal of NOM [29]. When ozonation is employed in conjunction with other treatment methods, NOM is degraded and low molecular weight molecules are formed, which are then adsorbable by granular activated carbon (GAC). However, adsorption of these smaller fragments onto GAC is usually hindered by their increased mobility and polarity [31].

Inorganic coagulants are considered ineffective in the removal/degradation of herbicides and pesticides from drinking water and wastewater [12]. Most of these agricultural pollutants are chemically stable and therefore not easily degradable species. Herbicides and pesticides belong to a group of persistent organic pollutants (POPs), and are they are not removed to desired regulatory levels by conventional

wastewater treatment plants (WWTP). Basic water treatment procedures such as coagulation-flocculation, chemical precipitation and biological oxidation have been only partially successful in the removal of a small selection of pesticides. Mitlner *et al.,* [12] have established that hydrophobic pesticides do not form complexes with humic substance, which can be partially removed by coagulation . Adams *et. al,* [30]. has also established low removal efficiencies of pesticides by coagulants, proving that the sole use of coagulation is not efficient in the removal of pesticides from water

Advanced oxidation techniques are one of the alternative treatment options for removing NOM and pesticides. AOPs are a type of oxidation processes centred on the *in situ* production of extremely reactive and oxidizing radicals (mostly hydroxyl radicals, •OH), which react with organic pollutants, leading to gradual degradation of the pollutants [32]. AOPs have been used to remove numerous pesticides and herbicides, according to extensive research that has been conducted [33, 34]. The UV treatment , Fenton process (H_2O_2 and Fe^{2+}), UV-H_2O_2 process, ozonation (O_3), photo-Fenton and heterogeneous photocatalysis employing TiO_2 have all been investigated among the many suggested AOPs [35]. Some of these AOPs are discussed in **Section 2.5**, with special attention being paid to heterogeneous photocatalysis

2.5 Advanced oxidation processes for degradation of organic pollutants in water

Advanced oxidation processes use the powerful oxidative property of the hydroxyl radical (OH•) to degrade organic compounds [36]. All AOPs comprise of two mechanisms for organic pollutant degradation, namely: production of reactive oxidative species *in situ* and oxidant reactions with target pollutants [32]. The mechanisms of radical production are influenced by water quality and system design and are dependent on process-specific characteristics. Other factors (radical mass transfer in surface-based AOPs, hydrodynamics) contribute to the efficient elimination of pollutants in addition to radical scavenging [27]. Other important radical species involved in AOPs include sulfate and superoxide radicals, which have a lower oxidation potential compared to the hydroxyl radical.

Generally, the hydroxyl radical has a greater oxidation potential (2.8 V) than common oxidants such as ozone (2.07 V) and hydrogen peroxide (1.8 V) (**Table 2.1**); this means that the hydroxyl radical can oxidize target compounds more rapidly than other oxidants [37]. In the event of mineralization, the interaction between organic pollutants and $HO^{\bullet}$ radical generate smaller organic compounds that are easy to remove or are transformed to carbon dioxide, water, and inorganic salts [35]. Advanced oxidation processes have many benefits over conventional techniques, including transforming organic compounds into CO_2 and H_2O, no production of sludge and other post-treatment is rarely required for further removal of organic compounds.

Table 2.1: Oxidation potentials of selected oxidants [37]

OXIDANT	OXIDATION POTENTIAL (V)
Fluorine	3.03
Hydroxyl radical	2.80
Sulfate radical	2.60
Atomic oxygen	2.42
Ozone	2.07
Hydrogen peroxide	1.77
Hypochlorous acid	1.49
Chlorine	1.36
Chlorine dioxide	1.27
Bromide	1.09

Hydrogen and oxygen atoms make up hydroxyl radicals, making them extremely reactive and allowing them to easily abstract hydrogen atoms from other molecules to generate water molecules [38]. Various organic, inorganic and microbial pollutants can be oxidized by hydroxyl radicals. Hydroxyl radicals oxidize organic compounds *via* three main mechanisms, namely:

(i) removal of a hydrogen atom from an aliphatic carbon

(ii) electrophilic addition to aromatic carbons

(iii) electron transfer (An organic substituent provides an electron to $HO^{\bullet}$)

The H-atom abstraction taking place in saturated compounds is mostly from C-H bonds, and this results in the generation of an organic radical as illustrated in **Eq. 2.1** [39]. The H-abstraction method includes significant separation of charges in the

transition state and requires more energy than the •OH radical formation reactions. For the electrophilic addition to the aromatic carbons, the OH radical is more likely to attack and abstract a hydrogen from a tertiary rather than a primary carbon. There is a low probability of the electrophilic addition of the OH radicals onto the saturated carbons occurring due to the C-atom's electron deficiency; therefore, preferential addition of the OH radical to the C-atom occurs in unsaturated bonds **(Eq. 2.2**).

Adding OH radicals to the aromatic ring takes place through a short-lived pi-complex, which is in equilibrium with the initial reactants and thereafter develops into a sigma-complex in which the OH is attached to a specific C-atom (**Eq. 2.3**) [40]. The electron transfer reaction of the hydroxyl radical may involve both inorganic and organic compounds. In both cases, the primary step is the formation of a two, three electron-bonded radical-adduct followed by electron transfer [41]. Subsequently, these organic radicals undergo a series of oxidative interactions resulting in the degradation of the organic molecule. Apart from the hydroxyl radical, more than a few other radicals such as superoxide, ozonide, sulfate and hydroperoxyl radicals also participate in the degradation of the organic contaminants. However, hydroperoxyl radicals have lower oxidation potential compared to the hydroxyl radical [42].

$$^{\bullet}OH + R\text{-}H \rightarrow [R\text{---}H^{+}\text{--}O^{-}H^{+}] \rightarrow {}^{\bullet}R + H_2O \quad [2.1]$$

$$^{\bullet}OH + H_2C{=}CHR \rightarrow [HO\text{---}CH_2\text{---}CH{-}R] \rightarrow HOCH_2{-}{}^{\bullet}CH \quad [2.2]$$

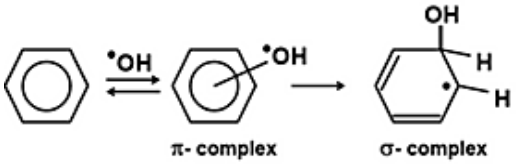

[2.3]

2.5.1 Different classes of advanced oxidation processes

Advanced oxidation processes are classified as either homogeneous or heterogeneous processes. Homogeneous processes are further classified into those that require energy and those that do not. Homogeneous AOPs refer to processes that exclude the use of a solid catalyst such as TiO_2 (**Figure 2. 3**) [43].

Ultraviolet (UV) or ultrasonic energy is used to drive homogeneous AOPs for the elimination of a range of pollutants from wastewater. More often, ultraviolet radiation is employed in combination with other oxidants such as UV-O_3, UV-H_2O_2, UV-O_3-H_2O_2, UV-Fe^{2+}-H_2O_2 (photo-Fenton) [37]. For example, UV-O_3 was observed to be more efficient than direct UV photolysis and ozonation in the removal of carbofuran, a very toxic carbamate pesticide [44]. A comparative analysis of Fenton and photo-Fenton processes has revealed that photo-Fenton are better at mitigating organic pollution than TiO_2 photocatalysis [45, 46].

Heterogeneous AOPs involve the addition of a catalyst, which may be metal oxides, sulphides, halides or nonmetal, to facilitate the degradation reactions [35]. By comparison with homogeneous AOPs, heterogeneous AOPs are more convenient for catalyst separation and recovery from treated water. The most studied heterogeneous AOPs are photocatalytic ozonation (UV-TiO_2-O_3), catalytic ozonation (Fe^{2+}-O_3, TiO_2-O_3), and heterogeneous photocatalysis [47].

Heterogeneous photocatalysis has recently gained popularity for degrading organic contaminants that are resistant to oxidation by other standard AOPs. The next sub-section (**Subsection 2.4.2**) introduces and provides a detailed overview of heterogeneous photocatalysis.

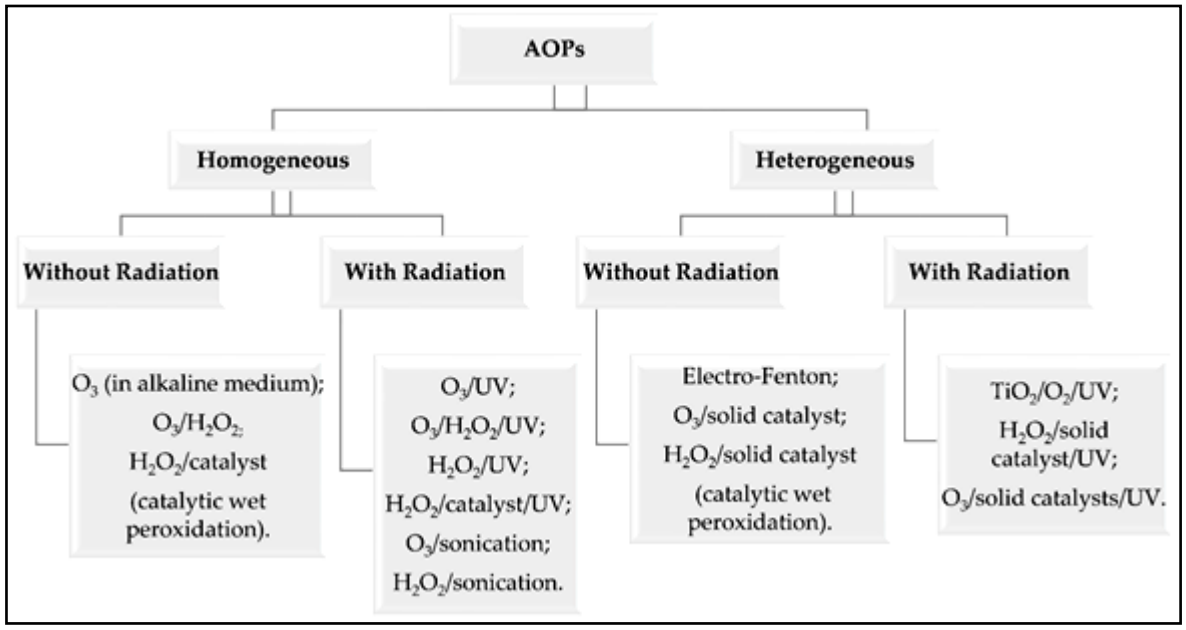

Figure 2. 2: Advanced oxidation processes (AOPs) classification [48].

2.5.2 Heterogeneous photocatalysis

Photocatalysis is one of the most promising heterogeneous AOPs in the removal/ degradation of a variety of organic, inorganic and microbial pollutants. As a typical AOP, the creation of the hydroxyl radicals transpires in the company of an energy source (e.g., light) and a light harvesting material (photocatalyst) [49]. Positive holes result from the excitation of electrons in the valance to the conduction band of a semiconductor, and this is only possible if a semiconductor is irradiated with a photon of energy larger than its band gap energy [17]. Reduction of an electron acceptor such as oxygen is possible in the conduction band to produce the superoxide radical [17]. Meanwhile, in the valence band, oxidation of suitable electron donors such as the hydroxide ion or water, can take place to yield hydroxyl radicals. As a result, the superoxide and hydroxyl radicals can oxidize pollutants on the exterior of the photocatalyst (**Figure 2. 4**) [50]. Alternatively, the recombination of electrons and holes leads to a dispersion of the input energy as light. This results in inadequate radical production which, leads to poor photocatalytic activity [51].

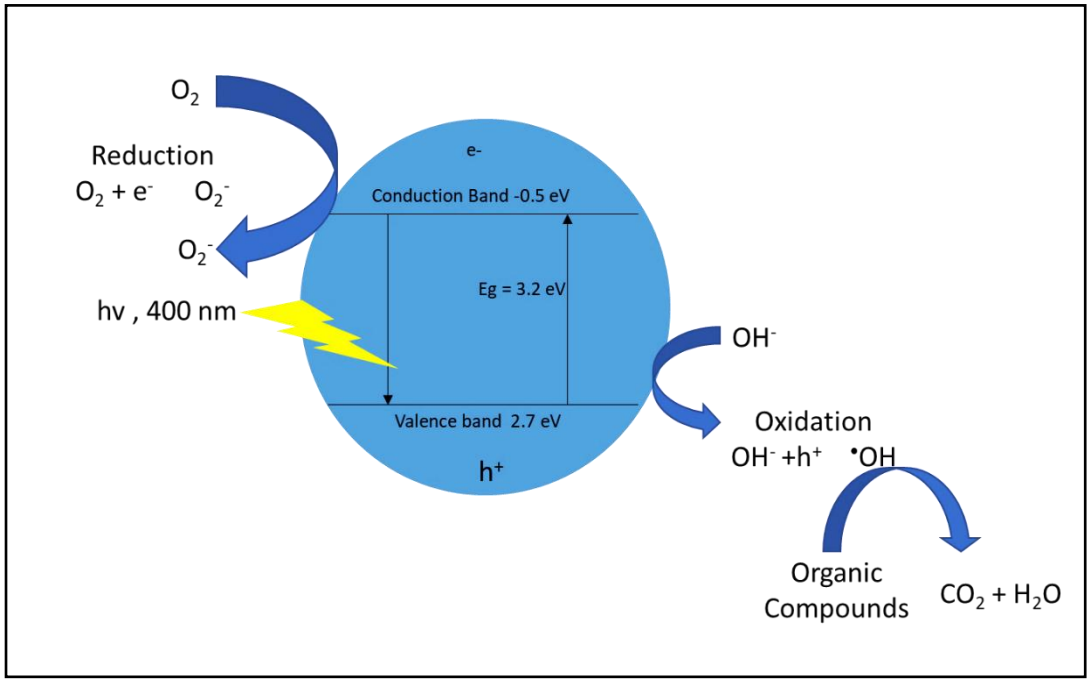

Figure 2.3: Schematic presenting the mechanism of TiO_2 photocatalysis (oxidation of organic compounds) [4].

The position of the redox potential of the organic substrate in relation to the standard electrode and the valence band of the substrate in question determines the redox potential required to oxidize it [52]. If the organic substrate's redox potential is lower than that of the photogenerated hole, it may reduce h^+ to form an organic substrate cation radical ($S^{\bullet+}$). Following that, the organic substrate cation radical ($S^{\bullet+}$) undergoes a faster reaction than back electron transfer, culminating in the creation of a product. Water or absorbed OH ions may reduce the holes, resulting in the generation of HO• and/or other radicals, allowing organic molecules to be oxidized (**Figure 2. 3**) [53]. Since the TiO_2 semiconductor conductivity band is virtually isoenergetic with the potential for oxygen reduction, the O_2 molecule has the ability to scavenge the electron from the TiO_2 semiconductor conductivity band, creating a superoxide radical ($O_2^{\bullet-}$) [54]. Photocatalytic activity inclines to be repressed in the absence of oxygen. Under ambient conditions, the photocatalytic decontamination rate is affected by the steady-state oxygen concentration as well as back-electron transfer from active species on photocatalytic surfaces [4].

2.6 Titanium dioxide as a photocatalyst for organic pollution mitigation

Since its commercial manufacturing, titanium dioxide (TiO_2) has been broadly used as a pigment and as a component of sunscreens, paints, ointments, and toothpastes. Water splitting on a TiO_2 electrode was studied during the early 1970s by Fujishima and Honda [55]. Since then, tremendous effort has gone into researching TiO_2, which has resulted in a deal of potential applications ranging from photocatalysis and photovoltaics to sensors and photo/electrochromics [56]. TiO_2 exists in three natural forms, namely: rutile, anatase, and brookite [34]. Anatase is stable at low temperature and rutile is more common in high temperature preparations. In the near UV band (350/400 nm), rutile absorbs almost no light. Chemically stable and abundantly available as a photocatalyst for oxidation reactions, the anatase form of titanium dioxide is a popular choice [43].

Amongst many semiconductors, TiO_2 is an excellent photocatalyst. The main advantages of TiO_2, which make it a suitable material for many photocatalytic applications, are its chemical stability in acidic and basic environments, nontoxicity, low cost, and high oxidation potential [57]. The unique properties of TiO_2 lend

themselves to various applications such as decontamination, water purification, air purification, UV protection ,and antibacterial activity [57]. The TiO_2 semiconductor photocatalyst acts as a powerful oxidizing agent when exposed to UV light, minimizing the amount of activation energy required for the disintegration of organic and inorganic molecules [37]. In general, when the surface of TiO_2 is illuminated, holes result in the valence band (VB) and electrons in the conduction band (CB), respectively (**Eq. 2.4**). The amount of energy that photons must supply to promote electrons is determined by the band gap of the semiconductor material in question [40]. The band gap of a semiconductor is outlined as the energy variation between the electrons in the uppermost permissible energy level in the valence band and the lowest permissible energy level in the conduction band [4].

Titanium dioxide (anatase) has a band gap energy (Eg) of 3.2 eV and can be activated by photons in the UV range of the sun spectrum with a wavelength of 388 nm [38]. A donor molecule (D) near the TiO_2 surface can be rapidly oxidized by the photoinduced hole (**Eq. 2.5**). Additionally, an acceptor molecule (A), may also be reduced in the conduction band by an electron (**Eq. 2.6**). An interaction between electron oxidation action and water produces a hydroxyl radical (•OH) due to the hole's considerable oxidation power (**Eq. 2.7**) [58]. Oxygen acts as an electron acceptor when adsorbed to the surface of TiO_2, and this leads to the production of a superoxide ion. The superoxide ion is a highly reactive particle capable of oxidizing organic material (**Eq. 2.8**) [55]. This mechanism was illustrated earlier in **Figure 2. 4**.

$$TiO_2 + hv \rightarrow h^+ + e^- \quad [2.4]$$

$$D + h^+ \rightarrow D^+ \quad [2.5]$$

$$A + e^- \rightarrow A^- \quad [2.6]$$

$$H_2O + h^+ \rightarrow OH\bullet + H^+ \quad [2.7]$$

$$O_2 + e^- \rightarrow O_2^{\bullet -} \quad [2.8]$$

Some of the drawbacks of using TiO_2 as a photocatalyst include low adsorption of pollutants, wide bandgap, fast electron hole recombination, difficult recovery of the

catalyst, and the agglomeration of suspended TiO_2 powder at high loading, all of which limit TiO_2 practical application in water treatment [59]. The strategies that are employed to address these drawbacks are discussed in the sections that follow. Special emphasis is placed on addressing the challenges associated with poor visible light absorption and recovery of TiO_2 NPs, as a subject that is at the core of this research study.

2.7 Strategies for improving TiO_2 photocatalytic activity

Some of the strategies for improving TiO_2 such as dye sensitization, incorporation of carbon materials, metal and nonmetal doping are discussed in the below subsections. These strategies include the improvements of bandgap reduction of TiO_2 for activation in the visible light range and resolving problems related to filtering and recovering the photocatalyst.

2.7.1 Coupling with carbon nanomaterials

Carbon comes in a variety of shapes and sizes, each with its own set of microtextures (or morphologies). Diamond, black carbon, carbon nanotubes, fullerenes, and graphene are only a few examples of carbon allotropes. Due to its widespread applicability in energy and the environment, graphene is one of the most investigated nanomaterials [55]. Recently, the advanced properties of graphene quantum dots (GQDs) have made these carbon nanomaterials very popular in the field of photocatalysis. Due to their excellent quantum confinement, graphene quantum dots are far more appealing as peroxidase mimetic catalysts than semiconductive quantum dots and organic dyes in terms of great photostability and low toxicity [64]. Hydrothermal techniques of GQD production commonly endow GQDs with functional groups such as carboxyl and hydroxyl groups, which aid in the formation of bonds with TiO_2 [55]. Fast electron transfer in the interfacial region of the GQDs/TiO_2 composite structure is facilitated by this bonding, which prevents carrier recombination [21]. Despite these advantages, GQDs' absorption band is primarily in the UV range, limiting their solar energy activation [54].

2.7.2 Dye sensitization

The TiO_2 photocatalyst primarily absorbs UV light, the wavelength of which is less than 400 nm [60]. As part of the endeavor to develop a visible light active TiO_2 photocatalysts, adsorbing and supporting various photosensitizing dyes was explored. In this approach, solar light is used to excite dye molecules anchored on TiO_2 and create electrons that are transported to the TiO_2 conduction band. The electrons in the TiO_2 conduction band are then transferred to electron acceptors, resulting in a range of redox reactions [61]. During this process, an electron is absorbed from a dye molecule or an adsorbate in order to reduce the dye molecule back to its original state (**Figure 2**. **5**) [62]. However, the photosensitizing dyes in these systems are generally thermally and/or photochemically unstable [63].

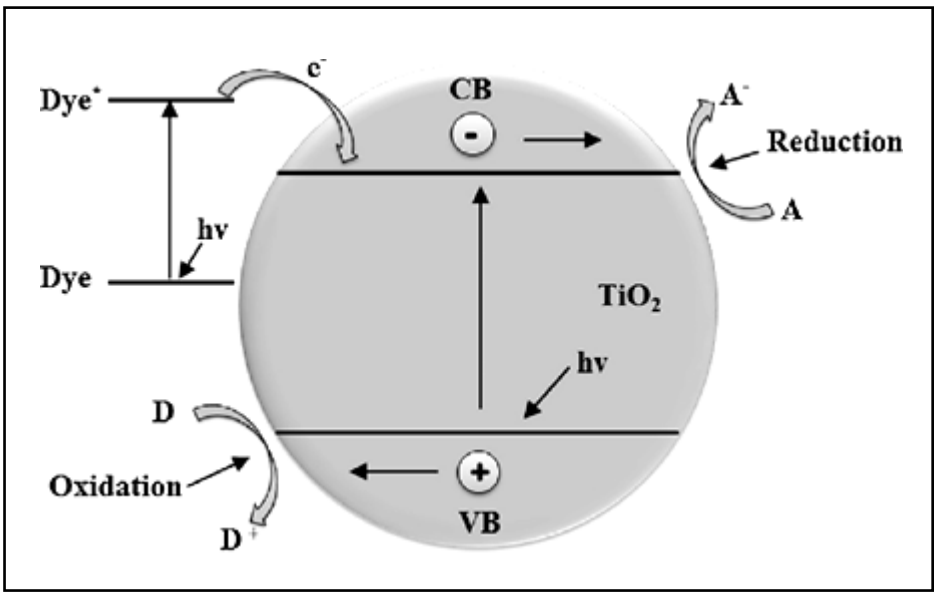

Figure 2. 4: Photocatalytic mechanism of dye sensitized of TiO_2 [71].

2.7.3 Doping of TiO_2

Over the past few years, huge efforts have been directed towards extending the light absorption of TiO_2. Ion doping is a new method for improving adsorption efficiency and photocatalytic activity. Doping may alter the chemical composition of TiO_2. The optical properties can be altered by substituting the metal, which is the titanium ion and the nonmetal, which is the oxygen atom [64]. More importantly, it is

desirable to retain the integrity of the host photocatalyst crystal structure while enhancing the electrical structure.

Incorporating ions into the TiO_2 matrix results in the introduction of new energy levels into the TiO_2 band structure. In addition to trapping electrons/holes and removing carriers from bands, the new energy levels allow for additional carriers to diffuse to the surface [63]. That is, the objective of doping is fairly straightforward, namely: to adjust the large band gap and electronic structure of TiO_2 to enhance its optical properties for visible light harvesting, to optimize each stage of the charge kinetics in order to prevent significant photogenerated carrier recombination and increase interface and surface properties [64]. Self-doping, nonmetal doping, transitional metal doping, and rare earth metal doping are all examples of TiO_2 doping [65]. Doping of TiO_2 can either be by a single metal, nonmetal or rare earth metal. Also, co-doping with two metals or two nonmetals or either a metal and a nonmetal is possible. To expand the responsiveness of TiO_2 to visible light, monodoping with 3d transitional metal ions has been widely researched [66]. While this method was able to reduce the band gap of TiO_2 to some degree, it also suffers from the presence of a carrier recombination centre and the creation of highly localized d states within the band gap, which greatly reduces carrier mobility [45]. Co-doping with two or more external atoms passivates the bands of impurities and minimizes the rising of recombination centre by increasing the solubility limit of dopants [67] In consequence, co-doping of TiO_2 can significantly enhance its photocatalytic properties.

2.7.4 Metal doping of TiO_2

Metal and nonmetal doping of TiO_2 are the two types of chemical doping. A particular amount of metal ions, such as Cr^{3+}, $Fe^{3+,}$ Ru^{2+}, V^{5+},Ce^{4+}, and La^{3+} is introduced into the TiO_2 lattice in the metal doping process [68]. Several studies suggest that metal doping has a bathochromic response on the edge of the TiO_2 absorption band because the outer Ti 3d orbitals overlap with the outer metal d orbitals. This band gap shift improves the visible light activity of TiO_2 subject on the type and concentration of metal dopant [60]. Doping TiO_2 with metal improves both the lifetime of electron/hole pairs generated by photolysis, as well as the rate at which

electron/hole pairs can be transferred, which precedes to an enhancement in the photocatalytic activity of doped TiO_2 [69]. Metal doping is also capable of effectively extending the adsorption edge into the visible region and lowering the band gap in TiO_2. Metal doping, on the other hand, has various disadvantages, including electron trapping by metal centres and the introduction of electron/hole recombination sites [70]. **Figure 2. 6** illustrates the activation mechanism of metal doped TiO_2.

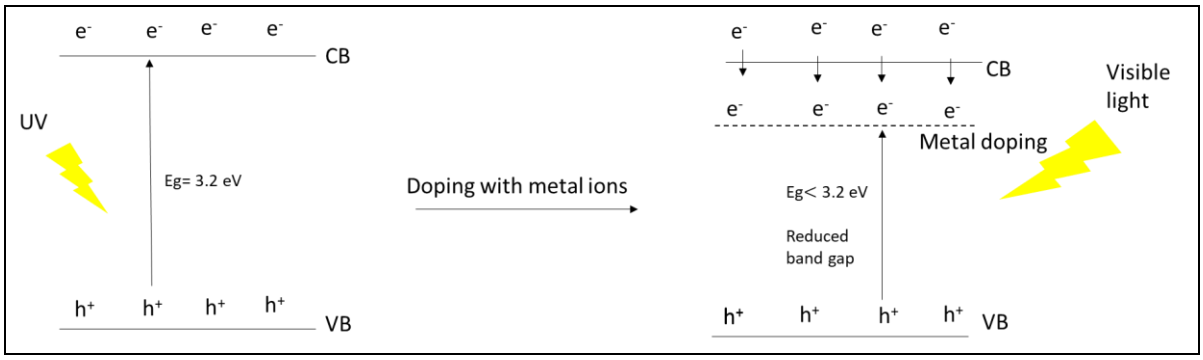

Figure 2. 5: Metal doping effect on TiO_2.

2.7.5 Non-metal doping of TiO_2

Nonmetal doping is another method for modifying TiO_2, and it is achieved by the substitution or interstitial addition on lattice oxygen of the TiO_2 by nonmetal elements [71]. Asahi *et al.,* [72] reported an improvement in the degradation of methylene blue and gaseous acetaldehyde by nitrogen doped TiO_2 under visible light irradiation. Since then, a lot of effort has gone into researching nonmetal doped TiO_2 photocatalysts like N, B, C, F, S, and P [17]. In the titania lattice, sulfur or nitrogen would be able to substitute for oxygen or titanium. As a consequence, it has been shown that S 3p states mixed with the valance band help to decrease the band gap [73]. N doping in TiO_2 does not lower the band gap, but rather allows the development of localized midgap states above the valence band, which improves the material's visible light sensitivity and photoactivity, according to recent experimental and theoretical research (**Figure 2. 7**) [74]. Additionally, sulfur doped TiO_2 has attracted considerable attention because increasing quantities of S can reduce the band gap and lead to high absorption under visible light [75]. Umebayashi *et al.,* [76] reported that sulfur only decreases the band gap of TiO_2 by 0.9 eV. However, more significant decrease in TiO_2 band gap was achieved by

Tachikawa *et al.,* [77] and Bacsa *et al.,* [78] and the calculated band gaps were 2.7 and 2.65 eV, respectively. Szatmáry *et al.,* [79] concluded the possibility of visible light activation of S-doped TiO_2. During the research, they discovered that sulphur is substituted for oxygen as an anion in the TiO_2 matrix. In the TiO_2 lattice, however, Ohno *et al.,* [80] discovered that S atoms were integrated and substituted Ti^{4+} ions.

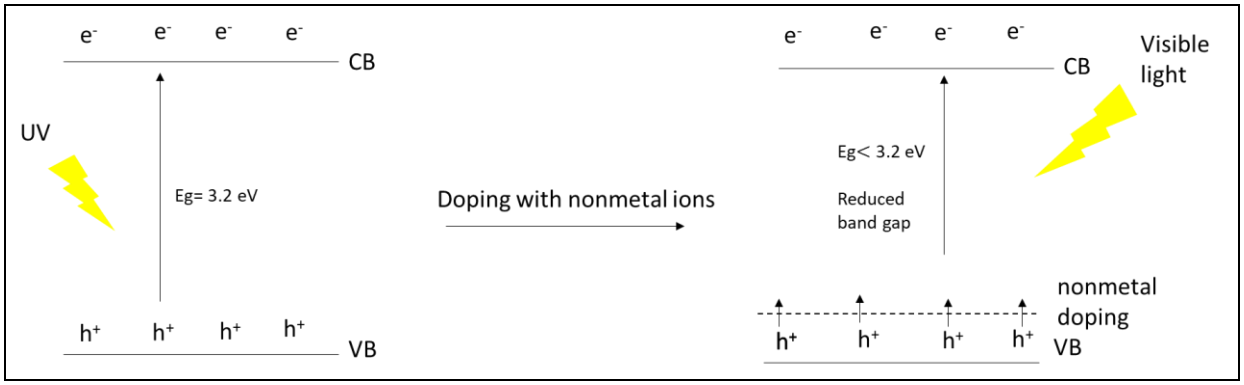

Figure 2. 6: Nonmetal doping effect on TiO_2.

2.7.6 Co-doping of TiO_2

There has been interest in co-doping TiO_2 with different elements in order to improve its photocatalytic performance under visible light illumination. Co-doping TiO_2 involves introducing either two metals or two nonmetals, or a nonmetal and a metal into the TiO_2 lattice. The different methods of co-doping have different effects on improving the performance of TiO_2 and each method will be discussed in detail in the succeeding sections.

2.7.7 Metal, metal co-doping

Several transition metal ion dopants were found to improve the photodegradation of a selection of organic pollutants. Al^{3+} doping of rutile crystals boosted photo efficiency, whereas Cr^{3+} doping allowed the photo-response to be extended to the visible region [32]. A combination of Al^{3+} and Cr^{3+} doping has been used to improve both the visible and the UV responses of rutile [14]. Recent work on the co-doping of TiO_2 with Fe and Mn was carried out by Lin *et al.,* [81]and they observed lower photocatalytic performance in all the co-doped TiO_2 thin films compared to undoped TiO_2 thin films under visible light irradiation. A doping ion's position for interfacial charge transfer or as recombination centres was a determinant of photocatalytic

efficiency in this case. A decrease in distance between trapping sites as a result of a surge in the number of doping ions, leads to an increase in the rate of recombination.

2.7.8 Metal, nonmetal co-doping

Metal and nonmetal co-doping of TiO_2 with N/Fe [82], V/N [83], and C/V [84] has been studied. Co-doping TiO_2 with a nonmetal and a metal ion can occur v*ia* two mechanisms. In the first mechanism, both metal and nonmetal are doped into the TiO_2 lattice, resulting in the development of impurity energy levels within the TiO_2 band gap, which increases visible light absorption and hence leads to increased photocatalytic activity [85]. In the second mechanism, the metal acts as a doping energy level substitution at the Ti position in the lattice, whereas nonmetallic species could exist as surface species capable of absorbing visible light [86]. By co-doping of metal and nonmetal ions, photocatalytic efficiency is increased significantly.

2.7.9 Nonmetal, nonmetal co-doping

Another option is co-doping TiO_2 with two nonmetals. TiO_2 co-doped with suitable nonmetal ions has been shown to have much greater photocatalytic activity than mono-doped photocatalysts in several studies. The occurrence of synergistic effects between the doping elements explains this phenomenon, which promotes visible light absorption while also enabling photogenerated electron/hole pair separation efficiency [69]. After preparing and analysing the effect of co-doping TiO_2 with boron and sulphur, Sun *et al.,* [72] observed an improvement in visible light response and photocatalytic performance of the TiO_2.

TiO_2 semiconductors have the Ti 3d orbitals dominating the conduction band and the O 2p orbitals dominating the valence band, according to semiconductor band theory [69]. The negative energy levels of the 2p orbitals of nonmetals such as C, P, N, and S are greater than those of the 2p orbital of the O As a result, incomplete substitution of impurity dopants C, P, N, S, and other nonmetals with lattice oxygen would follow in the development of additional energy bands above the TiO_2 valence band, improving the TiO_2 photocatalytic activity in visible light [69]. In the TiO_2 framework, nonmetal ions are doped to produce 2p orbital energy levels that help

synthesize new energy states within the bandgap of TiO_2 [55]. As these two dopants have similar structural characteristics, NF co-doped TiO_2 was explored as a visible light photocatalyst. The synergetic benefits of co-doping were determined to be due to N doping, which improved visible light response, and F doping, which delayed charge separation [87]. Additionally, it was proposed that co-doping N, S was capable of decreasing the band gap in anodically generated TiO_2 and enhancing the photocatalytic properties that it exhibited [54]. Massoudinejad *et al.,* [88] reported a decrease in the band gap of TiO_2 after doping with nitrogen and sulphur (from 3.17 to 2.77 eV) and thus improved activation of the catalyst by visible light. Another study by Asiri *et al.,* [89] showed that the prepared S and N doped TiO_2 co-doped was highly active as a photocatalyst for successful photodegradation of colorants such as eosin, and rhodamine B under visible light irradiation.

The following is an explanation of the difference between metal and nonmetal doping: Metal doping ions can present traps for electrons, lowering the electron/hole recombination rate, while nonmetal doping ions can increase TiO_2 absorption in the visible light range [72]. Since nonmetal co-doping of TiO_2 has shown interesting benefits in the improvement of visible light activation of TiO_2.This work focused on the design and development of nitrogen and sulphur co-doped TiO_2 for the degradation of NOM in water under visible light irradiation.

2.7.10 Charaterisation techniques for photocatalysts

2.7.10.1 Field emission scanning electron microscopy and electron dispersive X-ray spectroscopy

In a typical analysis, an electron beam is focused on a sample's surface in scanning electron microscopes, creating images of the sample. When electrons interact with atoms in a sample, a variety of signals are generated, each of which comprises of information regarding the sample's surface topography and composition [94].

2.7.10.2 High resolution transmission electron microscope

Transmission electron microscopy is a technique of creating images by using an electron beam that passes through a specimen [95].

2.7.10.3 Ultraviolet-visible spectroscopy-diffuse reflectance

As a powerful analytical technique, UV-vis spectroscopy can be utilised to evaluate the optical properties of solids and liquids (transmittance, reflectance, and absorbance) [95].

2.7.10.4 Brunauer-Emmett-Teller analysis

By measuring nitrogen adsorption as a function of relative pressure, Brunauer Emmett Teller (BET) analysis gives an accurate specific surface area evaluation of materials [95].

2.7.10.5 X-ray diffraction

X-ray crystallography is an experimental science that uses an X-ray beam to diffract in a variety of ways according to the crystalline structure to determine the atomic and molecular structure of a crystal [96].

2.7.10.6 Fourier transform infrared

Infrared is a powerful identification tool for functional groups due to similar adsorption frequencies observed for the different groups present in different molecules [97].

2.7.11 Coagulation-photocatalysis coupled system for the removal of dissolved organic matter from water

Natural organic matter (NOM) is a combination of high molecular weight (MW) compounds, such as extracellular polymers and biopolymers, and low MW chemicals originating from the decomposition of organic material that is commonly found in surface water supplies and landscape water bodies [90]. Presently, the purification of water and wastewater usually involves a phase of coagulation, which is recommended for the efficient removal of NOM by the U.S Environmental

Protection Agency [98]. Combining coagulation with advanced water purification procedures such as adsorption, oxidation, or membrane filtration can result in a higher NOM removal rate [28].

In coagulation-flocculation, NOM is predominantly removed, in particular the hydrophobic fraction, which usually contains more aromatic components and is of a larger molecular size than the hydrophilic fraction Coagulation-flocculation also allows DBPs to be reduced by physically removing organic precursor material [19]. On the other hand, is ineffective, eliminating just 60-70% of NOM under optimum treatment circumstances [28]. The hydrophilic component of humic substances, which can also induce the synthesis of DBPs, makes up the majority of the residual organic matter (about 30 to 40 percent) following coagulation [19]. Since existing water treatment processes have proven to be inefficient in the removal of this part of the humic substances or other organic pollutants such as pesticides, the development of advanced treatment methods for tackling such pollutants is therefore important

The efficacy of heterogeneous photocatalysis such as titanium dioxide when used in combination with ultraviolet (UV) in the removal of NOM from raw and drinking water (real water) has been demonstrated [91]. Furthermore, the coagulation-flocculation cycle is commonly employed to reduce DBP formation by producing flocs, and heterogeneous photocatalysis provides superior protection against DBP production in drinking water delivery systems by mineralising organic contaminants [16]. The portion of organics that is not removed by coagulation can be mineralised through oxidation by photocatalysis [44].

The combination of coagulation and photocatalysis work in a synergistic manner to mineralise and remove organic pollutants. The combination of photocatalysis and coagulation is a cost-effective solution because it can be easily retrofitted into the current treatment plan. Another advantage of this hybrid treatment method relates to the simultaneous removal of TiO_2 *via* coagulation post treatment, which ensures minimal secondary pollution due to the presence of nanoparticles [92].

Titanium dioxide NPs are used widely for a variety of applications, and this has resulted in their disposal into water bodies such as rivers, lakes, dams or aquifers

thus posing a significant threat to human and animal health [36]. Many treatment approaches, including as adsorption, coagulation, and membrane filtration, have been investigated to remove NPs from aquatic environments in order to control the health and environmental concerns caused by them. The recovery of suspended nanosized photocatalysts from vast quantities of reaction solutions by filtration and centrifugation is hard, time-consuming, and expensive, which makes these photocatalysts impractical for industrial use [22]. A strategy for addressing this problem involves introducing magnetic nanoparticles such as Fe_3O_4 NPs, to the nanosized photocatalyst matrix. When magnetic nanoparticles are incorporated into TiO_2, the photocatalyst can be efficiently recycled by utilizing an external magnetic field [64]. However, Fe_3O_4 can act as recombination centres, which decrease the oxidation efficiency of the catalyst [66].

Several studies have confirmed that nanoparticles such as TiO_2, and ZnO can be recovered by coagulation and the removal is mainly through the destabilisation mechanism. For example, Wang *et al.,* [93] investigated the use of PFS and $FeCl_3$ in the removal of TiO_2 NPs. The TiO_2 removal rate by $FeCl_3$ was slightly greater than that of PFS, but its working pH range is narrow. A study by Honda *et al.,* [76] examined the coagulation and removal of TiO_2 nanoparticles from groundwater and surface water with three different coagulants (ferrous sulfate ferric chloride, and ferric sulfate). TiO_2 nanoparticles have been found to outclass ferric chloride in the coagulation of nano-TiO_2 spiked surface water. Sun *et al.,* [31] investigated the elimination of silver nanoparticles using $Al_2(SO_4)_3$, PFS, PAC, and $FeCl_3$ as coagulants. The bridging effect of the hydrolysis product of $FeCl_3$ was discovered to destabilise silver NPs. From the evidence presented here, the removal of nanoparticles by coagulation-flocculation is a plausible method in this regard. Ferric coagulants seem to be the best performing coagulant for the removal of nanoparticles for water.

2.8 Chapter summary

The pollution of drinking water sources by organic pollutants is a matter of concern as this may lead to multiple detrimental effects on the environment and human health. Such effects include birth defects, cancer of the bladder, spontaneous

abortions, growth pattern irregularities, childhood neurodevelopment delays, fluctuations in immune function. Furthermore, the presence of DOM puts a strain on conventional water treatment methods as most of the treatments do not remove DOM completely or to the required levels. Coagulation and flocculation processes have been reported to remove NOM, but not pesticides. Attempts have been made to design and develop techniques for the mitigation of organic pollutants in water, more specifically NOM and pesticides. Heterogeneous photocatalysis is one of the AOPs that have attracted attention over the years due to their ability to completely oxidize organic pollutants in water. In photocatalysis, TiO_2 has been widely studied due to its numerous benefits. However, the disadvantages relating to the utilization of TiO_2 as a photocatalyst include fast recombination rate, NP aggregation and restricted activation in the UV range and recovery problems. Several modification strategies targeted at enhancing the activity of TiO_2 have been reported in the literature, and these include dye sensitization of TiO_2 as well as metal and non-metal doping (mono and co-doping). The strategy that was adopted in this research study was co-doping TiO_2 with nonmetal ions to enhance the visible light adsorption of TiO_2. However, TiO_2 NPs have been reported to contribute to secondary pollution and for this reason, recovery measures should be put in place after treatment. Several studies have explored coagulation as a method of choice for the recovery of NPs, and the process has proven to be successful in that regard.

Considering both photocatalysis and coagulation, and their ability to remove DOM from water and the possible recovery of TiO_2 *via* coagulation, combining the two processes would be advantageous. The individual processes are envisaged to work in a synergistic manner to remove DOM. For instance, portions of DOM that cannot be removed be coagulation would be degraded by photocatalysis. Furthermore, the advantage of TiO_2 recovery makes the photocatalysis-coagulation combined process worth exploring.

This work explored the efficiency of combining coagulation with photocatalysis for the degradation of a pesticide (mecoprop) and NOM using commercial TiO_2 and nitrogen, sulphur co-doped TiO_2 under UV and visible light, respectively. Furthermore, the efficacy of the combined system will be evaluated for the removal of TiO_2/NS-TiO_2 NPs *via* coagulation-flocculation processes.

References

[1] Monterey Starkey, “The Water Crisis in Third World Countries” Monterey Starkey A, Liberty University Spring Water treatment plant design, 2012.

[2] J. T. O’Connor, T. O’Connor, and R. Twait, “Water treatment plant design”, *Water treatment*, 4th ed., McGraw-Hill Professional, 2009.

[3] K. M. Mostofa, C. Q. Liu, M. A. Mottaleb, G. Wan, H. Ogawa, D. Vione, T. Yoshioka, and F. Wu, “Dissolved organic matter in natural waters”, *Photobiogeochemistry of organic matter*, Springer, Berlin, Heidelberg, pp. 1-137, 2013.

[4] C. Corniciuc and M. R. Teixeira, “The effect of TiO_2 nanoparticles removal on drinking water quality produced by conventional treatment C/F/S“, *Water research*, vol. 109, pp. 1–12, 2017.

[5] J. F. Gomes, A. Lopes, M. Gmurek, R. M. Quinta-Ferreira, and R. C. Martins, “Study of the influence of the matrix characteristics over the photocatalytic ozonation of parabens using Ag-TiO_2”, *Science of the total environment*, vol. 646, pp. 1468–1477, 2019.

[6] F. L. Rosario-Ortiz, S. A. Snyder, and I. H. Mel. Suffet, “Characterization of dissolved organic matter in drinking water sources impacted by multiple tributaries”, *Water research*, vol. 41, pp. 4115–4128, 2007.

[7] J. Peuravuori and K. Pihlaja, “Characterization of freshwater humic matter”, *Handbook of water analysis*, vol. 2, pp. 435–438, 2007.

[8] D. Yonge, “A comparison of aluminum and iron-based coagulants for treatment of surface water in Sarasota County, Florida”, Masters thesis, Department of civil, environmental, and construction engineering, College of engineering and computer science, University of central Florida Orlando, 2011.

[9] F. Meng, A. Drews, R. Mehrez, V. Iversen, M. Ernst, F. Yang, M. Jekel, and M. Kraume, “Occurrence, source, and fate of dissolved organic matter (DOM) in a pilot-scale membrane bioreactor”, *Environmental science and technology*, vol. 43, pp. 8821–8826, 2009.

[10] F. J. Beltrán, “Ozone-UV radiation-hydrogen peroxide oxidation technologies”, *Chemical degradation methods for wastes and pollutants: Environmental and industrial applications*, CRC Press, pp. 1–75, 2003.

[11] C. Costa, S. Maia, P. Silva, J. Garrido, F. Borges, and E. M. Garrido, "Photostabilization of phenoxyacetic acid herbicides MCPA and mecoprop by hydroxypropyl-β-cyclodextrin", *International journal of photoenergy*, vol. 2013, 2013

[12] P. T. Thuy, K. Moons, J. C. Van Dijk, N. V. Anh, and B. Van Der Bruggen, “To what extent are pesticides removed from surface water during coagulation – flocculation ?”, *Water and environment journal*, vol. 22, pp. 217–223, 2008.

[13] H. Juretić, G. Smoljanić, and M. Barta, “Degradation of natural organic matter in water by using UV-C/H_2O_2 process”, *The holistic approach to environment*, vol. 5, pp. 135–149, 2015.

[14] H. Spanjers, “Fundamentals of drinking water and wastewater treatment fundamentals of drinking water and wastewater treatment”, Sanitary engineering department, Delft university of technology, 2010.

[15] I. García, “Removal of natural organic matter to reduce the presence of trihalomethanes in drinking water”, Doctoral dissertation, KTH royal institute of technology, 2011.

[16] Y. H. H. Dong, G. Zeng, L. Tang, C. Fan, C. Zhang, X He, “An overview on limitations of TiO_2 based particles for photocatalytic degradation of organic pollutants and the corresponding countermeasures”, *Water research*, vol. 79, pp. 128–146, 2015.

[17] A. Peter, “Taste and odor in drinking water: Sources and mitigation strategies”, Doctoral dissertation, ETH Zurich, 2008.

[18] M. R. Teixeira, S. M. Rosa, and V. Sousa, “Natural organic matter and disinfection by-products formation potential in water treatment”, *Water resources management*, vol. 25, pp. 3005–3015, 2011.

[19] M. Sillanpää, M. C. Ncibi, A. Matilainen, and M. Vepsäläinen, “Removal of natural organic matter in drinking water treatment by coagulation: A comprehensive review”, *Chemosphere*, vol. 190, pp. 54–71, 2018.

[20] R. E. Adam, G. Pozina, M. Willander, and O. Nur, “Synthesis of ZnO nanoparticles by co-precipitation method for solar driven photodegradation of Congo red dye at different pH”, *Photonics and nanostructures - fundamentals and applications*, vol. 32, pp. 11–18, 2018.

[21] A. Bhatnagar, “Chemosphere removal of natural organic matter (NOM) and its constituents from water by adsorption: A review”, *Chemosphere*, vol.166, pp.497-510, 2017

[22] K. J. Ives, "The scientific basis of flocculation", *Springer science & business media*, vol. 27, 2012.

[23] B. Eikebrokk, T. Juhna, and S. W. Osterhus, “Operation of water treatment facilities–optimization effort and modelling if unit process operation”, *Coordinator project HOVEN TV, Nieuwegen, olanda*, vol. 26, 2006.

[24] B. Jiménez and J. Ramos, “High-rate sedimentation for wastewater treatment processes”, *Environmental technology (United Kingdom)*, vol. 18, pp. 1099–1110, 1997.

[25] B. E. Rittmann, T. Juhna, and S. W. Osterhus, “Treatment of a colored groundwater by ozone-biofiltration: Pilot studies and modeling interpretation”, *Water research*, vol. 36, pp. 3387–3397, 2002.

[26] C. Y. P. Ayekoe, D. Robert, and D. G. Lanciné, “Combination of coagulation-flocculation and heterogeneous photocatalysis for improving the removal of humic substances in real treated water from Agbô River (Ivory-Coast)”, *Catalysis today*, vol. 281, pp. 2–13, 2017.

[27] N. Vela, G. Pérez-Lucas, J. Fenoll, and S. Navarro," Recent overview on the abatement of pesticide residues in water by photocatalytic treatment using TiO_2", *Applications of titanium dioxide. Intech, Croatia*, pp.147-177, 2017.

[28] M. M. C. Adams, M. Asce, Y. Wang, K. Loftin, “Removal of antibiotics from surface and distilled Water in vonventional water treatment processes”, *Journal of. environmental engineering*, vol. 128, pp. 253–260, 2002.

[29] T. I Nkambule, R. W. M. Krause, B. B. Mamba, and J. Haarhoff, “Characterisation of natural organic matter (NOM) and its removal using cyclodextrin polyurethanes”, *Water institute of southern africa (WISA),* vol. 35, pp. 200–203, 2009.

[30] I. Levchuk, J. J. Rueda Márquez, and M. Sillanpää, “Removal of natural organic matter (NOM) from water by ion exchange – A review”, *Chemosphere*, vol. 192, pp. 90–104, 2018.

[31] M. Sillanpää, M. C. Ncibi, and A. Matilainen, “Advanced oxidation processes for the removal of natural organic matter from drinking water sources: A comprehensive review”, *Journal of environmental management*, vol. 208, pp. 56–76, 2018.

[32] R. Andreozzi, V. Caprio, A. Insola, and R. Marotta, “Advanced oxidation processes (AOP) for water purification and recovery”, *Catalysis today*, vol. 53, pp. 51–59, 1999.

[33] B. J. P. Jarvis, J. Banks, R. Molinder, T. Stephenson, S. A Parsons, “Processes for enhanced NOM removal: beyond Fe and Al coagulation”, *Water science technology: Water supply*, vol. 8, pp. 709–716, 2008.

[34] H. S. C. S. Uyguner, M. Bekbolet, “A comparative approach to the application of a physico-chemical and advanced oxidation combined system to natural water samples”, *Separation science technology*, vol. 42, pp. 1405–1419, 2007.

[35] R. Lamsal, M. E. Walsh, and G. A. Gagnon, “Comparison of advanced oxidation processes for the removal of natural organic matter”, *Water research*, vol. 45, pp. 3263–3269, 2011.

[36] S. Guerra-rodr and D. N. Singh, “Assessment of sulfate radical-based advanced oxidation processes for water and wastewater treatment : A review”, *Water,* vol. 10, pp. 1828, 2018.

[37] M. C. Vagı and A. S. Petsas, “Advanced oxidation processes for the removal of pesticides from wastewater : Recent review and trends”, *15th International conference on environmental science and technology. CEST2017, Rhodes, Greece*, vol. 31, 2017

[38] Z. Cai and M. M. Benjamin, “NOM fractionation and fouling of low-pressure membranes in microgranular adsorptive filtration”, *Environmental science and technology*, vol. 45, pp. 8935–8940, 2011.

[39] O. Legrini, E. Oliveros, and A. M. Braun “Photochemical processes for water treatment”, *Chemical reviews*, vol. 93, pp. 671–698, 1993.

[40] A. Primo, A. Corma, and H. Garcia, “Titania supported gold nanoparticle as photocatalyst”, *Physical chemistry chemical physics*, vol. 13, pp. 886–910, 2011.

[41] J. Zhao, T. Wu, T. X. Wu, K. Oikawa, H. Hidaka, and N. Serpone “Photo-assisted degradation of dye pollutants. Degradation of the cationic dye rhodamine B in aqueous anionic surfactant/TiO_2 dispersions under visible light irradiation: Evidence for the need of substrate adsorption on TiO_2 particles”, *Environmental science & technology*, vol. 32, pp. 2394–2400, 1998.

[42] D. Chatterjee and S. Dasgupta, “Visible light induced photocatalytic degradation of organic pollutants”, *Journal of photochemistry and photobiology C: photochemistry reviews*, vol. 6, pp.186-205, 2005.

[43] A. Rodriguez Arreola, M. Sanchez Tizapa, F. Zurita, J.P. Morán-Lázaro, R. C. Valderrama, J. L. Rodríguez-López, and A. Carreon-Alvarez., “Treatment of tequila vinasse and elimination of phenol by coagulation-flocculation process coupled with heterogeneous photocatalysis using titanium dioxide nanoparticles”, *Environmental technology*, vol. 41, pp. 1–11, 2018.

[44] C. A. Orge, M. F. R. Pereira, and J. L. Faria, “Applied Catalysis B : environmental photocatalytic ozonation of model aqueous solutions of oxalic and oxamic acids”, *Applied catalysis B, environmental,”* vol. 174–175, pp. 113–119, 2015.

[45] S. Bagheri and N. M. Julkapli, “Magnetite hybrid photocatalysis: Advance environmental remediation”, *Reviews in inorganic chemistry*, vol. 36, pp. 135–151, 2016.

[46] W. T. M. Audenaert, D. Vandierendonck, S. W. H. Van Hulle, and I. Nopens, “Comparison of ozone and HO induced conversion of effluent organic matter (EfOM) using ozonation and UV/H_2O_2 treatment”, *Water research*, vol. 47, pp. 2387–2398, 2013.

[47] O. C. N. and A. M. T. S. M. Sousa, N. F .F. Moreira, G. Macedo, A. R. Ribeiro, L. Barreiros, M. Pedrosa, J. L. Faria, M. Fernando, R. Pereira, S. Castro-Silva, M. A. Segundo ,C. M. Manaia, “Photocatalytic ozonation of urban wastewater and surface water using immobilized TiO_2 with LEDs : micropollutants, antibiotic resistance genes and estrogenic activity”, *Water research*, vol. 94, pp. 10–22, 2016.

[48] C. Amor, L. March, M. S. Lucas, and J. A. Peres, “Application of advanced oxidation processes for the treatment of recalcitrant agro-Industrial wastewater : A review”, *Water*, vol. pp. 205, 2019

[49] J. Li, W. Guan, X. Yan, Z. Wu, and W. Shi, “Photocatalytic Ozonation of 2 , 4-Dichlorophenoxyacetic Acid using - $LaFeO_3$ Photocatalyst under visible light irradiation”, *Catalysis letters*, vol. 148, pp. 23–29, 2018.

[50] M. Castellote, and N. Bengtsson, "Principles of TiO_2 photocatalysis", *Applications of titanium dioxide photocatalysis to construction materials*. Springer, Dordrecht, pp. 5-10, 2011.

[51] M. Castellote and N. Bengtsson, “Applications of titanium dioxide photocatalysis to construction materials”, S*tate-of-the-art report of the RILEM technical committee 194-TDP*. *Springer science & business media*, vol. 5, 2011.

[52] X. Li, J. Yu, S. Wageh, A. A. Al-ghamdi, and J. Xie, “Graphene in Photocatalysis : A Review”, *Small*, vol.12, pp. 6640–6696, 2016.

[53] X. Chen and S. S. Mao, “Titanium dioxide nanomaterials : Synthesis , properties , modifications , and applications”, *Chemical reviews*, vol. *107*, pp. 2891-2959, 2007.

[54] S. Lam, X. D. Low, K. Wong, and J. Sin, “Sequencing coagulation – photodegradation treatment of Malachite Green dye and textile wastewater through ZnO micro / nanoflowers”, *Chemical engineering communications*, vol. 205, pp. 1143–1156, 2018.

[55] M. M. Khan, S. F. Adil, and A. Al-Mayouf, “Metal oxides as photocatalysts”, *Journal of saudi chemical society*, vol. 19, pp. 462–464, 2015.

[56] S. Tsoumachidou, A. Kouras, and I. Poulios, “Heterogeneous and homogeneous photocatalytic degradation of psychoactive drug fluvoxamine: kinetic study , inorganic ions and phytotoxicity evaluation”, *Journal of chemical technology & biotechnology,* vol. *93, pp. 1705–1713,* 2018.

[57] H. Wang, G. Wang, Y. Zhang, Y. Ma, Z. Wu, and D. Gao, “Preparation of RGO / TiO_2 / Ag Aerogel and Its photodegradation performance in gas phase

formaldehyde", *Scientific reports*, vol. 9, pp. 1–12, 2019.

[58] H. Tian, K. Shen, X. Hu, L. Qiao, and W. Zheng, "N , S co-doped graphene quantum dots-graphene-TiO_2 nanotubes composite with enhanced photocatalytic activity N,S co-doped graphene quantum dots-graphene-TiO_2 nanotubes composite with enhanced photocatalytic activity", *Journal of alloys and compounds*, vol. 691, pp. 369–377, 2016.

[59] D. Ma, S. Zhai, Y. Wang, A. Liu, and C. Chen, "Synthetic approaches for C-N bonds by TiO_2 Photocatalysis", *Frontiers in chemistry*, vol. 7, pp. 1–8, 2019.

[60] X. Sun, J. Xing, and J. Qiu, "Preparation and photocatalytic activity of nonmetal co-doped titanium dioxide photocatalyst", *Russian journal of physical chemistry A*, vol. 90, pp. 1151–1156, 2016.

[61] N. Serpone, "Heterogeneous photocatalysis and prospects of TiO_2-based photocatalytic DeNOxing the atmospheric environment", *Catalysts*, vol. 8, p.553, 2018

[62] J. Moma, and J. Baloyi, "Modified titanium dioxide for photocatalytic applications", *Photocatalysts-applications and attributes*, vol. 18, 2019

[63] H. Liu, G. Liu, G. Xie, M. Zhang, Z. Hou, and Z. He, "Gd^{3+},N-codoped trititanate nanotubes: Preparation, characterization and photocatalytic activity", *Applied surface science*, vol. 257, pp. 3728–3732, 2011.

[64] A. Naldoni, M. Altomare, G. Zoppellaro, and N. Liu, "Photocatalysis with reduced TiO_2 : from black TiO_2 to cocatalyst- free hydrogen production", *ACS catalysis*, vol. 9, pp. 345−364, 2019.

[65] L. Szatmáry, S. Bakardjieva, J. Subrt, P. Bezdiˇ, V. Brezová, and M. Korenko, "Sulphur doped nanoparticles of TiO_2", *Catalysis today*, vol. 161, pp. 23–28, 2011.

[66] F. Huang, A. Yan, and H. Zhao, “Influences of doping on photocatalytic properties of TiO_2 photocatalyst”, *Semiconductor photocatalysis—materials, mechanisms and applications*, *Cao, W., Ed,* pp. 31–80, 2016.

[67] M. Humayun, F. Raziq, A. Khan, and W. Luo, “Modification strategies of TiO_2 for potential applications in photocatalysis: a critical review”, *Green chemistry letters and reviews*, vol. 11, pp. 86–102, 2018.

[68] N. Serpone, D. Chimica, and U. Pavia, “Heterogeneous photocatalysis and prospects of TiO_2 -based photocatalytic denoxing the atmospheric Environment”, *Catalysts*, vol. 8, p. 553, 2018.

[69] R. Long and N. J. English, “Tailoring the electronic structure of TiO_2 by cation codoping from hybrid density functional theory calculations”, *Physical review B*, vol. 83, pp. 155–209, 2011.

[70] J. V. Hernandez, “Structural and morphological modification of TiO_2 doped metal ions and investigation of photo-induced charge transfer processes”, Doctoral dissertation, Université du Maine; Instituto politécnico nacional, México, 2017.

[71] M. Fan, Y. Wang, N. Xue, Y. Zhao, Z. Wang, M. Wang, Y. Zhao, B. Gao “Coagulation of TiO_2 nanoparticles-natural organic matter composite contaminants in various aquatic media : Fluorescence characteristics , flocs properties and membrane fouling abilities”, *Separation and purification technology*, vol. 205, pp. 113–120, 2018.

[72] R. J. Honda, V. Keene, L. Daniels, and S. L. Walker, “Removal of TiO_2 nanoparticles during primary water treatment: Role of coagulant type, dose, and nanoparticle concentration”, *Environmental engineering science*, vol. 31, pp. 127–134, 2014.

[73] L. Rizzo, G. Lofrano, M. Grassi, and V. Belgiorno, “Pre-treatment of olive mill wastewater by chitosan coagulation and advanced oxidation processes”,

Separation purification technology, vol. 63, pp. 648–653, 2008.

[74] M. I. Badawy, F. E. l. Gohary, M. Y. Galey, and M. E. M. Ali, "Enhancement of olive mill wastewater biodegradation by homogeneous and heterogeneous photocatalytic oxidation", *Journal of hazard materials*, vol. 169, pp. 673–679, 2009.

[75] R. Y. Asahi, T. A. Morikawa, T. Ohwaki, K. Aoki, and Y. Taga, "Visible-light photocatalysis in nitrogen-doped titanium oxides", *Science*, vol. 293, pp. 269–271, 2001.

[76] T. Umebayashi, T. Yamaki, H. Itoh, and K. Asai, "Band gap narrowing of titanium dioxide by sulfur doping", *Applied physics letters*, vol. 81, pp. 454–456, 2002.

[77] T. M. T. Tachikawa, S. Tojo, K. Kawai, M. Endo, M. Fujitsuka, T. Ohno, K. Nishijima, Z. Miyamoto, "Photocatalytic oxidation reactivity of holes in the sulfur-and carbon-doped TiO_2 powders studied by time-resolved diffuse reflectance spectroscopy", *The journal of physical chemistry B*, vol. 108, pp. 19299–19306, 2004.

[78] B. S. P. V. Ramacharyulu, J. P. Kumar, G. K. Prasad, "Sulphur doped nano TiO_2: Synthesis, characterization and photocatalytic degradation of a toxic chemical in presence of sunlight", *Materials chemistry and physics*, vol. 148, pp. 692–698, 2014.

[79] R. Bacsa, J. Kiwi, T. Ohno, P. Albers, and V. Nadtochenko ,"Preparation, testing and characterization of doped TiO_2 active in the peroxidation of biomolecules under visible light", *The journal of physical chemistry B*, vol. 109, pp. 5994–6003, 2005.

[80] M. K. Szatmáry, L. Bakardjieva, S. Šubrt, P. Bezdička, J. Jirkovský, Z. Bastl, V. Brezová, "Sulphur doped nanoparticles of TiO_2", *Catalysis today*, vol. 161, pp. 23–28, 2011.

[81] P. S. Basavarajappa, S. B. Patil, N. Ganganagappa, K. R. Reddy, A. V. Raghu, and C. V. Reddy, “Recent progress in metal-doped TiO_2, non-metal doped/codoped TiO_2 and TiO_2 nanostructured hybrids for enhanced photocatalysis”, *International journal of hydrogen energy*, vol. 45, pp. 7764–7778, 2020.

[82] M. Z. Lin, H. Chen, W.-F. Chen, A. Nakaruk, C. C. P. Koshy Sorrell ,“Effect of single-cation doping and codoping with Mn and Fe on the photocatalytic performance of TiO_2 thin films”, *International journal hydrogen energy*, vol. 39, pp. 8526–8531, 2014.

[83] M. J. Yang, C. Hume, S. Lee, Y.-H. Son, J. K. J. Lee, “Correlation between photocatalytic efficacy and electronic band structure in hydrothermally grown TiO_2 nanoparticles”, *The journal of physical chemistry C*, vol. 114, pp. 15292–15297, 2010.

[84] E. Wang, T. He, L. Zhao, Y. Chen, and Y Cao, “Improved visible light photocatalytic activity of titania doped with tin and nitrogen”, *Journal of materials chemistry*, vol. 21, pp. 144–150, 2011.

[85] H. Liu, Y. Wu, and J. Zhang, “A new approach toward carbon-modified vanadium-doped titanium dioxide photocatalysts”, *ACS applied materials & interfaces*, vol. 3, pp. 1757–1764, 2011.

[86] Y. Y. Li, D. Xu, J. I. Oh, W. Shen, X. Li, “Mechanistic study of codoped titania with nonmetal and metal ions: a case of C^+, Mo codoped TiO_2”, *ACS catalysis*, vol. 2, pp. 391–398, 2012.

[87] Y. Meng, J. Chen, Y. H. Wang, Y. Ding Shan, “(N, F)-Codoped TiO_2 nanocrystals as visible light-activated photocatalyst”, *Journal of material. science and technology*, vol. 25, pp. 73–76, 2009.

[88] M. Massoudinejad, A. Paseban, A. Yazdanbakhsh, and M. Reza, “Preparation , characterization , and application of N , S-codoped TiO_2/montmorillonite

nanocomposite for the photocatalytic degradation of ciprofloxacin: Optimization by response surface methodology", *Polish journal of chemical technology,* vol. 20, pp. 66–74, 2018.

[89] M. Asiri, M. S. AAl-Amoudi, T. A. Al-Talhi, and A. D. Al-Talhi, "Photodegradation of rhodamine 6G and phenol red by nanosized TiO_2 under solar irradiation", *Journal of the saudi chemical society*, vol. 15, pp. 121–128, 2011.

[90] B. Kwon, S. Lee, J. Cho, H. Ahn, D. Lee, and H. S. Shin, "Biodegradability, DBP formation, and membrane fouling potential of natural organic matter: Characterization and controllability", *Environmental science and technology*, vol. 39, pp. 732–739, 2005.

[91] A. L. F Yee, M. P. Abdullah, A. Abdullah, B. K. N. Z Ishak, "Hydrophobicity characteristics of natural organic matter and the formation of THM", *The malaysian journal of analytical science and technology*, vol. 13, pp. 94–99, 2009.

[92] D. Gerrity, B. Mayer, H. Ryu, J. Crittenden, and M. Abbaszadegan, "A comparison of pilot-scale photocatalysis and enhanced coagulation for disinfection byproduct mitigation", *Water research*, vol. 43, pp. 1597–1610, 2009.

[93] K. C. Lee, and K. H. Choo, "Optimization of flocculation conditions for the separation of TiO_2 particles in coagulation-photocatalysis hybrid water treatment", *Chemical engineering and processing: Process intensification*, vol. 78, pp. 11–16, 2017.

[94] K. D. Vernon-Parry, "Microscopy : An introduction," *III-Vs Review*, vol. 13, no. 4, pp. 40–44, 2000.

[95] B. Kwiecińska, S. Pusz, and B. J. Valentine, "Application of electron microscopy TEM and SEM for analysis of coals , organic-rich shales and

carbonaceous matter," *International Journal of Coal Geology*, vol. 211, no. December 2018, p. 103203, 2019.

[96] H. Y. A.-E. A. A. Bunaciu, E. G. UdriŞTioiu, "X-ray diffraction: instrumentation and applications," *Critical reviews in analytical chemistry*, vol. 45, pp. 289–299, 2015.

[97] P. D. C. D. Lopes, P. H. Limirio, V. R Novais, "Fourier transform infrared spectroscopy (FTIR) application chemical characterization of enamel, dentin and bone," *Applied spectroscopy reviews*, vol. 53, pp. 747–769, 2018.

CHAPTER 3
EXPERIMENTAL METHODOLOGY

3.1 Introduction

The study was divided into two parts: namely: 1) Development and application of an integrated commercial TiO_2 photocatalysis-coagulation system for the removal of a mecoprop under UVC irradiation, 2) The removal of humic acid by a NS-TiO_2 photocatalysis-coagulation system under visible light irradiation. The first part of the work was done in the United Kingdom at the Cranfield Water Science Institute. While the second part was done in South Africa at the Institute of Nanotechnology and Water Sustainability (iNanoWS). This chapter outlines the experimental procedures that were followed for the execution of both parts of the study.

3.2 Materials and reagents

Reagents used in the UK study were as follows: Mecoprop (99.5% purity) was purchased from Sigma Aldrich (UK), LCMS grade methanol (>99.9%) and ammonium formate (≥99.0%) were purchased from Fisher Scientific (Loughborough, UK). Titanium dioxide (Aeroxide® TiO_2 P25 Degussa) was purchased from Lawrence Industries (Tamworth, UK), ferric sulphate (Ferripol XL, 13% w/v) was purchased from Huntsman Tioxide Europe. Ultra-pure (UP) water was produced using a Purelab Option-S7/15 system (Elga process water, Buckinghamshire, UK). The surface water was collected from the Chicheley Brook stream at Cranfield University (UK) (characterized non-purgeable organic carbon (NPOC) concentration of 7.30 mg L^{-1}, UV_{254} measurement of 0.12 cm^{-1}, turbidity measurement of 1.53 NTU) and stored in the dark at 4 °C. All the reagents used for the second part of the study were as follows: NaOH (≥98%), titanium (IV) butoxide (≥97.0%) formic acid (99.9%) thiourea (≥99.0%), sulphuric acid (95-99%), butanol (99.4%), and humic acid were purchased from Sigma Aldrich (South Africa) of analytical grade. These reagents were used as received without any further purification.

3.3 Part 1 – Commercial TiO_2-UVC-Coagulation for the removal of mecoprop

This section details the experimental procedures followed for investigating the removal of mecoprop using a photocatalysis-coagulation hybrid system. This includes coagulation experiments for commercial TiO_2 removal evaluation, degradation experiments of mecoprop from natural water samples, control experiments, instrument descriptions and water sample analysis procedures.

3.3.1 Coagulation of commercial TiO_2

Commercial TiO_2 (P25) suspensions in water (20, 40, 60, 80, 100 mg/L) were sonicated and stirred for 5 minutes. The jar test procedure was as follows: 1) dispersion of TiO_2 NPs in solution by sonication , 2) Coagulant (ferric sulphate) was dosed immediately into the jars (jars filled with TiO_2 solutions) at 0.0125 (0.7), 0.025 (1.4), 0.0375 (2.1), 0.05 (2.8), 0.1 (5.6), 0.15 (8.4), 0.2 (11.2) mM (mg/L) as [Fe] at the start of the rapid mix phase (250 rpm for 1 minute). This was followed by slow mixing at 45 rpm for 15 minutes. Finally, a 30 minute period of non-mixing was allowed for settlement of the flocs. The jar test apparatus used in these experiments is displayed in **Figure 3. 1**. Samples (5 mL) were taken at the end of the sedimentation and the turbidity (Thermo Scientific Orion AQUAfast®AQ3010), zeta potential (Malvern zetasizer, UK) and UV_{254} (PerkinElmer, LAMBDA 650 ultraviolet-visible) were measured.

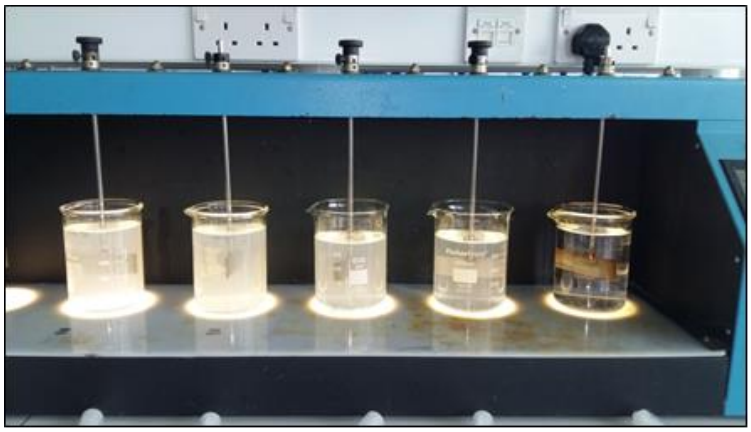

Figure 3. 1: Jar test experiment.

3.3.2 Photocatalysis-coagulation removal of mecoprop under UVC irradiation

All experiments were carried out in a Wedeco AG quasi-collimated beam setup (Herford, Germany), which was equipped with four 30 W low pressure Hg lamps that emit monochromatic light at 254 nm (**Figure 3. 2**). To maintain consistent light output, a 30-minute warmup period was permitted. Varying concentrations of commercial TiO_2 (20, 40, 60, 80, 100 mg/L) were added to the test solution. The solution was sonicated for 5 minutes to ensure equal distribution of the TiO_2 NPs in the solution. Test solutions of the pesticide (10 µg/L) were prepared by spiking surface water with MCPP.

The test solution (250 mL) was placed in a petri dish (Petri dish factor, PF=1, water depth= 2 cm) situated 22 cm from the source of light. The oxidation results reported herein are represented as C/C_0 (final concentration divided by initial concentration) vs UV fluence (UV dose over time). There is a tendency to report micropollutant degradation as a function of time in many studies, but this does not take into account the experimental setup, leading to a lower level of direct comparison between studies [1]. Using UV fluence (rather than irradiation time) to rate a pollutant's degradation allows for better comparisons among different studies on pollutant degradation. For this reason, the micropollutant degradation vs UV fluence approach was adopted for this study. The irradiation time was converted to UV fluence using **Eq. 3.1**:

$$\text{UV Fluence} = \text{Fluence rate} \times \text{Exposure time} \qquad [3.1]$$

Subsequent to fast mixing for 1 minute and addition of the catalyst, the coagulant ($Fe_2(SO_4)_3$) was added to the test solution. The mixture was then exposed to UV irradiation with an intensity of 67.5 $W.m^2$ for 20 minutes under slow mixing conditions. Thereafter, the suspension was allowed to settle for 10 minutes [2, 3]. A number of control experiments were conducted: removal of mecoprop by photolysis under UVC irradiation, removal under TiO_2 mediated photocatalysis, and removal of mecoprop using coagulation with and without UV irradiation. Furthermore, the influence of adsorption was evaluated by conducting the experiments in the presence of TiO_2 under dark conditions. Prior to quantitative analysis for mecoprop

and DOC, the samples were filtered through Millex-HA 0.45 m syringe filters to isolate TiO_2 particles. An amount of 1.5 mL was sampled after 10 fluences for MCPP quantification and 20 mL for DOC analysis at the end of each degradation treatment. All experiments were conducted at the optimum pH of 5 (adjusted by addition of 0.1 M NaOH, 0.1 M H_2SO_4) as evidenced by the coagulation tests DOC was measured in the non-purgeable organic carbon (NPOC) mode, using a Shimadzu 5000-A TOC analyser, Japan.

Figure 3. 2: Lab scale photocatalysis experimental set-up.

3.3.3 LC-MS quantification of mecoprop herbicide

An ammonium formate solution (0.01% w/v) used for the LC-MS analysis was prepared by dissolving a 2 mM solution of ammonium formate in ultrapure water (1:1). The herbicide was identified and quantified using a Sciex, Exion MS liquid chromatograph-Sciex QTRAP 6500^+ mass spectrometer. The flow rate was 0.4 $mL.min^{-1}$ and the sample injection volume was 10 µL [4]. Prior to each sequence, a new calibration curve was created, which displayed satisfactory linearity between concentrations of 0 and 20 µg/L (r^2 > 0 99). After every 10 samples, standards in

the concentration range of 1 – 20 µg/L were analysed to guarantee that the data produced was of high quality. All of the experiments were done in duplicates.

3.3.4 Degradation kinetics

The rate of pesticide degradation by UV-TiO_2 was calculated using the Langmuir-Hinshelwood model. This model divides the kinetics observed from the removal of contaminants into components for reaction (oxidation) and adsorption **Eq. 3.2** is a basic description of the Langmuir-Hinshelwood model:

$$r = d[P]/dt = k_r K[P]/ 1+K[P] \quad [3.2]$$

The rate of pollutant degradation (P) is represented by r, K represents the adsorption coefficient of P, kr the reaction rate constant, and P_0 is the initial concentration of compound P.

Integration of **Eq. 3.2** gives **Eq. 3.3**:

$$\ln[P_o]/[P] + K([P]_o - [P]) = k_r Kt \quad [3.3]$$

This equation is the summation of the zero and first order rate equations. The contribution of the equation to the overall response is determined by the pollutant's initial concentration. Since the contaminants being extracted in drinking water treatment are usually at very low concentrations, P_0 is typically very high, and **Eq. 3.3** can be transformed to **Eq. 3.4** as follows:

$$\ln[P]_0 - [P] = k_r Kt = k't \quad [3.4]$$

Where k' is apparent constant of the pseudo first order rate constant. A plot of $\ln[P]_0/[P]$ vs t leads to a straight line in which the slope reflects the apparent constant of first order (k') [3]

3.4 Part 2: NS-TiO_2-visible light-coagulation for the removal of humic acid

In this sub section, experimental procedures for the preparation and characterisation of photocatalysts (TiO_2 and NS-TiO_2) are detailed as well as model humic acid solution preparation. Further, an analysis of the process for degrading humic acid,

a description of the instrumentation utilised in the process of degradation, and a description of the experimental method for recovering NS-TiO_2 following the coagulation process is explained.

3.4.1 Synthesis of nitrogen, sulphur co-doped titanium dioxide

The procedure for the preparation of nitrogen, sulphur co-doped titanium dioxide (NSTiO_2) was adopted from work done by Mamba *et al.,* [5]. Typically, a mixture of titanium (IV) butoxide (10 mL) dissolved in butanol (20 mL) was sonicated for 30 minutes. Thereafter, solutions of thiourea (1 g, 2 g, 4 g) were dissolved in formic acid (15 mL) was added dropwise to the mixture under stirring conditions. The resultant mixture was left to stir for an additional 2 hrs after the addition of the thiourea solution. Subsequently, a white to yellowish precipitate formed. The pure TiO_2 photocatalyst was prepared using the same approach, but this time without adding thiourea. In both cases, the NS-TiO_2 and TiO_2 products were washed with ethanol (50 mL x 3) and thereafter dried at 100 °C for 12 hrs. This was followed by milling and calcination of the resultant solid at 400 °C for 3 hrs. Prior to application, the solid NS-TiO_2 and TiO_2 photocatalysts were stored at room temperature in glass vials.

3.4.2 Analytical techniques

The characterization of the prepared photocatalysts was done using Field Emission Scanning Electron Microscope and Energy Dispersive X-ray Spectroscopy (FE-SEM EDX), Ultra-Violet Visible Diffuse reflectance spectroscopy (UV-Vis DRS), Brunauer-Emmett-Teller (BET), X-ray Diffraction (XRD), Transmission Electron Microscope (TEM), and Fourier Transformer Infrared (FTIR).

3.4.2.1 Field emission scanning electron microscopy and electron dispersive X-ray spectroscopy

The surface morphology of the produced photocatalysts was studied using field emission scanning electron microscopy and electron dispersive x-ray spectroscopy. The material was placed onto glass slides with double-sided carbon tape and gold coating before being loaded into the Field Emission Scanning Electron Microscope

(FE-SEM, Joel JSM-7800F SEM Field Emission Electron Microscope, Japan). The elemental composition of the photocatalyst was determined using an energy dispersive X-ray spectrophotometer coupled with the SEM Joel JSM-7800D SEM.

3.4.2.2 High resolution transmission electron microscope

The surface morphology of the produced photocatalyst was examined using a high-resolution transmission electron microscope (HRTEM). To analyse the prepared photocatalyst, ethanol was used to disperse a small portion of the sample and a droplet of the dispersion was placed on a copper grid and permitted to dry prior to analysis. The analysis was undertaken using a Jeol JEM 2100 Transmission Electron Microscope, Japan.

3.4.2.3 Ultraviolet-visible spectroscopy-diffuse reflectance spectroscopy

The optical properties of the prepared photocatalysts were determined using a PerkinElmer, LAMBDA 650 ultraviolet-visible spectroscopy-diffuse reflectance spectrophotometer (UV-Vis-DRS) fitted with an integrating sphere . For baseline correction, a $BaSO_4$ standard was employed as a reference sample. To perform the analysis, the photocatalyst was mounted onto the sample holder and placed in the instrument (range 250 nm to 800 nm).

3.4.2.4 Brunauer-Emmett-Teller analysis

The surface area of the photocatalysts were determined using the BET method on an AUTOSORB-IQ-MP, USA. The photocatalyst samples was degassed under vacuum at 200 °C for 4 hrs to eliminate moisture and other solvents.

3.4.2.5 X-ray Diffraction

X-ray diffraction (XRD) was used to gain insight into the mineral phases of NS-TiO_2, the degree of crystallinity and the average size of the NS-TiO_2 crystallites. Powder XRD measurements were recorded on a PAnalytical XPERT/PRO diffractometer using Ni filtered CuKα radiation (λ = 1 5406 Å) at 45 kV/40 mA. The diffraction

measurements were conducted at room temperature in a Bragg-Brentano geometry.

3.4.2.6 Fourier transform infrared

FTIR was utilised to identify the functional groups present in the prepared photocatalyst. Samples were analysed as KBr pellets. In a ratio of 1:20, the sample was mixed with KBr, ground and pressed to form the pellet that was then mounted and analysed on the FTIR sample holder. The analyses were undertaken on a PerkinElmer Spectrum 100 FT-IR spectrophotometer.

3.4.3 Degradation studies

3.4.3.1 Preparation of stock solutions of humic acid

A solution containing humic acid 10 mg/L was prepared from a stock solution of 100 mg/L humic acid. Humic acid stock solution was prepared by dispersing 100 mg of humic acid in Milli-Q water (1 L) [7]. Dilutions of 10 mg/L were prepared from the stock solution as test solution that would be used in the degradation experiments. The pH of the stock solution was altered to 10 using a 0.1 M NaOH solution followed by 20 minutes of stirring. Lastly, the stock solution was stored at 4 °C prior to each experiment.

3.4.3.2 Coagulation of NS-TiO_2

A laboratory procedure that simulates coagulation-flocculation described in **Section 3.5.1** with differing $FeCl_3$ doses was adopted (15, 20, 30, 40 mg/L) NS-TiO_2 suspensions (150 mg/L) were sonicated and stirred for 5 minutes and added to each jar, stirred, and the settling of solids was observed. The water in the degradation tests was treated with the lowest dosage ([$FeCl_3$]= 30 mg/L of chemicals that provided adequate settling. Turbidity of the water was measured to determine the extent of removal of suspended particles in the solutions. Furthermore, UV_{254} (LAMBDA 650 from Perkin Elmer) was measured to evaluate the relationship

between humic acid removal in the presence of NS-TiO_2. Zeta potential (Malvern zetasizer, UK) of the resultant solutions was measured to optimize coagulant dose

3.4.3.3 The removal of humic acid by treatment with a photocatalysis-coagulation hybrid system

The NS-TiO_2 samples with varying N and S loadings were investigated for the degradation of humic acid. The photocatalyst (50, 100, 150, 200 mg/L) was added to the humic acid solution (10 mg/L) in a beaker. Prior to irradiation, the photocatalyst-humic acid mixture was agitated in the dark for 15 minutes to allow adsorption desorption equilibrium. This was followed by addition of the coagulant ($FeCl_3$), and fast mixing for 1 minute. Thereafter, the mixture was exposed to visible light irradiation (250 W), with slow mixing for 15 minutes. Subsequently, a settling period of 30 minutes was allowed in the absence of light and agitation [8, 9]. For comparison, an experiment was performed where photocatalysis was done first for 120 minutes followed by the coagulation process. Humic acid degradation was monitored by drawing (20 mL) aliquots at 20 minutes intervals. Filtration through a 0.45 µm glass fibre syringe filter followed to separate the photocatalyst from the test solution. Thereafter, the samples were analysed using TOC (Teledyne Tekmar TOC Fusion Analyser Ohio, USA), FEEM (Horiba Aqualog spectrometer) and UV-Vis (LAMBDA 650 from Perkin Elmer). In addition to the photocatalysis-coagulation experiments, HA removal by photolysis, NS-TiO_2 in the dark, coagulation-adsorption and coagulation-photolysis, was investigated as controls. The apparatus used to

conduct these photodegradation-coagulation experimental set-up displayed in **Figure 3. 3**.

Figure 3. 3: Photoreactor used for the photocatalysis and photocatalysis-coagulation experiments.

3.4.3.4 Total Organic Carbon (TOC) analysis

Analyses of total organic carbon (TOC) were performed, using a Teledyne Tekmar TOC Fusion Analyser (Ohio, USA), following degradation studies to quantify the amount of organic carbon in the samples. Standard solutions were prepared by dissolving 1 mg/L, 5 mg/L, 10 mg/L, 20 mg/L, and 30 mg/L potassium hydrogen phthalate (KHP) in de-ionized water.

3.4.3.5 Fluorescence excitation emission matrices (FEEM) analysis

In this method (FEEM), humic and non-humic substances are identified and differentiated according to their sources. This procedure is commonly used to distinguish among humic compounds (fulvic acids, humic acids, and humin) and other NOM constituents [4]. In addition to the UV/Vis spectrophotometer, a Horiba Aqualog, JobinYvon spectrometer was used for humic acid characterisation. Fluorescence EEMs, absorbance spectra, and simulated synchronous scans at λ= 60 nm, were obtained using a fluorescence spectrometer in the wavelength range 200–600 nm at 2 nm excitation intervals, and 250-600 nm at 3 nm emission interval

References

[1] B. Jefferson, P. Jarvis, G. K. Bhagianathan, H. Smith, O. Autin, E. H. Goslan, J. MacAdam, I. Carra, “Effect of elevated UV dose and alkalinity on metaldehyde removal and THM formation with UV/TiO_2 and UV/H_2O_2”, *Chemical engineering journal*, vol. 288, pp. 359–367, 2016.

[2] S. Martinez, M. Delgado, and P. Jarvis, “Removal of herbicide mecoprop from surface water using advanced oxidation processes (AOPS)”, *International journal of environmental research*, vol. 10, pp. 291–296, 2016.

[3] O. Autin, "Micropollutant removal by advanced oxidation processes", PhD thesis, Cranfield Water Science Institute, School of applied sciences, Cranfield University, Cranfield, 2012.

[4] E. S. Majzik, F. Tóth, L. Benke, and Z. Kiss, “SPE-LC-MS-MS determination of phenoxy acid herbicides in surface and ground water”, *Chromatographia*, vol. 63, pp. 105–109, 2006.

[5] G. Mamba, M. A. Mamo, X. Y. Mbianda, and A. K. Mishra, “Nd, N, S-TiO_2 decorated on reduced graphene oxide for a visible light active photocatalyst for dye degradation : Comparison to Its MWCNT/Nd,N,S-TiO_2 analogue”, *Industrial & engineering chemistry research*, vol. 53, pp. 14329−14338, 2014.

[6] K. D. Vernon-Parry, “Microscopy : An introduction”, *III-Vs Review,* vol. 13, no. 4, pp. 40–44, 2000.

[7] C. D. Lopes, P. H. Limirio, V. R Novais, and P. Dechichi, “Fourier transform infrared spectroscopy (FTIR) application chemical characterization of enamel, dentin and bone”, *Applied spectroscopy reviews*, vol. 53, pp. 747–769, 2018.

[8] H. Juretić, G. Smoljanić, and M. Barta, “Degradation of natural organic matter in water by using UV-C/H_2O_2 process”, *The holistic approach to environment*, vol. 5, pp. 135–149, 2015.

[9] B. J. O. Autin, J. Hart, P. Jarvis, J. MacAdam, S. A. Parsons, “Comparison of

UV/H_2O_2 and UV/TiO_2 for the degradation of metaldehyde: Kinetics and the impact of background organics", *Water research*, vol. 46, pp. 5655–5662, 2012.

CHAPTER 4:
AN INTEGRATED PHOTOCATALYSIS-COAGULATION SYSTEM FOR THE REMOVAL OF A PESTICIDE UNDER UVC IRRADIATION

4.1 Introduction

This chapter gives detailed discussions of experimental results following the investigation of 1) the removal of commercial TiO_2 by coagulation-flocculation processes using ferric sulphate, 2) the performance of the integrated photocatalysis-coagulation system for the removal of mecoprop under UVC irradiation.

4.2 Materials and methods

The details on the materials and methods employed are as discussed in **Chapter 3**, **Section 3 2** of the experimental methodology.

4.3 Results and discussion

This section covers detailed discussions based on the results obtained for the investigation of the removal of mecoprop by a photocatalytic-coagulation hybrid system. The first aspect involved is the optimisation of the reaction conditions of the coagulation-flocculation step used in the recovery of the TiO_2 photocatalyst. Once optimised, these conditions were then adopted and tested in the actual experiments involving the photocatalytic degradation of mecoprop from an aqueous medium. In the last step, the removal of mecoprop using the photocatalysis-coagulation hybrid process was evaluated under UVC irradiation. A detailed presentation and discussion of the results that emanated from these three stages is undertaken in the subsections that follow.

4.3.1 Optimization of coagulation-flocculation conditions for the recovery of TiO_2 (P25)

This section presents the experimental data and discussions following the investigation of the elimination of TiO_2-P25 from water by coagulation-flocculation process using ferric sulphate. As illustrated in **Figure 4. 1**, the turbidity of the raw water was found to be 3 NTU in the absence of a coagulant. However, the turbidity

increased from 50 to 233 NTU when TiO_2-P25 was varied between 20 and 100 mg/L. The turbidity levels observed following the addition of the TiO_2-P25 were reduced after the addition of the coagulant ($(Fe_2(SO_4)_3$) (**Figure 4. 1**). This is evident from the observation of a rapid decrease in the measured turbidity after coagulation with 0.0125 mM [Fe] (decrease from 233 to 25 NTU at 100 mg/L of TiO_2). When the coagulant dose was increased from 0. 0125 mM to 0. 0500 mM, the turbidity decreased to between 2.5 and 5 NTU for the different TiO_2 doses. However, the lowest residual turbidity was observed for the system where no TiO_2 was added**.** This serves as evidence of the need to recover the TiO_2 NPs from water after treatment and removal of organic pollutants.

The addition of ferric sulphate coagulant contributes to the destabilisation of TiO_2 NPs *via* the neutralisation of the negative TiO_2 charges by the hydrolysed Fe^{3+} [1]. Once the TiO_2 NP were destabilised, they agglomerated to form flocs, which eventually settled out of solution to enable their easy removal [2]. Removal of the flocs significantly reduced the turbidity of the solution, which signified the success of the coagulation process. Furthermore, the effectiveness of the coagulation process was evaluated by monitoring the change in the system's zeta potential at increased coagulant dose. Evidently, the zeta potential became more positive and reached 0 mV when the Fe^{3+} hydrolysis material was adsorbed onto the surface of the NPs or NOM. The TiO_2 nanoparticles were destabilised at coagulant doses of between 0.0375 and 0.0500 mM [Fe] (**Figure 4 1**). Under these conditions, the surface charge of TiO_2 was near neutral and the nanoparticles aggregated owing to the reduced electrostatic repulsion amongst the nanoparticles [3]. Additionally, as the coagulant dose increased, the zeta potential also increased. Notably, when the coagulant dose was increased to above 0.1000 mM [Fe], the system became more positive within the zeta potential thus increasing from 3 to 5 mV. However, the increased positive charge failed to have an impact on the removal of TiO_2 from the water thus indicating that particle re-stabilisation had not occurred. From **Figure 4. 1**, an optimal coagulant dose of 0.0375 mM [Fe], that is in agreement with the obtained zeta potential (**Figure 4. 2**), was achieved. The zeta potential was found to be above 0 mV (over coagulated) at coagulation dosages exceeding 0.0375 mM [Fe].

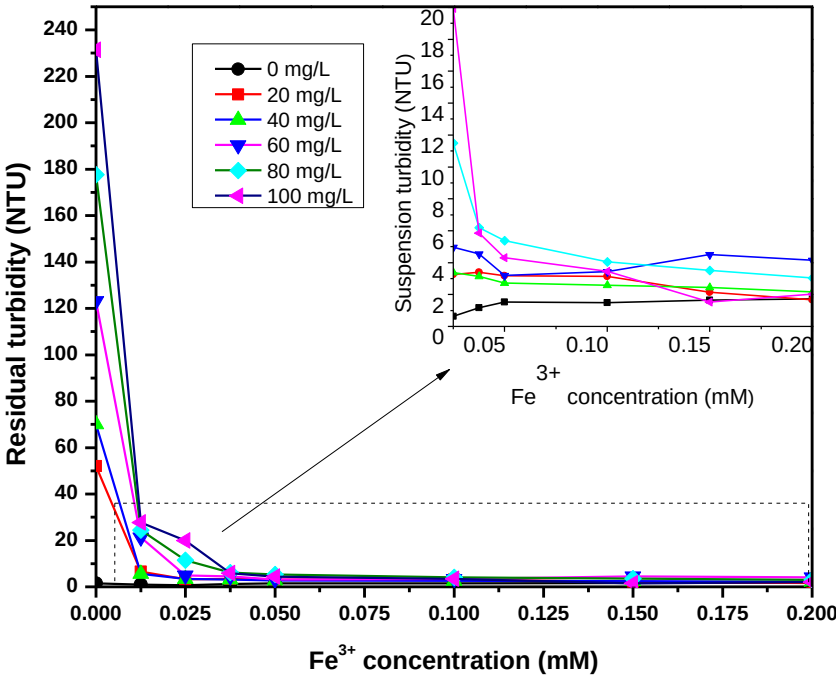

Figure 4. 1: Removal of TiO_2 as indicated by reduction of turbidity as a function of coagulant dosage (TiO_2 = 20 to 100 mg/L, $Fe_2(SO_4)_3$ = 0 to 0 2 mM, pH = 5).

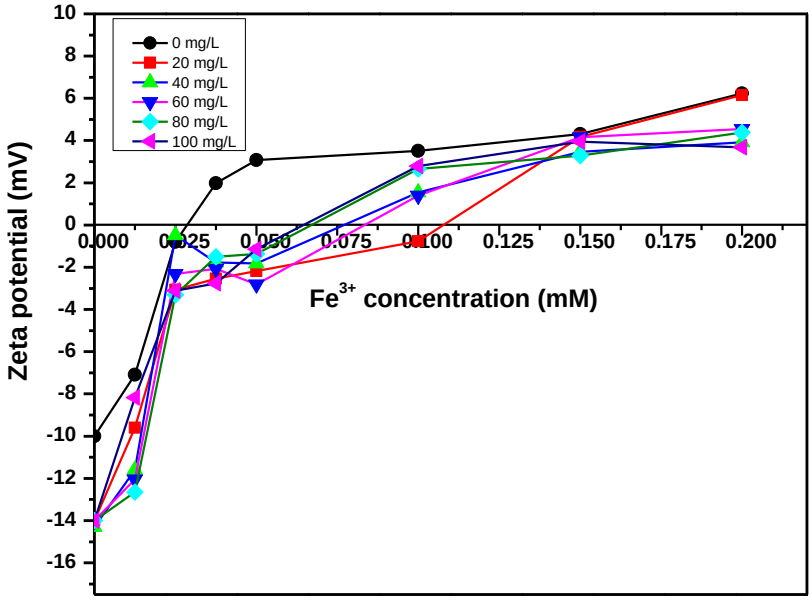

Figure 4. 2: Zeta potential measurements for coagulation of TiO_2 by ferric sulphate (TiO_2 = 20 to 100 mg/L, $Fe_2(SO_4)_3$ = 0 to 0 2 mM, pH = 5).

Furthermore, coagulation-flocculation experiments were conducted at pH 4, 5 and 6 to examine the influence of pH on the TiO_2 surface charge and its subsequent removal by coagulation. When the coagulation pH was increased to above 5, an

improvement in the residual turbidity was noted indicating better removal of the TiO_2 (**Figure 4. 3**). Titanium dioxide NPs have a positive surface charge at pH values between 2.5 to 4. Conversely, at pH 5 to 7.3, the TiO_2 NPs have a negative surface charge [4]. The lower removal rates obtained for TiO_2 at pH values lower than 5 are attributed to the repulsive forces that occur between the Fe^{3+} and the TiO_2 NPs [5].

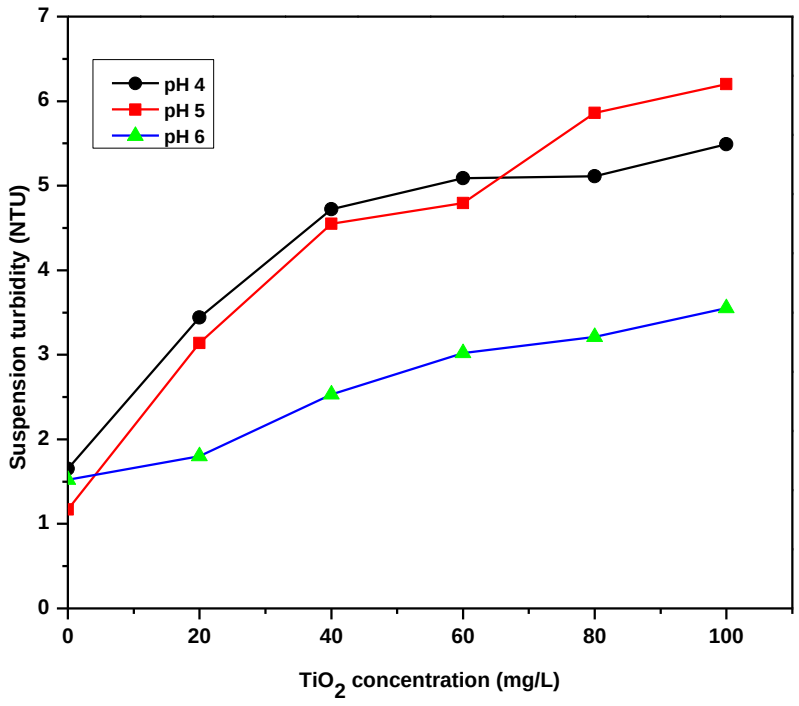

Figure 4. 3: Turbidity removal during coagulation of varying concentrations of TiO_2 suspensions using ferric sulphate (TiO_2 = 20 to 100 mg/L, [Fe^{3+}] = 0 0375 mM).

The effect of TiO_2 on the removal of NOM by coagulation-flocculation was evaluated, and the results thereof follow. Removal of UV_{254} absorbing organic matter (OM) was not affected by the presence of TiO_2 during the coagulation process illustrated in **Figure 4. 4**. This removal profile was similar to the one observed for turbidity, whereby a rapid decrease in the UV_{254} absorbing organic matter was observed (decreased from 0.1300 to 0.0300 cm^{-1}) following treatment with an Fe concentration of 0.0125 mM. Subsequently, a slight reduction in UV_{254} was observed when the coagulant dosage was increased from 0.0125 mM to 0.0375 mM. No further removal was observed beyond the Fe dosage of 0.0500 mM. Two mechanisms were postulated for the removal of OM in the combined TiO_2-coagulation process, namely: 1) removal by coagulation; and 2) removal by

adsorption onto the TiO_2. Different types of organic matter (e.g., fulvic acids, humic acids, and non-humic substances) have been shown to adsorb onto the surface of TiO_2 NPs and thereafter extracted from water following the settling of TiO_2 NPs [6]. Previous studies have shown that the physicochemical properties of NOM, such as molecular weight distribution and hydrophobic and hydrophilic properties, have a significant impact on the interaction of NOM with NPs.

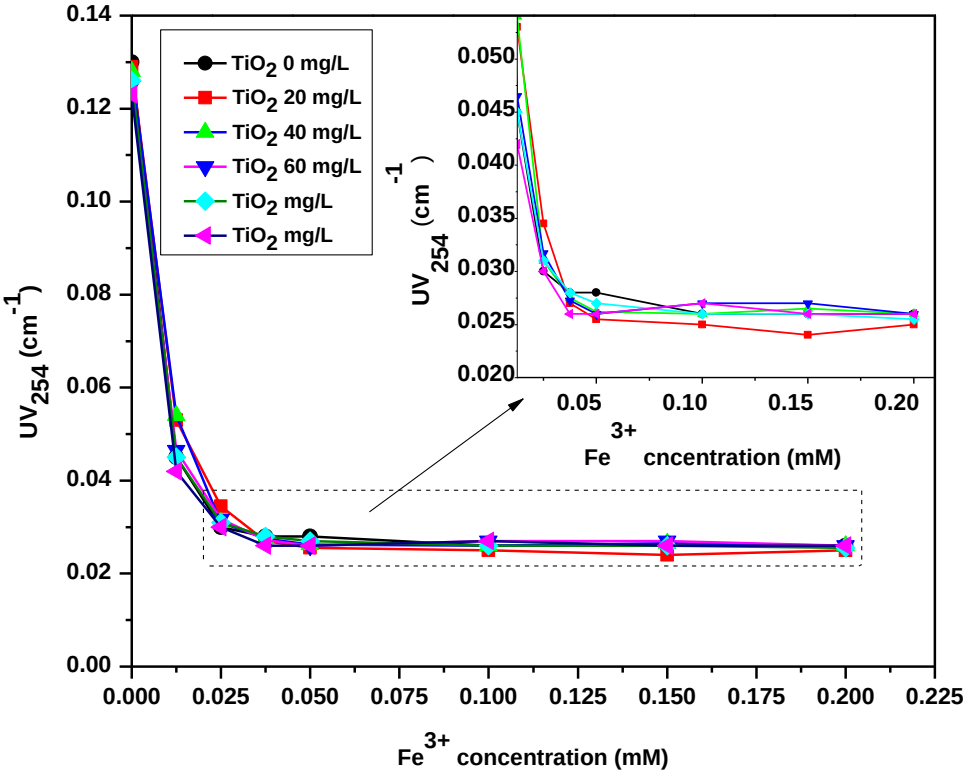

Figure 4. 4: UV_{254} removal by ferric sulphate in the presence of TiO_2 (TiO_2 = 20-100 mg/L, [Fe]= 0 012 mM to 0 2 mM, pH= 5).

Removal of OM by coagulation is one of the most effective methods in water treatment [7]. According to Yan *et al.,* [8] peak NOM removal happens under vaguely acidic conditions for coagulants that are not pre-hydrolysed such as alum and ferric salts (pH < 6.0) [8]. This coincides with the results presented in **Figure 4. 5**, where the best OM removal by ferric sulphate was achieved at pH 5. However, for the pH that was used in these tests (pH 5), both the TiO_2 surface and OM are negatively charged [3,6] (**Figure 4. 3**), thus reducing the opportunities for adsorption. Since no difference was observed in the removal of UV_{254} absorbing NOM in the presence of various concentrations of TiO_2 (20 to 100 mg/L), it is unlikely

that the removal proceeded *via* adsorption of NOM onto TiO_2, rather than by direct coagulation. An increase in NS-TiO_2 concentration does not alter or improve UV_{254} removal, proving that no NOM was adsorbed to the NS-TiO_2 surface and consequently removed.

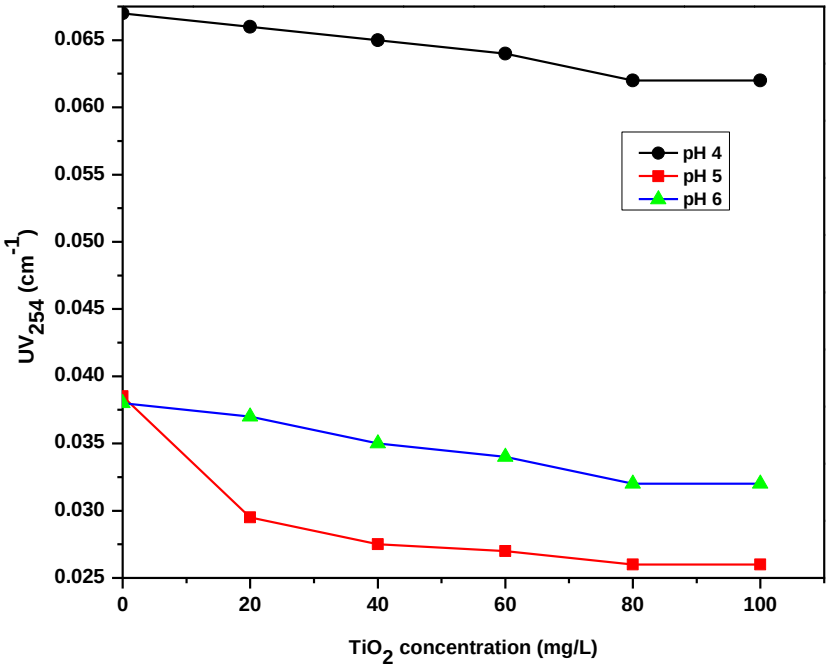

Figure 4. 5: UV_{254} removal post coagulation by ferric sulphate in the presence of TiO_2 (TiO_2 = 20-100 mg/L, [Fe^{3+}] = 0.0375 mM)**.**

4.3.2 Removal of mecoprop by photocatalysis-coagulation hybrid process

The simultaneous treatment and removal of mecoprop with ferric sulphate coagulation and UV-mediated TiO_2 photocatalytic degradation was investigated to determine the efficacy of the coupled process. To evaluate the effect of the coupling of the two processes on the removal of mecoprop, detailed control experiments (photolysis, photocatalysis, coagulation, UV-coagulation, and coagulation-TiO_2) were performed under conditions similar to those of the hybrid treatment process. **Figure 4. 6** shows that mecoprop was degraded by photolysis reaching a removal efficiency of 88% (at a maximum UV fluence applied at 8000 $cm^2.mJ^{-1}$). Mecoprop absorbs UV light in the range 230 and 280 nm thus leading to its degradation [8]. Cátia *et al.,* [9] reported over 80% photodegradative removal of mecoprop under simulated solar irradiation. It is clear that the photodegradation profile of mecoprop

under UVC irradiation is similar to the photocatalytic degradation when TiO_2 concentrations of 20 and 40 mg/L were employed. The results suggest that photolysis by UVC irradiation is an effective tool for the degradation of mecoprop in water. However, coupling catalysis and photolysis show a greater removal efficiency of mecoprop at higher TiO_2 concentrations (100 mg/L).

The photocatalytic degradation curves displayed in **Figure 4. 6** show a direct relationship between degradation rate of mecoprop, TiO_2 concentration, and UV fluence. Complete degradation of mecoprop into smaller fragments occurred at TiO_2 concentrations of 80 mg/L and 100 mg/L and UV fluences of 8000 $cm^2.mJ^{-1}$ and 4356 $cm^2.mJ^{-1}$, respectively. The high removal of mecoprop following treatment at these conditions ([TiO_2] = 80 mg/L and 100 mg/L, UV fluence =8000 cm^2 mJ^{-1} and 4356 cm^2 mJ^{-1}) is ascribed to increased production of hydroxyl radicals at higher dosage of TiO_2. However, at lower TiO_2 concentrations (20, 30, 60 mg/L), incomplete MCPP degradation was observed, which resulted in residual concentrations of MCPP between 0.0650 µg/L and 3.6300 µg/L. The degradation rates at these lower TiO_2 concentrations were similar to those recorded for the photolytic treatment of MCPP (photolysis at 8000 $cm^2.mJ^{-1}$ = 88% removal, photocatalysis at [TiO_2] of 60 mg/L, 8000 $cm^2.mJ^{-1}$ = 92% removal). The results are consistent with the findings of Martinez *et al.,* [10] which showed that the highest degradation of MCPP was achieved with TiO_2 concentrations of about 100 mg/L.

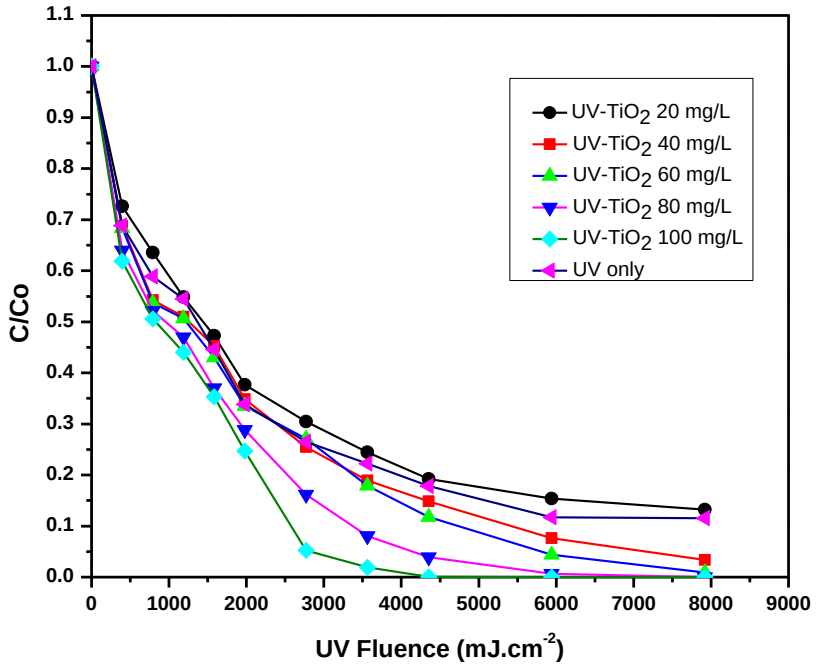

Figure 4. 6: Photocatalytic degradation of mecoprop over commercial TiO_2 UVC light irradiation (TiO_2= 20 to 100 mg/L, pH = 5).

Figure 4. 7 shows the removal of MCPP in the presence of various concentrations of TiO_2 without light. This test was carried out to evaluate the extent to which MCPP can be removed *via* absorption onto the TiO_2 surface. Limited removal of mecoprop *via* adsorption with TiO_2 NPs was observed after a contact time of 20 minutes; mecoprop removal rates ranging from 0 to 30% were obtained even under inconsistent TiO_2 concentration levels. The poor adsorption of mecoprop onto the TiO_2 NP surface suggests that the use of adsorption alone is not sufficient for the removal of mecoprop. However, adsorption is an essential step in photocatalysis, with the reactions taking place at the photocatalyst/liquid interface [11]. However, while close contact between the contaminant and photocatalyst is required, excessive adsorption (more than 50% of pollutant adsorbed onto catalyst surface) is unnecessary. Throughout photocatalysis, molecules may be degraded when they are adsorbed by or are near the TiO_2 surface [12].

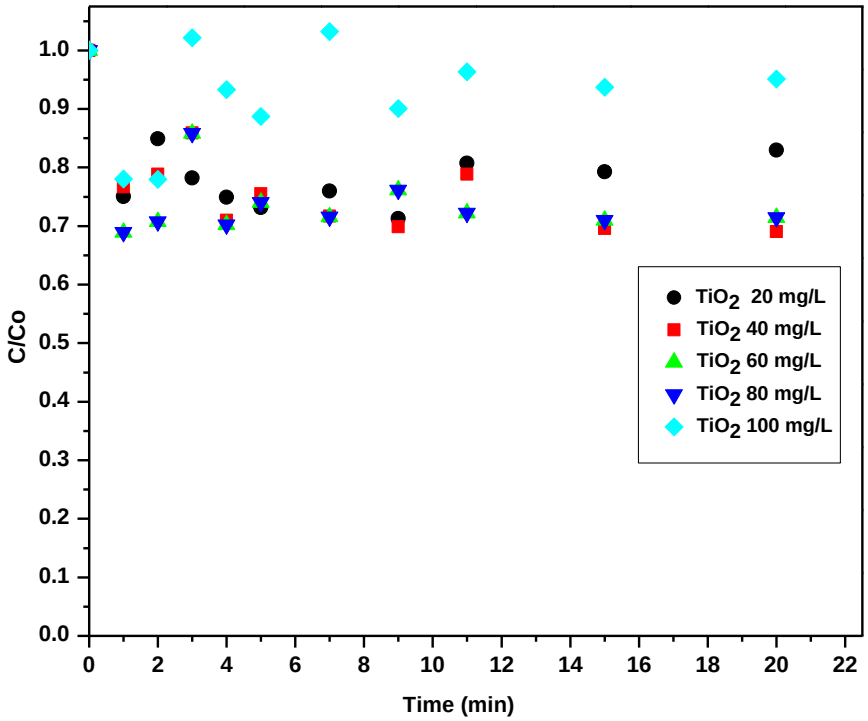

Figure 4. 7: Adsorption of mecoprop onto TiO_2 surface ([TiO_2] = 20 to 100 mg/L)**.**

Coagulation is a mandatory process in conventional water treatment. Despite this process targeting organic pollutants in water, it has never been used at pilot scale for the simultaneous removal of NPs and mecoprop. Results seen in **Figure 4. 8** explore the removal of NPs using ferric sulphate. All reactions were carried out at pH 5 and $Fe_2(SO_4)_3$ coagulant dosage of 7.5 mg/L (i.e., [Fe] = 0 0375 mM). These conditions were selected based on the optimisation results. Two processes, namely photocatalysis and coagulation are combined for the removal of mecoprop and the recovery of TiO_2 and the results and discussions thereof follow.

The coagulation-photocatalysis hybrid system (**Figure 4. 8**) revealed an improved mecoprop removal compared to coagulation, direct photolysis, catalysis, photolysis-coagulation and photocatalysis under the same experimental conditions (TiO_2 concentration, pH, UV fluence). The results show an increase in the removal of MCPP when the $Fe_2(SO_4)_3$ coagulant was introduced in the presence of TiO_2 and under UV irradiation. Comparatively, the sole use of coagulation led to no significant removal of the mecoprop. This is consistent with a study conducted by Adam *et al.,* [13] on the coagulation-flocculation with alum and iron salts, which at 10% found no significant removal of chloroacetamide herbicide. In another study, coagulation-

flocculation was used to treat river water spiked with atrazine, and a low removal rate of 0 to 11% was achieved [14]. Therefore, to promote its adsorption onto the particles, not only did the pesticide fail to strongly adsorb onto the negatively charged particles, it also failed to complex the humic substance materials fraction of NOM [14]. It was found that the anionic component of the phenoxy acetic acid in the pesticide is hardly adsorbed onto the humic substances due to the repulsive force emanating from the anionic component of the pesticide and the negative charged humic substances [15].

Furthermore, mecoprop did not readily adsorb onto the surface of the TiO_2 nanoparticles. This was confirmed from the TiO_2-coagulation experiments in the absence of UV light, whereby no removal of mecoprop was observed (**Figure 4. 8**) The herbicide does not readily adsorb onto the inorganic coagulant, hence treatment with coagulation and catalysis alone could not enhance the removal of the mecoprop [14]. Interestingly, complete removal of the herbicide was observed at lower UV fluence for the photocatalysis-coagulation hybrid system and the UV-coagulation process (**Figure 4. 8**) compared to when photocatalysis or photolysis was employed individually (**Figure 4. 6**).

While photolysis results in relatively slow degradation kinetics of various organic compounds, the addition of Fe^{3+} into the system catalysed the formation of hydroxyl radicals [7]. From **Figure 4. 8**, it is evident that the UV-coagulation process (in the absence of TiO_2) resulted in fast degradation kinetics. The mechanism involved in the degradation of the pesticides proceeds *via* the generation of hydroxyl radicals from iron species upon exposure to UV light (**Eq. 4.1** and **4.2**).

$$Fe^{3+} + H_2O \rightarrow Fe^{2+} + HO^{\bullet} + H^{+} \quad [4.1]$$

$$Fe^{3+} + H_2O + h\nu \rightarrow Fe^{2+} + H^{+} + HO^{\bullet} \quad [4.2]$$

At pH 2.5 to 5, Fe^{3+} hydrolyses and produces a range of hydroxylated species (such $Fe(H_2O)_5(OH)^{2+}$ (written for convenience as $Fe(OH)^{2+}$), which are formed by deprotonation of the hexaquo Fe^{3+}. Upon photolysis, the $Fe(OH)^{2+}$ species decompose to yield Fe^{2+} and a hydroxyl radical (**Eq. 4.2**). This process has a number of advantages compared to conventional (photo) Fenton processes. In this

process, there is no requirement for the application of the Fenton reagent or H_2O_2 and the process is carried out across a pH range that is suitable for effective coagulation of other water contaminants The Fe^{3+}-UV process has been applied widely to degrade several organic compounds such as phenols and nitrobenzene, carboxylic acids and 4-chloro-alinine [11]. The formation of hydroxyl radicals will cease once the Fe^{3+} ions are no longer left in this system. Additionally, iron has been used as a dopant for amending the properties of TiO_2 to enhance photocatalysis processes, through lowering the band gap width for electron excitement and reducing the recombination of electron/hole pairs [18]. What is observed in the UV-TiO_2-Coagulation process can be explained as follows. In the present case, iron was not introduced into the catalyst structure, but hydrolysed Fe^{3+} remains close to the TiO_2 when in the floc, where it can act as an electron acceptor leaving behind the hole available for oxidation ($TiO_2 + h\nu \rightarrow e^- + h^+$). The iron species therefore help reduce recombination of electron/hole pairs, contributing to the increase in degradation rate of UV-TiO_2-Coag when compared to the UV-TiO_2 system.

In the coagulation-photocatalysis system, the two processes work in a synergistic manner to produce high amounts of hydroxyl radicals, which are accountable for the rapid degradation of mecoprop compared to the individual processes. Of interest, for the same coagulant dose, the incorporation of low concentrations of TiO_2 (20 to 80 mg/L) reduced the efficiency of the degradation of mecoprop when compared to the experiment without TiO_2 (UV-Coag), requiring the highest dose of catalyst to be added for an equivalent rate of removal to be achieved. While the presence of Fe improves the performance of UV-TiO_2, TiO_2 had an inhibitory effect on the UV-Coag process at low TiO_2 concentrations. Dissolved Fe^{3+} hydrolysis species are known to produce radicals under UV exposure [19, 20]. In the present experiments, iron species were predominantly present as precipitated solids in the floc. However, solid phase $Fe(OH)_3$ can also be activated under UV light, leading to the generation of $O_2^{-\bullet}$ radicals (**Eq. 4.3 and 4.4**), which in turn can lead to $OH^\bullet$ radical formation [21]:

$$Fe(OH)_3 + 2O_2 + h\nu \rightarrow Fe^{2+} + 2O_2^{-\bullet} + H_2O \qquad [4.3]$$

$$O_2^{-\bullet} + 2H_2O \rightarrow 2\ {}^{\bullet}OH + 2\ OH^- \quad [4.4]$$

Nonetheless, irradiation in the presence of TiO_2 contributed (100 mg/L) to an improved MCPP removal owing to more efficient radical formation. In the hybrid system, the formation of hydroxyl radicals proceeds according to **Eq. 4.5** to **4.8**, and from the reactions presented for the UV-Fe^{3+}process (**Eq. 4.1 - 4.4**) [17].

$$TiO_2 + hv \rightarrow e^- + h^+ \quad [4.5]$$

$$h^+ + H_2O \rightarrow OH^{\bullet} \quad [4.6]$$

$$h^+ + OH \rightarrow OH^{\bullet} \quad [4.7]$$

$$h^+ + OM \rightarrow OH^{\bullet} \quad [4.8]$$

The pseudo first order rate constant increased in the TiO_2 range 0 to 100 mg/L up to 0.0019 $cm^2.mJ^{-1}$ for UV-TiO_2 and up to 0.0034 $cm^2.mJ^{-1}$ for the photocatalysis-coagulation process, which was due to the growing photon absorption by TiO_2 particles. The UV-Fe^{3+} had a high-rate constant of 0.0031 $cm^2.mJ^{-1}$, which was close to the degradation rate constant obtained when mecoprop was treated with 100 mg-L TiO_2 at UV dosage of 1800 $cm^2.mJ^{-1}$ and coagulant dose of 0.0375 mM [Fe] (**Table 4.1**). A synergistic effect was expected from the combination of UV-TiO_2-Coagulation. However, addition of the TiO_2 to the system had no effect on the production of radicals or the degradation rate. The addition of TiO_2 shields light from penetrating the entire test solution, and this might hinder activation of the TiO_2 NPs and even direct photolysis. This assertion is supported by the results from the UV-Coagulation system as compared to the UV-TiO_2-Coagulation system. The kinetic rate of the two processes are almost similar (0.0031 and 0.0034 $cm^2\ mJ^{-1}$, respectively), thus rendering the addition of TiO_2 useless in this photocatalysis-coagulation process.

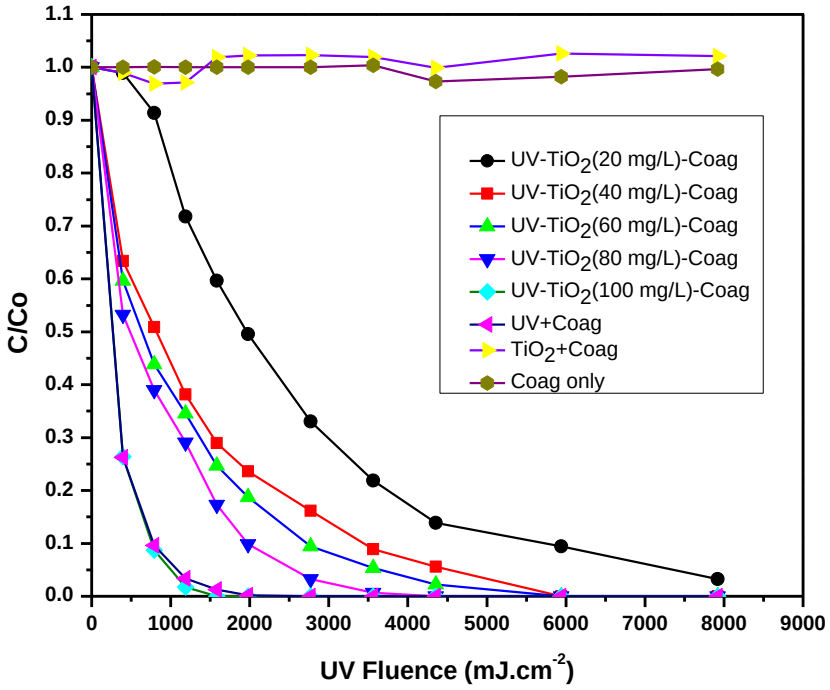

Figure 4. 8: Coagulation, photolysis-coagulation, photocatalysis-coagulation of mecoprop under UVC irradiation ([TiO_2] = 20 to 100 mg/L, [Fe^{3+}] = 0.0375 mM, pH = 5).

Table 4. 1: First order kinetics for the removal of mecoprop by photocatalysis combined with coagulation

PROCESS CONDITIONS	**K' ($CM^2 MJ^{-1}$)**	**R^2**
UV+TiO_2 (20 mg/L)	0 .0003	0.9332
UV+TiO_2 (40 mg/L)	0.0005	0.9904
UV+TiO_2 (60 mg/L)	0.0007	0.9648
UV+TiO_2 (80 mg/L)	0.0010	0.9531
UV+TiO_2 (100 mg/L)	0.0019	0.8948
UV+TiO_2 (20 mg/L) + Coagulation	0.0004	0.7117
UV+TiO_2 (40 mg/L) + Coagulation	0.0009	0.9899
UV+TiO_2 (60 mg/L) + Coagulation	0.0017	0.9333
UV+TiO_2 (80 mg/L) + Coagulation	0.0022	0.8508
UV+TiO_2 (100 mg/L) + Coagulation	0.0034	0.9886
UV	0.0005	0.9708
UV + Coagulation	0.0031	0.9501

4.3.3 TOC removal during photocatalysis-coagulation

The DOC of the treated water is presented in **Figure 4. 9a and 4. 9b** to illustrate an evaluation of the performance of the photocatalysis-coagulation hybrid system in the removal of background DOM (mecoprop and other dissolved organic matter in

the water). The results presented in **Figure 4. 9** reveal a 65% removal of DOC over a UV fluence of 8000 $cm^2.mJ^{-1}$ when a TiO_2 concentration of 100 mg/L was used. Under these conditions, mecoprop was completely removed from the water (**Figure 4. 6**). The removal percentage of 65% is ascribed to the difference in the concentrations of the mecoprop (10 µg/L) and DOC (7.35 mg/L). The photocatalysis-coagulation hybrid system displayed DOC removal percentage that is higher than that of the photocatalysis or UV irradiation when applied individually. However, photolysis and UV-Fe^{3+} also removed almost half of the organic matter present in the test solutions (**Figure 4. 9a and 4. 9b**). The DOC removal percentage after treatment with UV is higher than expected, and this could be ascribed to irradiation of a clear solution when no TiO_2 is added to the water solution. Combining UV with coagulation led to an increase in the degradation compared to when the treatment was undertaken with UV only. The power of UV and the Fenton-like process played a noteworthy role in the degradation of the organic matter.

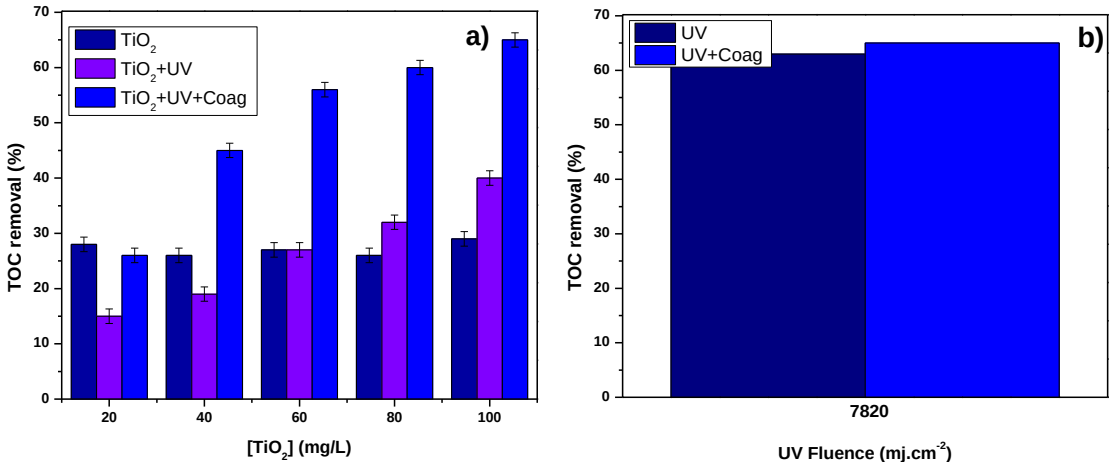

Figure 4. 9: DOC removal post photocatalysis-coagulation treatment, a) TiO_2 (adsorption), UV/TiO_2, UV-TiO_2-Coagulation, b) UV and Coagulation-UV.

4.4 Chapter summary

In this study, the removal of mecoprop using a photocatalysis-coagulation hybrid system was investigated. The hypothesis was that the two processes would work in a synergistic manner to improve the removal of mecoprop from water. These results highlight the complexities of the system, with potential for four separate mechanisms

for removal of organic matter (both bulk and micropollutants) from the system: adsorption onto TiO_2, oxidation by TiO_2, oxidation by Fe processes and coagulation by Fe. This research has shown the proof of concept of activating the coagulation process through the excitation of iron present in a system coagulated using an iron coagulant or an introduced catalyst particle using UV light.

Moreover, the recovery of TiO_2 NPs would be achieved by coagulation following treatment. The complete removal of TiO_2 by coagulation with ferric sulphate ($Fe_2(SO_4)_3$) was not achieved However, about 80% removal was observed at optimal conditions of [Fe] = 0.037 mM and pH = 5. Additionally, at high concentrations of TiO_2 (60, 80, 100 mg/L), no further enhancement in TiO_2 removal was achieved at Fe dosages exceeding 0.0500 mM. Furthermore, the combined photocatalysis-coagulation system for the degradation and removal of mecoprop proved to be more effective than when the individual treatment processes were used. A synergistic effect was observed between photolysis (UV) and the Fe^{3+} processes, however, the addition of TiO_2 to the system did not improve the degradation rate significantly (only 0.0031 $cm^2.mJ^{-1}$ was recorded in the degradation rate of UV + Coagulation process). Owing to mecoprop absorbing in the UVC region, the sole use of photolysis led to a high degradation rate. The UV-Fe^{3+} system could be applied in a pilot scale water treatment plant for the mitigation of mecoprop as the photolysis equipment could be retro-fitted into existing coagulation systems. Such an arrangement will result in the improvement of the removal of mecoprop in drinking water or wastewater.

References

[1] J. M. Santos, J. P. S. Valente, S. M. A. Jorge, P. M. Padilha, M. J. Saeki, G. R. Castro and A. O. Florentino, "Coagulation-flocculation of TiO_2 in suspension used in heterogeneous photocatalysis", *Orbital: electronic journal of chemistry*, vol. 5, pp. 233-241 , 2013.

[2] K. C. Lee, and K. H. Choo, "Optimization of flocculation conditions for the separation of TiO_2 particles in coagulation-photocatalysis hybrid water treatment", *Chemical engineering and processing: Process intensification*, vol. 78, pp. 11–16, 2017.

[3] F. Azeez, E. Al-Hetlani, M. Arafa, Y. Abdelmonem, A. A. Nazeer, M.O. Amin, and M. Madkour, "The effect of surface charge on photocatalytic degradation of methylene blue dye using chargeable titania nanoparticles", *Scientific reports*, vol. 8, pp. 1–9, 2018.

[4] A. Matilainen, R. Liikanen, M. Nyström, N. Lindqvist, T. Tuhkanen, and N. LIndqvist, "Enhancement of the natural organic matter removal from drinking water by nanofiltration", *Environment technology*, vol. 25, pp. 283–291, 2004.

[5] K. C. Lee and K. H. Choo, "Hybridization of TiO_2 photocatalysis with coagulation and flocculation for 1,4-dioxane removal in drinking water treatment", *Chemical engineering journal*, vol. 231, pp. 227–235, 2013.

[6] M. Fan, M. Fana, Y. Wanga, N. Xuea, Y. Zhaob, Z. Wanga, M. Wanga, Yi Zhaoa, B. Gaoa, "Coagulation of TiO_2 nanoparticles-natural organic matter composite contaminants in various aquatic media : fluorescence characteristics , flocs properties and membrane fouling abilities", *Separation and purification technology*, vol. 205, pp. 113–120, 2018.

[7] C. Y. Ayekoe, D. Robert, and D. G. Lanciné, "Combination of coagulation-flocculation and heterogeneous photocatalysis for improving the removal of humic substances in real treated water from Agbô River (Ivory-Coast)", *Catalysis today*, vol. 281, pp. 2–13, 2017.

[8] O. P. Sahu and P. K. Chaudhari, “Review on chemical treatment of Industrial waste water review on chemical treatment”, *Journal of applied sciences and environmental management*, vol.17, pp. 241-257.2013.

[9] A. Matilainen, "Removal of the natural organic matter in the different stages of the drinking water treatment process", PhD dissertation, Tampere University of Technology, Tampere, 2007.

[10] C. Costa, S. Maia, P. Silva, J. Garrido, F. Borges, and E. M. Garrido, “Photostabilization of phenoxyacetic acid herbicides MCPA and mecoprop by hydroxypropyl-β-cyclodextrin”, *International journal of photoenergy*, vol. 2013, 2013.

[11] O. Autin, J. Hart, P. Jarvis, J. MacAdam, S. A. Parsons, and B. Jefferson, “Comparison of UV/H_2O_2 and UV/TiO_2 for the degradation of metaldehyde: Kinetics and the impact of background organics”, *Water research*, vol. 46, pp. 5655–5662, 2012.

[12] A. L. Linsebigler, G. Lu, and J. T Yates Jr, “Photocatalysis on TiO_2 surfaces: principles, mechanisms, and selected results”, *Chemical reviews*, vol. 95, pp. 735–758, 1995.

[13] O. Autin, “Micropollutant removal by advanced oxidation process”, PhD dissertation, Cranfield water science institute, School of applied sciences, Cranfield University, UK, 2012.

[14] A. F. Iglesias A. Lopez R. Gondar D. Antelo J. Fiol “Effect of pH and ionic strength on the binding of paraquat and MCPA by soil fulvic and humic acids”, *Chemosphere*, vol. 76, pp. 107–113, 2009.

[15] M. Zhou and L. Lei, “An improved UV / Fe^{3+} process by combination with electrocatalysis for p -nitrophenol degradation”, vol. 63, pp. 1032–1040, 2006.

[16] B. C. Faust, J. Hoigne´, “Photolysis of Fe(III)-hydroxy complexes as sources of OH radicals in clouds, fog and rain”, *Atmospheric environment,* vol. 24, pp. 79–89, 1990.

[18] F. Sohrabi, S., Akhlaghian, "Surface investigation and catalytic activity of iron-modified TiO_2", *Journal of nanostructure chemicals*, vol. 6, pp. 93–102., 2016.

[19] D. Andreozzi, R. Di Somma, I. Marotta, R. Pinto, G. Pollio, A. and Spasiano, "Oxidation of 2, 4-dichlorophenol and 3, 4-dichlorophenol by means of Fe (III)-homogeneous photocatalysis and algal toxicity assessment of the treated solutions", *Water research*, vol. 45, pp. 2038–2048, 2011.

[20] J. R. Li, Q. Guo, B. Yu, J. Ran, J. Zhang, B. Yan, H. and Gong, "Highly efficient visible-light-driven photocatalytic hydrogen production of CdS-cluster-decorated graphene nanosheets", *Journal of the american chemical society*, vol. 133, pp. 10878–10884, 2011.

[21] G. Pan, M. Ding, J. Duan, L. and Gao, "Sunlight-driven photo-transformation of bisphenol A by Fe (III) in aqueous solution: Photochemical activity and mechanistic aspects", *Chemosphere*, vol. 167, pp. 353–359, 2017.

CHAPTER 5:
THE REMOVAL OF HUMIC ACID BY A PHOTOCATALYSIS-COAGULATION HYBRID METHOD UNDER VISIBLE LIGHT IRRADIATION

5.1 Introduction

The removal of humic acid from drinking water is crucial in water treatment as it improves the aesthetic merits of water and ensures that the water distributed to communities is safe for consumption. The work presented in this chapter covers the second part of the study which was conducted in South Africa. Specifically, results reported herein were obtained from the investigation of the removal of humic acid by a photocatalysis hybrid treatment method under visible light irradiation NS-TiO_2 and ferric chloride were used as photocatalyst and coagulant, respectively. The investigation concluded with an evaluation of the removal of NS-TiO_2 NPs using the coagulation method in the presence of ferric chloride. Following a detailed discussion of the results, an implication of these results towards water treatment is presented.

5.2 Materials and methods

Details on the materials and methods used are presented in **Chapter 3, Section 3. 4** of the experimental methodology.

5.3 Results and Discussion

This section presents results and a discussion pertaining to the removal of humic acid from water *via* a photocatalytic-coagulation hybrid system under visible light irradiation. Firstly, the removal of NS-TiO_2 *via* coagulation-flocculation process using ferric chloride ($FeCl_3$) was investigated, and this is discussed in **Section 5.3.1**. A detailed evaluation of the degradation of humic acid by the photocatalytic-coagulation hybrid system is presented in **Section 5.3.3.**

5.3.1 Simultaneous removal of NS-TiO_2 and HA by $FeCl_3$ coagulation

The removal of NPs such as TiO_2 from water has been mainly achieved through centrifugation, filtration and incorporation of magnetic components (magnetite and the ferrites) that permit separation of the NPs using an external magnetic field. Recently, the application of coagulation as a nanoparticle recovery tool has attracted a lot of interest because of its dual ability to also remove NOM from water. For this reason, the coagulation of NS-TiO_2 suspensions in HA aqueous solutions in the presence of $FeCl_3$ coagulant was investigated. **Figure 5. 1a** shows the water turbidity measurements, throughout the coagulation processes at different pH values (5, 6, 7), and different coagulant doses ([Fe^{3+}] = 0.0925, 0.1230, 0.1850, 0.2470 mM). It is clear from **Figure 5. 1a** that turbidity removal reached an optimum level (from 34 NTU to 4 NTU, 88.2% turbidity reduction) at pH 6 and Fe^{3+} coagulant dose of 30 mg/L. This means that $FeCl_3$ can remove 88.2% of NS-TiO_2 from water under optimized conditions. Water treatment plants target an NTU measurement of <1 NTU (SANS: 241 regulations) for final water that is distributed to communities. For this reason, the process of NS-TiO_2 removal *via* coagulation can be optimised further to obtain an NTU measurement <1 NTU. Furthermore, at pH 5 and coagulant dose of 15 mg/L, the lowest turbidity removal was obtained, decreasing from 34 NTU to 19 NTU (44.1% reduction). Zeta potential was measured (**Figure 5. 1b**) to determine the degree of neutralisation of HA and NS-TiO_2 by Fe^{3+} ions. Significantly, the zeta potential approached 0 mV (neutralisation) at a coagulant dose of 30 mg/L and pH 5; this result is consistent with the maximum turbidity removal. The pH of the solution has a direct impact on the hydrolysis of ferric salt coagulants [1, 2, 3, 4]. Since Fe^{3+} ions can only hydrolyse into the hydroxide form at near alkaline pH values, the removal of NS-TiO_2 nanoparticles using $FeCl_3$ is strongly influenced by pH when coagulated with $FeCl_3$, thereby removing NS-TiO_2 nanoparticles through adsorption bridging and enmeshment effect. Finally, UV_{254} was measured to monitor the coagulation and by extension the removal of HA in the presence of NS-TiO_2. **Figure 5. 1c** shows the removal of humic acid by coagulation in the presence of NS-TiO_2 at different pH conditions. The highest UV_{254} removal was realised at pH 5 and coagulant dose of 30 mg/L. Although these findings coincide with the turbidity measurements in respect of coagulant dose, the same cannot be said of the pH.

For non-prehydrolysed coagulants such as alum and ferric salts, according *to* Yan *et al.,* [5] maximal NOM elimination occurs under slightly acidic conditions (pH < 6.0). In an aqueous medium and a pH range of 4.5 to 6.0, $FeCl_3$ forms metal hydroxide that is responsible for the decrease in turbidity and humic substances (HS) by attaching to anionic sites of the HS and neutralizing the charge of HS to reduce solubility [5]. The poor removal of HA at higher coagulant dose is ascribed to excess coagulant, which results in coagulant residuals in the treated water and post treatment precipitation of particles that cause turbidity and increase UV_{254} readings ($[Fe^{3+}]$ = 0.18 mM) as demonstrated in **Figure 5. 1c** [6].

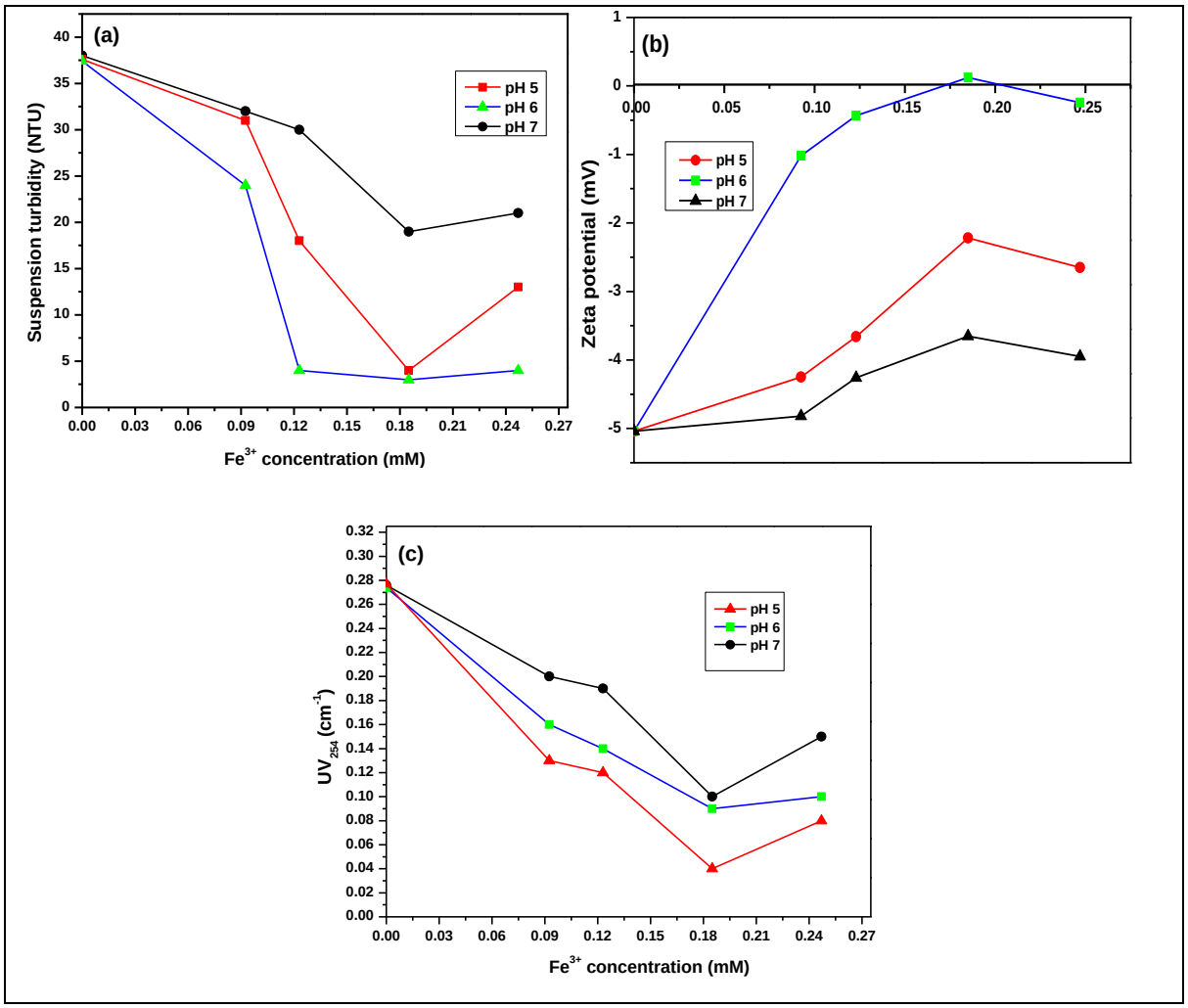

Figure 5. 1: Measurements of (a) Turbidity removal, (b) Zeta potential, and (c) UV_{254} during coagulation of 2NS-TiO_2 suspension (150 mg/L) in HA with $FeCl_3$ (pH = 5, 6, 7, $[Fe^{3+}]$ = 0.0925, 0.123, 0.185, 0.247 mM).

5.3.2 Degradation of HA by NS-TiO_2 samples

The photocatalytic performance of three previously synthesized NS-TiO_2 photocatalysts (i.e., 1NS-TiO_2, 2NS-TiO_2, and 4NS-TiO_2) was evaluated for HA degradation under visible light irradiation. The photocatalysts were obtained by varying the N and S loadings of the photocatalysts. The N and S loadings of the 1NS-TiO_2, 2NS-TiO_2, and 4NS-TiO_2 photocatalysts were in turn achieved by varying the amounts of the thiourea (1 g, 2 g and 4 g, respectively). **Figure 5. 2** provides a comparative analysis of the photocatalytic degradation of HA by the three photocatalysts (1NS-TiO_2, 2NS-TiO_2 and 4NS-TiO_2) under visible light illumination, photolysis, and dark conditions.

The photolysis experiment achieved only 10% removal of humic acid. As a photo/sensitizer and reaction substrate, humic substances may produce transient intermediates including reactive oxygen species or relatively stable free radicals when exposed to light [7]. This implies that a portion of the HA in water can be degraded into small fragments following irradiation with visible light. In the case of this study, only 10% of the HA was degraded *via* this mechanism. Furthermore, an investigation of the degradation of HA in the presence of 2NS-TiO_2 and absence of light revealed that nearly 20% HA degradation was observed after 120 minutes. The adsorption (absence of light) degradation percentage is not high (20%), however in photocatalysis, oxidation experiment occurs at the surface of the catalyst. Having the 20% adsorption is an added advantage as it improves the removal of HA. When the degradation of HA was studied under visible light irradiation in the presence of undoped TiO_2, an HA degradation efficiency of 10% was obtained within 120 minutes. This degradation is thought to proceed *via* adsorption of HA onto the TiO_2 surface and to some extent *via* HA photosensitisation. TiO_2 photocatalytic degradation is known to be limited to the UV region of the solar spectrum owing to the inherently wide band gap of the TiO_2, hence a low removal of HA was recorded for TiO_2-visible light process [8].

All the NS-TiO_2 samples show significantly improved visible light mediated HA degradation when compared with the pristine TiO_2. Among the doped TiO_2 samples, the 2NS-TiO_2 displayed the highest HA degradation efficiency at 98%. With a

degradation efficiency of 65%, the 4NS-TiO_2 was found to possess the lowest photocatalytic activity under the similar conditions (**Figure 5. 2**). Nonmetal doping is widely believed to introduce defect states localized at the impurity site, reducing the bandgap, and causing absorption in the visible portion of the spectrum. This explains the superior degradation activity of the N and S co-doped TiO_2 towards HA when compared with the undoped TiO_2. Furthermore, it has been shown that the defect states, which form below the conduction band, are good acceptors of electrons leading to an improvement of charge separation [9]. Nonmetal doping, on the other hand, promotes the creation of oxygen vacancies that may act as charge recombination centres when present in excess amounts. Therefore, these oxygen vacancies must be minimised to avoid their detrimental effect on photocatalytic reactions [10]. The number of defects grows as the amount of nonmetal dopant increases, and the photocatalytic activity diminishes as a result. This is consistent with the observed degradation kinetics where the highest HA removal was recorded at low N,S co-doping and decreased with increasing nonmetal loading. Therefore, in nonmetal doping, careful optimisation of the dopant concentration is important for attaining enhanced visible light absorption and improved photocatalytic activity [11,12].

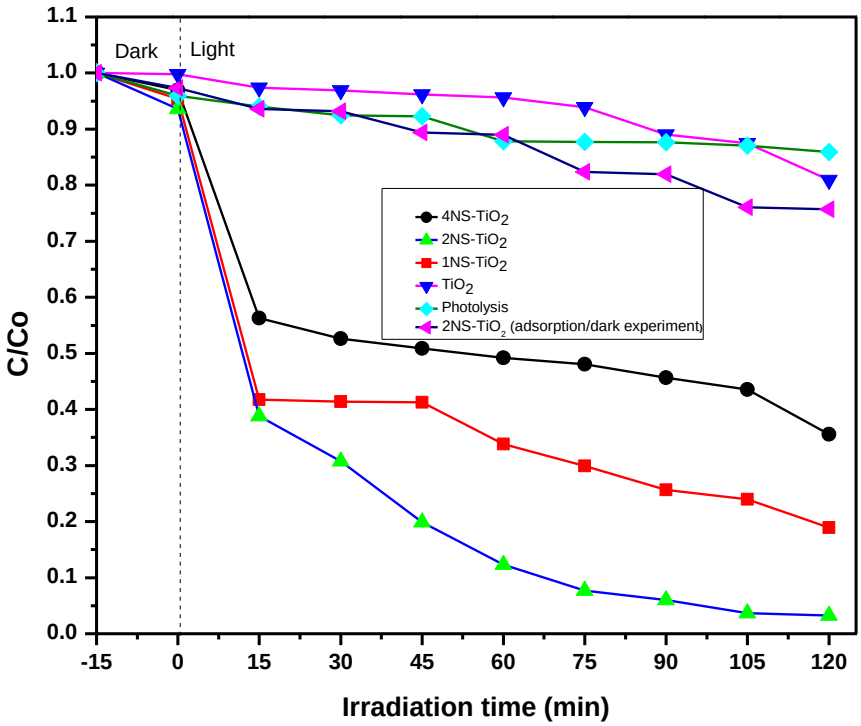

Figure 5. 2: Photocatalytic degradation of HA by NS-TiO_2 photocatalysts under visible light illumination, pH=5, photocatalyst dose = 150 mg/L.

5.3.2.1 Effect of catalyst concentration on the degradation of humic acid

To determine the optimum concentration of the photocatalyst, the effect of various concentrations (50, 100, 150, 200 mg/L) of 2NS-TiO_2 towards the photocatalytic degradation of HA under visible light was investigated (**Figure 5. 3**). Evidently, a dosage of 200 mg/L of 2NS-TiO_2 led to 100% HA degradation within 73 minutes following irradiation. In contrast, complete HA degradation was achieved within 120 minutes by 150 mg/L dosage of 2NS-TiO_2. An improvement in the removal of HA brought about by a rise in the catalyst concentration is due to a rise in the number of 2NS-TiO_2 particles. An increase in the number of 2NS-TiO_2 particles increases the susceptibility to photon absorption and adsorption of pollutants [12]. The 150 mg/L catalysts dosage was adopted for use in the next phase of the study because it allows for a decent HA degradation efficiency to be obtained at what is deemed as a fairly low dosage. Also, the low dosage may prove to be important in lowering the operational costs in terms of photocatalyst preparation and recovery *via* the coagulation process.

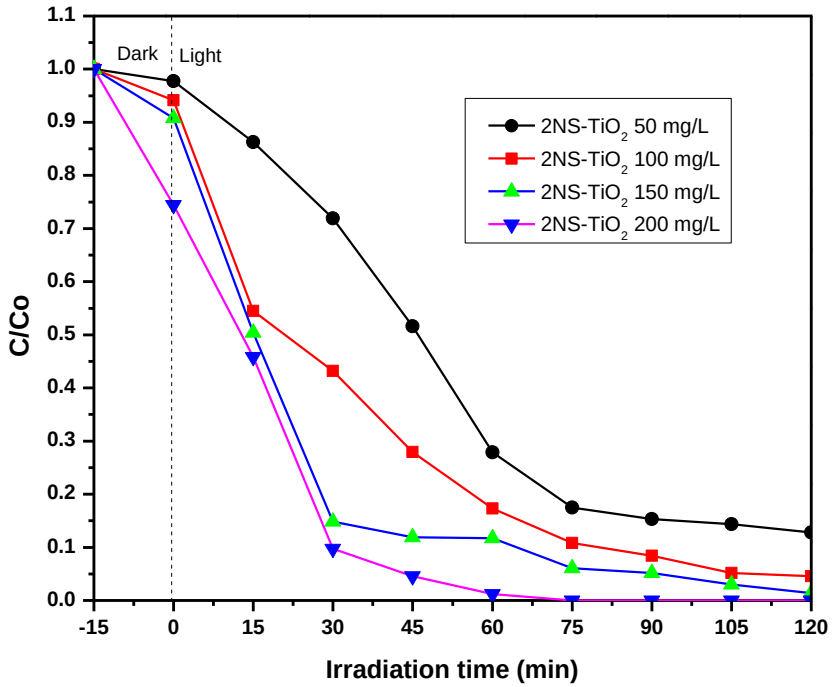

Figure 5. 3: Effect of the concentration of 2NS-TiO_2 on the degradation of an aqueous solution of HA (10 mg/L) under visible light irradiation ([2NS-TiO_2] = 50, 100, 150, 200 mg/L), pH = 5).

5.3.2.2 Effect of pH on the HA photocatalytic degradation

An investigation of the influence of pH (5, 6 and 7) on the activity of 150 mg/L of 2NS-TiO_2 towards the photocatalytic degradation of HA under visible light irradiation was conducted and the results are presented in **Figure 5. 4**. The highest degradation efficiency was realised at pH 5, with complete degradation being achieved after 120 minutes of irradiation. Under alkaline conditions, the carboxyl groups of the humic acid are ionised, leading to negatively charged humic acid molecules. Consequently, electrostatic repulsions between the HA and the negatively charged TiO_2 become predominant and thus discourage the interaction between the two species that is necessary for the degradation process to take place. By lowering the pH, the phenolic and carboxyl groups of the HA are able to interact less with each other, which allows them to adhere to the titanium dioxide more readily. A major problem arises from aggregation in that it lowers mass transport rates and reduces surface area available for adsorption of light [7].

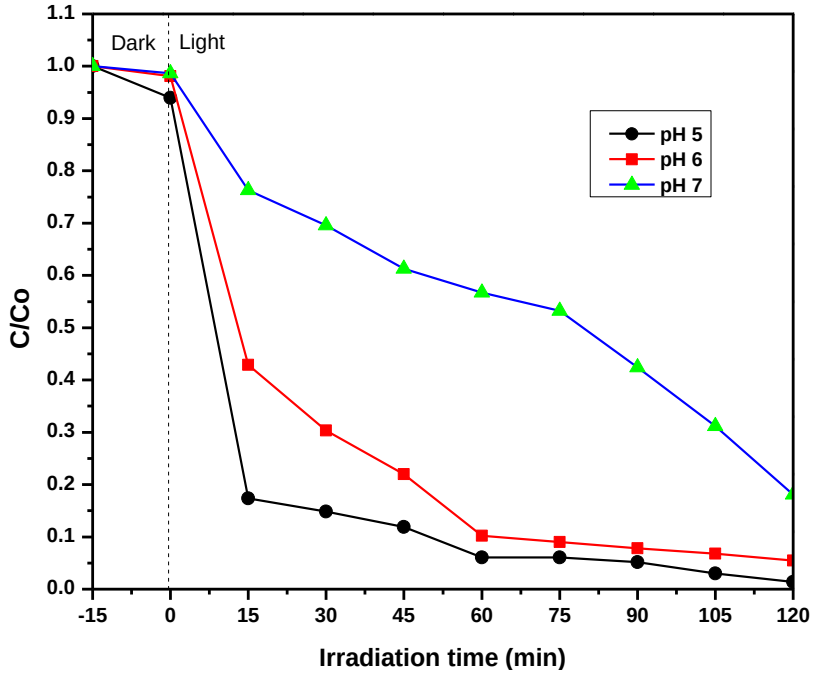

Figure 5. 4: Influence of pH (pH = 5, 6, 7) on the photocatalytic degradation of HA over 2NS-TiO_2 (150 mg/L).

5.3.2.3 Effect of HA initial concentration

Humic acid solutions of different initial concentrations (5, 10, 20 mg/L) were used to evaluate the degradation efficiency of 2NS-TiO_2 at a catalyst concentration of 150 mg/L and pH of 5. **Figure 5. 5** shows that, at HA initial concentrations of 5 and 10 mg/L, the degradation profiles are almost similar, with only a slightly higher degradation rate being observed at 5 mg/L. However, when the concentration was increased to 20 mg/L, the degradation rate decreased. Increases in pollutant concentrations result in a shorter path length for photons entering the pollutant (low penetration of photons through solution). In addition, a significant portion of visible light may be absorbed by pollutant molecules as opposed to the catalyst, resulting in a reduction in catalyst efficiency at high concentrations of pollutants [13]. For further investigations, a 10 mg/L HA solution was evaluated as this concentration is an average of NOM in many natural water samples.

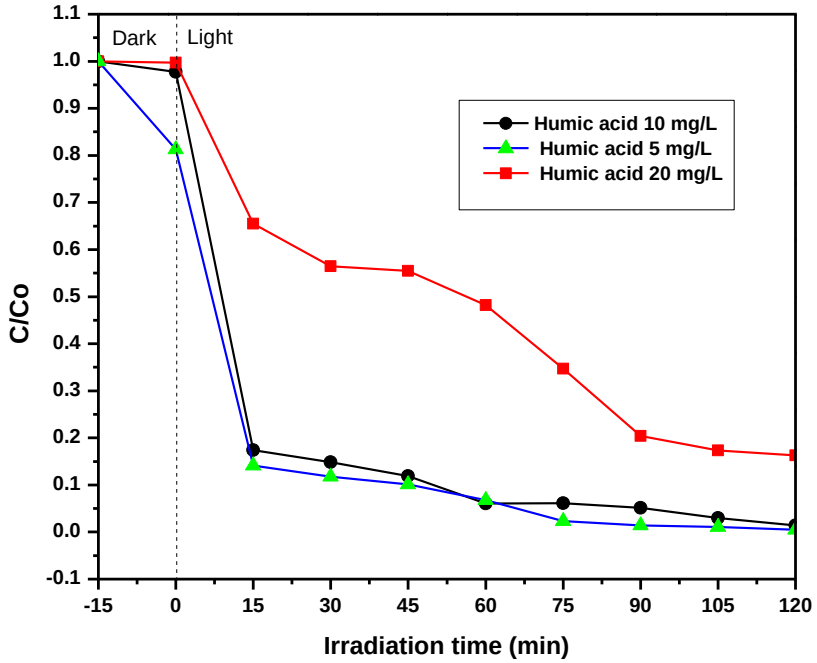

Figure 5. 5: Degradation of different concentrations of humic acid (5, 10 20 mg/L) in water by photocatalysis using 2NS-TiO_2 under visible light irradiation ([2NS-TiO_2 = 150 mg/L, pH 5).

5.3.3 Degradation of humic acid from water by a photocatalysis-coagulation hybrid system

A photocatalysis-coagulation hybrid system was evaluated for the removal of HA under optimized conditions (i.e., pH 5, [2NS-TiO_2] = 150 mg/L, [$FeCl_3$] = 30 mg/L) and the results are presented in **Figure 5. 7**. The individual coagulation and photocatalysis processes were conducted for 45 and 120 minutes, respectively. Since the coagulation process was the limiting process, the photocatalysis-coagulation hybrid system was adjusted to run for 45 minutes. The removal of HA using a photocatalysis-coagulation hybrid system (Photo-Coag, photocatalysis and coagulation occurring simultaneously) was investigated at three pH conditions (pH = 5, 6, and 7) (**Figure 5. 7a**). The Photo-Coag conducted at pH 6 under optimized conditions ([2NS-TiO_2] = 150 mg/L, [$FeCl_3$]= 30 mg/L) showed the highest HA removal of 98% and a rate constant of 0.0143 min^{-1} (**Table 5.2**) was achieved within 45 minutes. The removal efficiency of HA at pH 5 was slightly lower than that occurring at pH 6 under the similar experimental conditions.

Furthermore, an experiment was conducted where photocatalysis and coagulation processes were performed sequentially (Photo+Coag). In terms of the removal of HA, the photocatalysis-coagulation hybrid system (Photo-Coag; run for 48 minutes) performed better than the photocatalysis-coagulation sequential process (Photo+Coag; 120 minutes photocatalysis plus 45 minutes coagulation). The superior performance of the hybrid system is ascribed to the coagulant not reacting efficiently with the degradation products of HA resulting from the photocatalysis process. Furthermore, as seen in **Figure 5. 7b**, coagulation alone performed better than the photocatalysis-coagulation sequential system. From this observation, it can be concluded that coagulation is not as effective when performed after photocatalysis compared with when it is performed alone or in combination with photocatalysis. The results of a previous study have revealed that the conventional coagulation method is usually effective in eliminating high molecular weight organic compounds, but less so in removing smaller molecular weight fractions [14]. The removal of HA by coagulation following photocatalytic degradation into smaller low molecular weight fragments seems to corroborate the results [14].

A similar removal rate was observed for the removal of HA by photocatalysis and the sequential photocatalysis-coagulation process. However, a slight improvement in the removal of HA by the sequential photocatalysis-coagulation process was observed following the addition of the coagulation step to the photocatalysis step. Overall, the photocatalysis-coagulation hybrid system (Photo-Coag) performs better than the coagulation, photocatalysis and the photocatalysis-coagulation sequential process (Photo+Coag). The application of the photocatalysis-coagulation hybrid system (Photo+Coag) in the removal of HA has an advantage over the other processes (coagulation, photocatalysis, photocatalysis-coagulation sequential process) because the hybrid system works synergistically to degrade the HA.

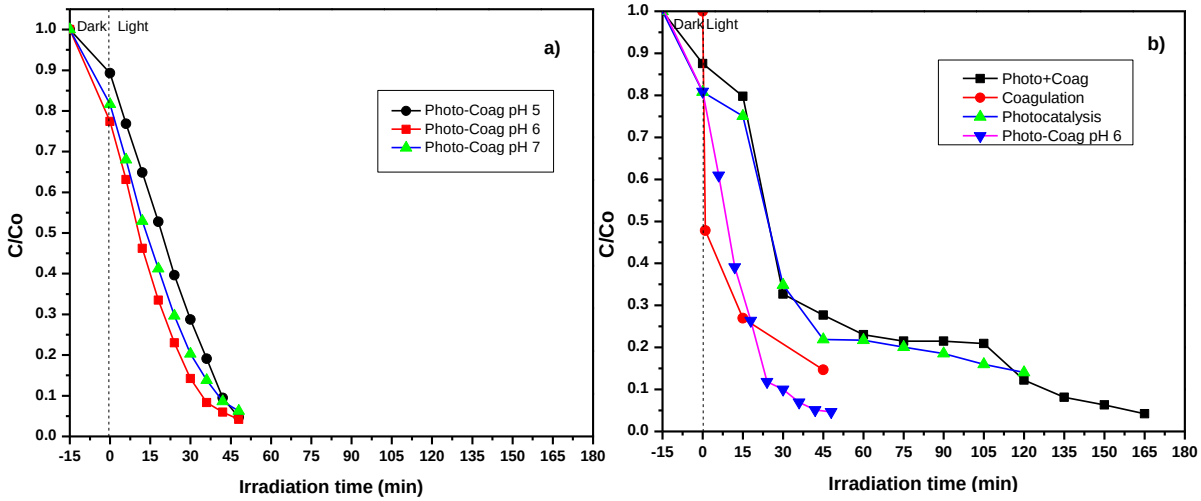

Figure 5. 6: Removal of humic acid (10 mg/L) using the: a) Photocatalysis-coagulation hybrid system (Photo-Coag), using 2NS-TiO_2 ([2NS-TiO_2] = 150 mg/L, pH 5, 6 and 7), b) Photocatalysis-coagulation hybrid system (Photo+Coag, Photo-Coag), and individual processes (coagulation (pH 6 and photocatalysis (pH 5)), 2NS-TiO_2 ([2NS-TiO_2] = 150 mg/L).

Table 5. 1: Degradation kinetics data for the removal of HA by the different processes

PROCESS	K_1 (MIN^{-1})	R^2
Photo-Coagulation at pH 6	0.0143	0.8316
Photo+Coagulation	0.0066	0.9486
Photocatalysis	0.0044	0.8458
Coagulation	0.0074	0.9677

5.3.4 Fluorescence emission excitation matrices, TOC and turbidity measurements

The principle of FEEM is the capability of a molecule to absorb light at a certain wavelength and to emit light of another wavelength depending on the specific molecular bonds. This method is particularly important because of its ability to detect changes in properties of the species of interest. In this case, FEEM was utilised to detect the changes in properties of humic acid through treatment with the proposed photocatalytic-coagulation hybrid process. However, for further extract of information and, in particular, changes in NOM composition between several samples, multivariate analysis techniques can be employed. Multivariate analysis methods such as PCA are able to reduce dimensionality of data sets by modelling variance between samples. **Figure 5. 8** displays the fluorescence emission spectra for the removal of HA over a period of 120 minutes of irradiation with visible light under the optimised conditions ([2NS-TiO_2] = 150 mg/L, pH = 5, [HA] = 10 mg/L) by the combined photocatalysis-coagulation system (Photo-Coag). Humic substances typically express fluorescence in the excitation wavelength range of 300–400 nm and the emission wavelength range of 400–500 nm. Moreover, humic like fluorescence show excitation between 220 and 250 nm

and emission between 400 and 460 nm [15]. The fluorescence emission excitation matrices (FEEM) spectra (**Figure 5. 8**) show contours at an excitation between 300 and 400 nm and an emission wavelength between 400 to 500 nm, which suggests the presence of humic like substances in the water. As treatment of the HA proceeds, the contours decrease significantly in size following 15 minutes of coagulation in the presence of 2NS-TiO_2 and absence of light. At this point, the reduction or florescence enhancement is ascribed to the removal of HA by coagulation and adsorption of HA onto the catalyst. Beyond the dark/adsorption phase of the experiment, contours continue to decrease further with some disappearing as the treatment proceeds. The FEEM spectra of HA following 120 minutes of irradiation show no contours. During the photocatalysis-coagulation hybrid process, the degradation of HA into smaller organic components is inevitable mainly as a result of treatment by photocatalysis. Since fluorescence enhancement is associated with a decrease in molecular weight [15], it can be concluded that a decrease in the fluorescence takes place as the photocatalysis successfully breaks down the chromophoric groups within the structure of HA.

The TOC measurements (**Figure 5. 9**) revealed that the photocatalysis-coagulation hybrid process showed the highest TOC removal (94%) compared to the other processes. TOC removals during coagulation (65%), Photocatalysis (55%), photocatalysis-coagulation sequential process (80%) were found to be lower than that of the photocatalysis-coagulation hybrid process. A measure of TOC represents the total carbon concentration of a sample, this includes carbon concentration in HA and its degradation products. Since FEEM only gives a representation of the presence HA and not concentration, a comparative analysis of the two sets of results (TOC and FEEM) is not possible.

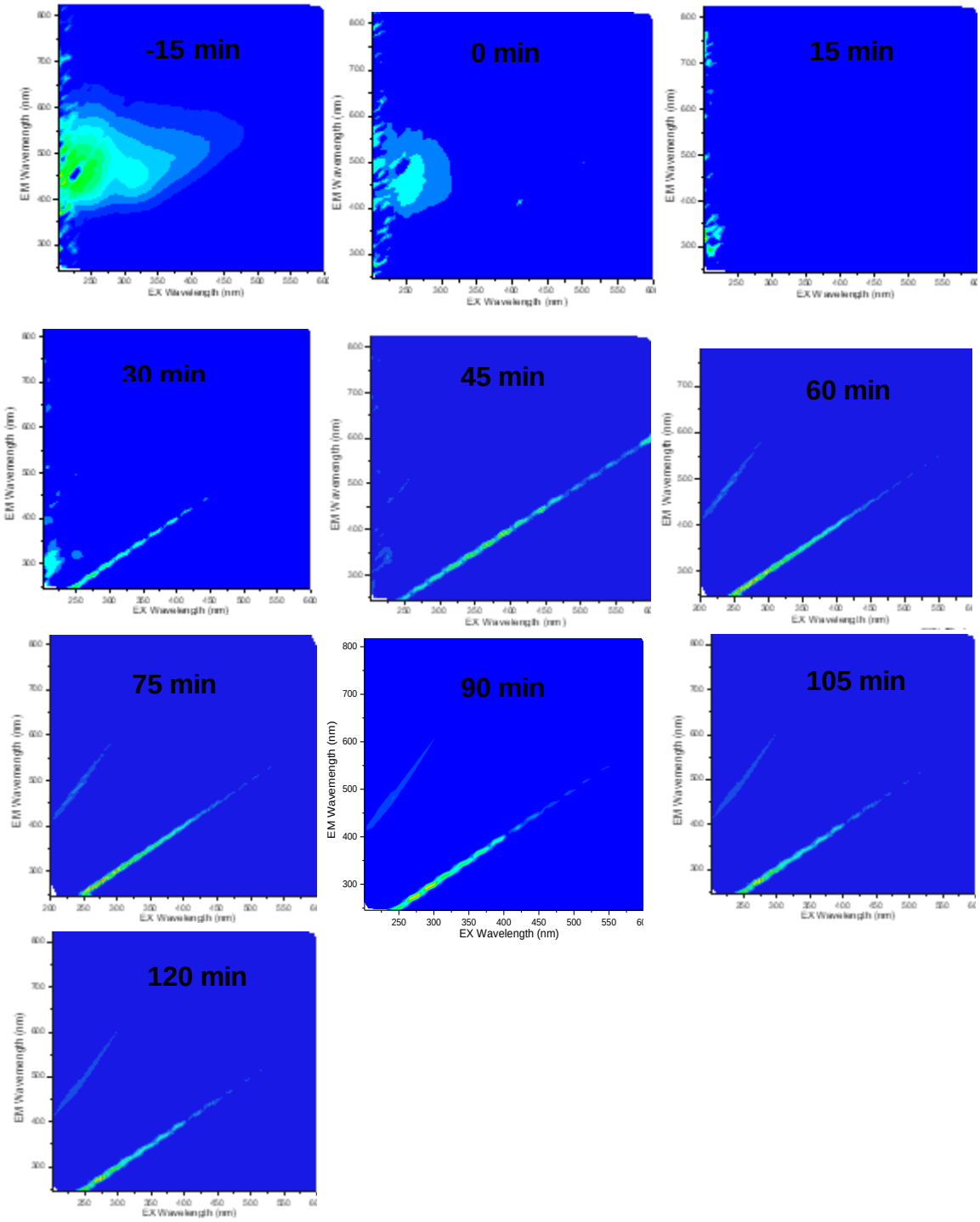

Figure 5. 7: FEEM spectra for the removal of humic acid (10 mg/L) using the photocatalysis-coagulation hybrid system with 2NSTiO$_2$ (catalyst concentration: 150 mg/L, pH 5, [FeCl$_3$] = 30 mg/L).

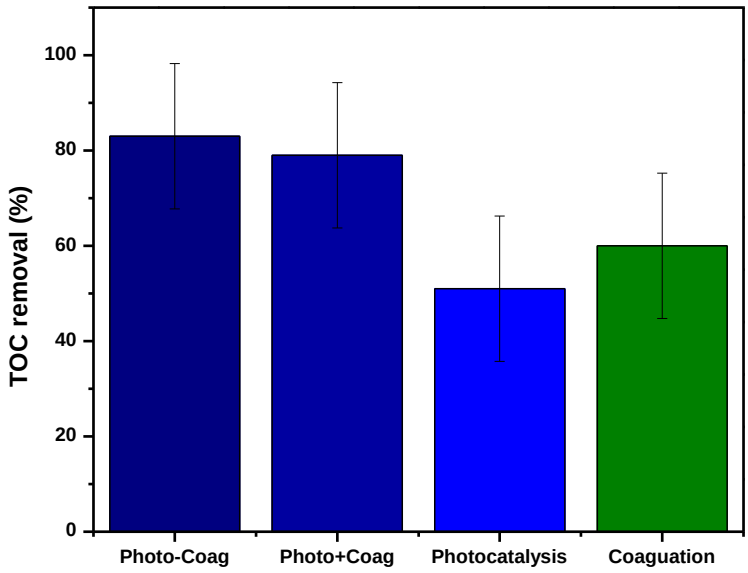

Figure 5. 8: TOC removal of HA following treatment with the photocatalysis-coagulation process ([2NS-TiO_2]= 150 mg/L, pH 5, [$FeCl_3$] = 30 mg/L)**.**

The changes in solution turbidity were measured to monitor the simultaneous removal of 2NS-TiO_2 and HA along with its degradation by-products during the photocatalytic-coagulation hybrid treatment **Figure 5. 9** depicts the changes in turbidity during HA removal by the hybrid process (Photo-Coag) and the photocatalysis-coagulation sequential process (Photo+Coag). Turbidity removal by the Photo-Coag is higher (58 NTU to almost 0 NTU) within 45 minutes of treatment, with the same removal seen Photo+Coag system after 120 minutes of treatment. It is evident from a comparative analysis of results displayed in **Figure 5. 9** with those displayed in **Figure 5. 1a** that coagulation achieved a turbidity removal (30 NTU) that is lower that of the two hybrid systems (Photo-Coag and Photo+Coag (~58 NTU). It is therefore evident that the photocatalysis component of the two hybrid systems (Photo-Coag and Photo+Coag) increases the removal of HA thus leading to greater turbidity removal in the two hybrid systems when compared with coagulation alone . Whereas coagulation is responsible for the removal of the 2NS-TiO_2 and HA, photocatalysis is mainly responsible for the removal of HA. An enhanced removal of HA in the photocatalysis-coagulation hybrid system is due to the synergistic effect of photocatalysis and coagulation in the removal of the pollutant.

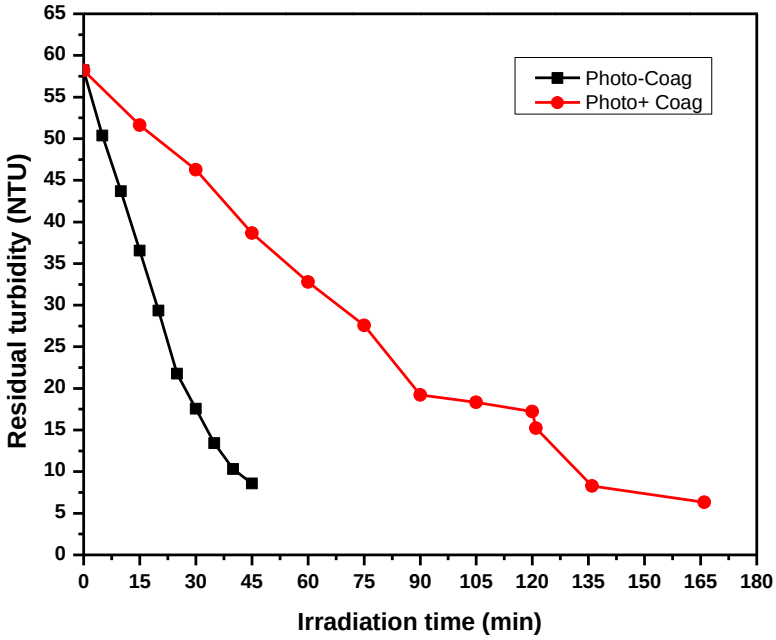

Figure 5. 9: Turbidity removal following treatment with photocatalysis combined with coagulation (Photo-Coag at pH 6, Photo+Coag for 120 minutes), [2NS-TiO_2] = 150 mg/L.

5.3.3.1 HA removal mechanism using the hybrid process

Typically, the hybrid process combines both photocatalysis and coagulation in a single step and the duration of the process is dependent on the coagulation component of the hybrid system. The coagulation component of the photocatalysis-coagulation hybrid system is responsible for removing the HA and its degradation by-products *via* charge neutralisation process (**Figure 5. 10**). The simultaneous removal of the NS-TiO_2 nanoparticles is also achieved through coagulation [15]. This mechanism aids with the adsorption of the pollutant (HA) onto the surface of the catalyst (TiO_2). Moreover, NOM could form complexes with TiO_2 NPs *via* steric and weak van der Waals forces, electrostatic attraction, and repulsive forces [16]. In addition to coagulation, the hybrid process facilitates HA degradation by photocatalysis as depicted in **Figure 5. 10.** The subsequent formation of hydroxyl radicals lead to the degradation of HA. **Eq. 5.1** to **5.5** illustrates the formation of the hydroxyl radicals following irradiation of NS-TiO_2 with visible light. The separation of two types of carriers occurs when the surface of the NS-TiO_2 is illuminated, namely (a) an electron (e^-) and (b) a hole (h^+) (**Eq. 5.1**). An oxidation process with water

produces a hydroxyl radical due to the hole's considerable oxidation strength (**Eq. 5.2**). The hydroxyl radicals produced in **Eq. 5.2** and **5.3** attack and degrade HA into smaller organic components or mineralize it into CO_2 and H_2O (**Eq. 5.4**). Additionally, a donor molecule (HA) adsorbed on TiO_2 can be oxidized by the photoinduced hole (**Eq. 5.5**). Furthermore, oxygen can behave as an electron acceptor and be reduced to a superoxide ion ($O_2^{\bullet -}$) by the promoted electron in the conduction band. Superoxide radicals also have oxidising power and their formation is depicted in **Eq. 5.6** [17].

$$NS\text{-}TiO_2 + \text{visible light} \rightarrow e_{cb}^- + h_{vb}^+ \quad [5.1]$$

$$h_{vb}^+ + H_2O \rightarrow H^+ + {}^{\bullet}OH \quad [5.2]$$

$$h_{vb}^+ + {}^-OH \rightarrow {}^{\bullet}OH \quad [5.3]$$

$$HA + {}^{\bullet}OH \rightarrow \text{degradation products} \quad [5.4]$$

$$HA + h_{vb}^+ \rightarrow \text{degradation products} \quad [5.5]$$

$$e_{cb} + O_2 \rightarrow O_2^{\bullet -} \quad [5.6]$$

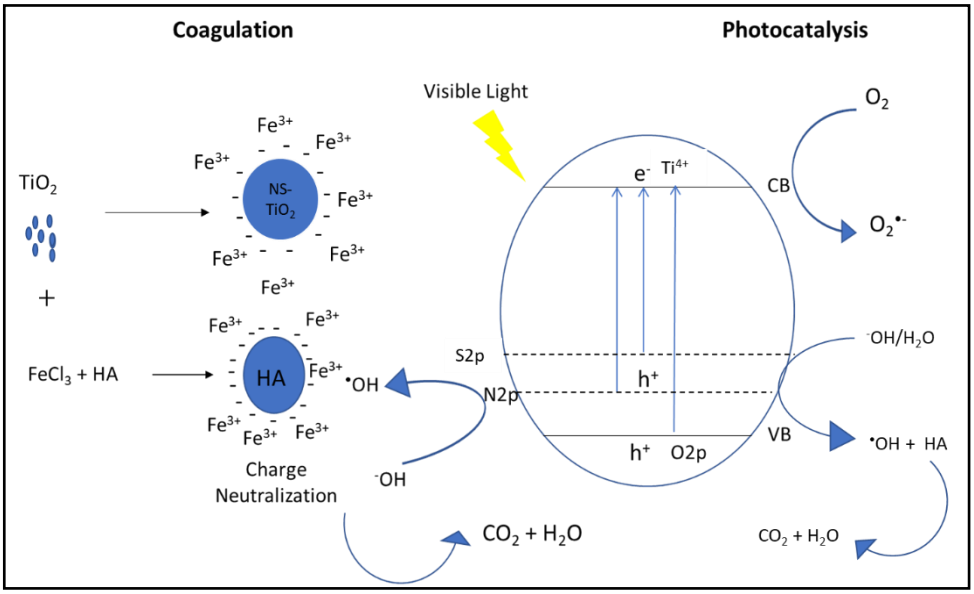

Figure 5. 10: Mechanism for the removal of HA by a photocatalysis-coagulation hybrid system.

The two processes work synergistically to improve the removal of HA in water, and this is evident in the degradation profiles of the photocatalysis-coagulation hybrid system compared to the individual processes (photocatalysis and coagulation). Comparatively, coagulation treatment allows for the simultaneous removal of NS-TiO2 and HA along with its degradation by-products. Alternatively, the photocatalytic process removes the pollutant through oxidation. The synergy of Photo+Coag process is observed with both photocatalysis and coagulation processes working collectively to remove HA from water, and this has proved to offer good removal of both NS-TiO2 and HA through charge neutralization and the oxidation of HA by hydroxyl radicals.

5.3.5 Characterization of NS-TiO2

To gain a good understanding of their physiochemical and morphological properties, the synthesized photocatalysts were characterized using the following techniques: Fourier Transform Infrared (FTIR), Ultraviolet-Visible Diffuse Reflectance Spectroscopy (UV-Vis-DRS), X-Ray Diffraction (XRD), Brunauer-Emmitt-Teller (BET), High Resolution Transmission Electron Microscopy (HRTEM), and Field Emission Scanning Electron Microscopy (FE-SEM).

5.3.5.1 Optical properties of NS-TiO_2

UV-Vis DRS was employed to evaluate the effect of co-doping TiO_2 with varying amounts of the non-metals, nitrogen and sulphur on the photo-response of the resultant doped TiO_2 material. **Figure 5. 11a** depicts the UV-Vis optical response of nitrogen and sulphur co-doped TiO_2 samples and pristine TiO_2. Pristine TiO_2 shows absorption limited to the UV region (< 400 nm). However, co-doping TiO_2 with N and S dramatically enhanced its photo-response in the visible region of the solar spectrum. This is evident in **Figure 5. 11a** where the adsorption edge increases from 395 nm for the undoped TiO_2 to 415, 548, and 580 nm for the TiO_2 doped with N and S by adding 1 g, 2 g and 4 g of thiourea (denoted as 1NS-TiO_2, 2NS-TiO_2 and 4NS-TiO_2), respectively. This shows that the synthesized NS-TiO_2 possessing different N and S loadings exhibited good visible light response compared to the undoped TiO_2. Moreover, an increase in the NS loading into the TiO_2 lattice leads to an increase of the adsorption edge to higher wavelengths. Interestingly, 1NS-TiO_2 shows two absorption edges, namely one at 395 nm corresponding to the typical valence band to conduction band transition and the second edge at longer wavelength (575 nm) emanating from transitions involving the mid-band gap states introduced by co-doping [18].

The band gap values of the synthesized photocatalysts were estimated using the Tauc model as expressed in **Eq. 5.6**

$$\alpha h\nu = B(h\nu - E_g)^{n/2} \qquad [5.6]$$

where h is the Planck's constant, v the vibration frequency, α the absorption coefficient, Eg the forbidden gap energy (eV) of the semiconductor and n can take the values 1/2, 2,3/2, and 3 for indirect allowed ,direct allowed, indirect forbidden transitions ,and direct forbidden respectively [19,20].

Figure 5. 11b shows the Tauc plots for the doped and pristine TiO_2 samples. As shown in **Figure 5. 11b**, the pristine TiO_2 has a significant decrease in the TiO_2 band gap from 3.20 to 3.18, 2.55 and 2.41 eV for 1NS-TiO_2, 2NS-TiO_2 and 4NS-TiO_2, respectively. The introduction of nitrogen into the crystalline lattice of the TiO_2 in the form N-Ti-O or O-N-Ti linkages has been linked to band gap modification

[21]. In the instance of S-doping, sulphur may be introduced as a cation (S^{6+}) that substitutes Ti^{4+} ions in the TiO_2 lattice, reducing the energy gap and the energy required for electronic transitions, and finally resulting in visible light absorption [22]. Various experimental and theoretical studies have demonstrated that adsorption of light in TiO_2 is shifted to higher wavelengths with the addition of heteroatoms (such as sulphur and nitrogen) due to a reduction of the energy gap between the highest occupied and lowest unoccupied bands. Accordingly, the observed red-shift in the optical adsorption of NS-TiO_2 samples occurs owing to the overlap of the 2p and 3p orbitals of N and S, respectively, with the valence band (VB) of TiO_2. This overlap results in the formation of additional energy levels just above VB, which ultimately results in improved visible light absorption [23].

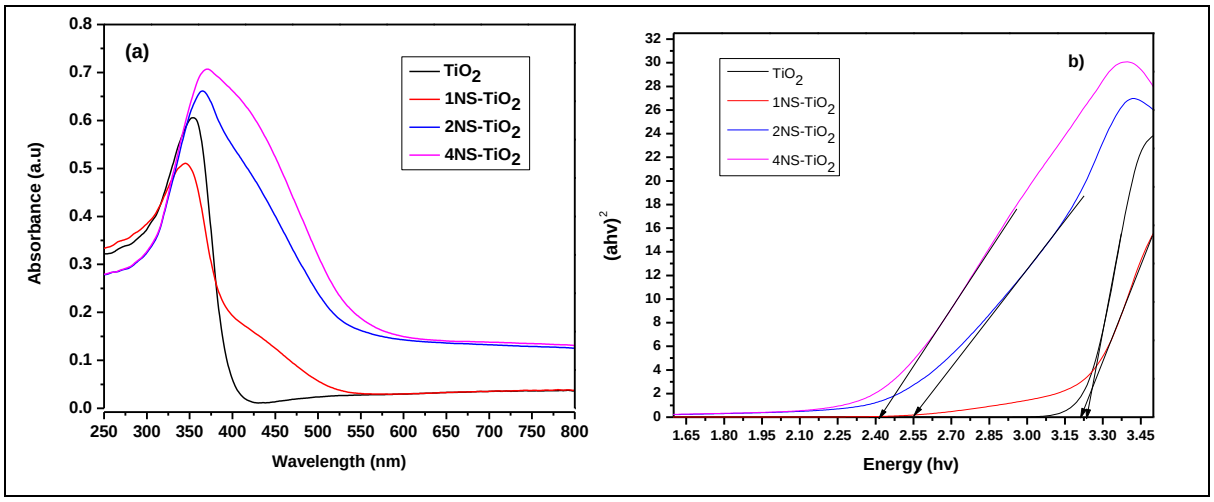

Figure 5. 11: a) UV-Vis DRS spectra for undoped TiO_2 and NS-TiO_2 with varying N, S loadings b) Corresponding Tauc plot for NS-TiO_2 photocatalysts and undoped TiO_2.

5.3.5.2 ATR-FTIR analysis of NS-TiO_2

The functional groups found in photocatalysts that have been synthesized were determined by FT-IR and the spectra are shown in **Figure 5. 12**. As moisture is absorbed from the air onto both the doped and undoped TiO_2, the peak observed at 3468 cm^{-1} and 1630 cm^{-1} is caused by both stretching and bending of the OH bonds in adsorbed water molecules. Furthermore, the Ti-O, O-Ti-O stretching vibrations are responsible for a large peak that appears between 600 and 800 cm^{-1}.Peaks at around 2348 cm^{-1} have been seen in co-doped TiO_2, which may

be linked to the NH stretching vibration, implying that nitrogenous species have been incorporated into photocatalysts [16]. These peaks appear at 1134, 1047, and 1202 cm^{-1} as a consequence of the presence of sulphur species. The presence of bidentate SO_4^{2-} coordinated to Ti^{4+} is associated to these peaks [24].

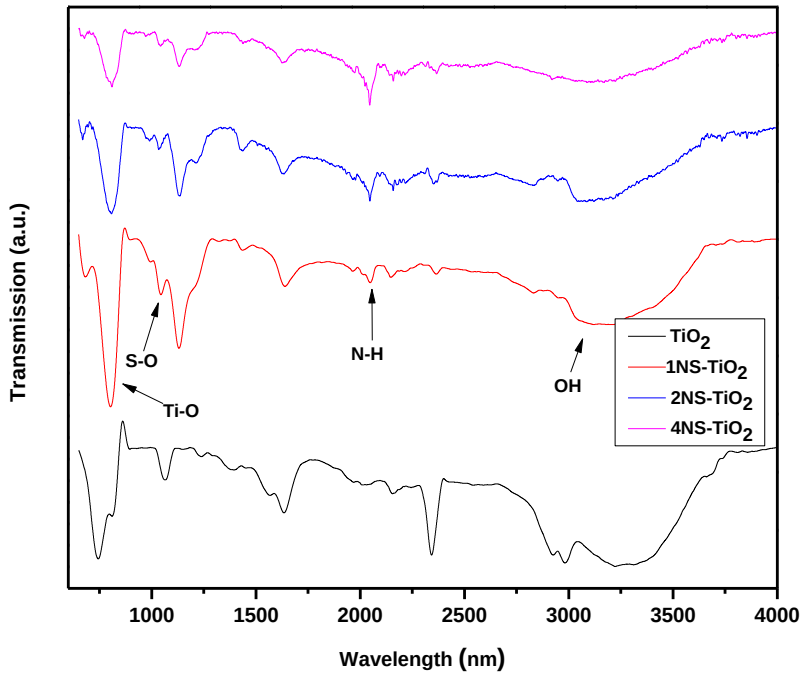

Figure 5. 12: The ATR-FTIR spectra of TiO_2 and NS-TiO_2 nanostructures.

5.3.5.3 X-ray Diffraction

The crystallinity of the synthesized photocatalysts was determined by X-ray diffraction spectroscopy. The X-ray diffraction spectrum depicted in **Figure 5. 13** confirms the mixed phases (rutile and anatase) of both the doped and undoped TiO_2. Peaks observed at 2θ 25.4°, 37.8°, 48.2°, 54.7°, and 63.1° are characteristic of the anatase phase of titania. These peaks emanate from the (101), (004), (200), (211), and (204) crystal planes (JCPDS No 21-1272). In addition, a rutile peak appears at 2θ 43.3°, which correspond to (220) crystal plane (JCPDS No 21-1276). There is no observable difference between the doped and undoped samples resulting from the incorporation of the N and S. This could be ascribed to the low dopant concentrations introduced into the TiO_2 lattice [24].

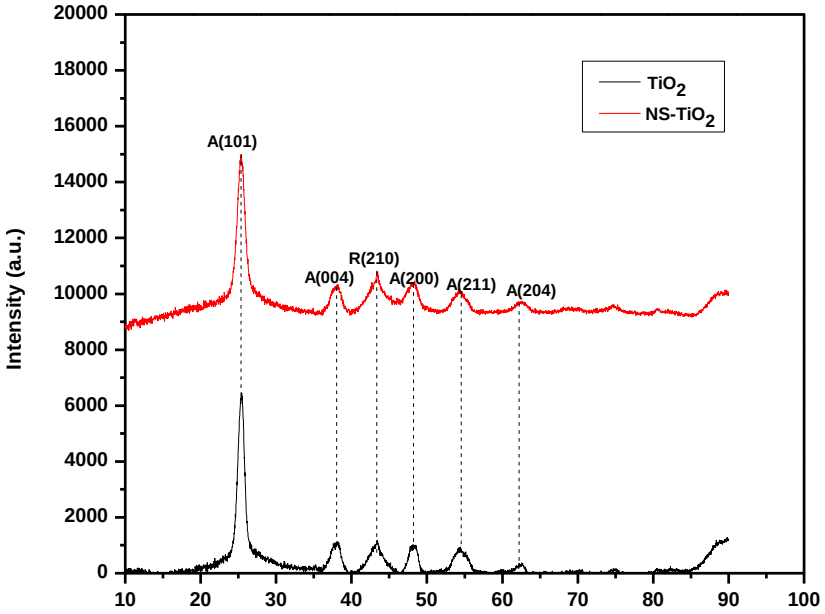

Figure 5. 13: XRD spectra of TiO_2 and 2NS-TiO_2.

5.3.5.4 BET analysis

Photocatalysis is a surface phenomenon where the oxidation reaction occurs at the surface of the photocatalyst [19]. Therefore, it is highly desirable for a photocatalyst to possess a large surface area to guarantee sufficient interaction with the pollutants. **Figure 5.14** illustrates the nitrogen adsorption/desorption isotherms of 2NS-TiO_2 and pristine TiO_2 materials. Evidently, the samples displayed a type IV isotherm, which is characteristic of mesoporous materials according to the IUPAC (International Union of Pure and Applied Chemistry) classification. The BET surface area and average pore diameter of 2NS-TiO_2, and the undoped TiO_2 photocatalyst are shown in **Table 5.3.** Notably, the BET surface area of the undoped TiO_2 (67.22 m^2/g) is smaller than that of 2NS-TiO_2 (96.78 m^2/g). The incorporation of the nitrogen and sulphur into the TiO_2 lattice improves the specific surface area of the TiO_2 and this could be due to the inhibition of particle size growth (slow nucleation and growth rate) of TiO_2 during calcination [21]. This ultimate increase in surface is desirable for improved catalytic oxidation.

Table 5. 2: Pore size, pore volume and surface area of TiO_2 and 2NS-TiO_2

CATALYST NAME	PORE SIZE (NM)	PORE VOLUME (CC/G)	SURFACE AREA (M^2/G)
TiO_2	6.522	$2.518x10^{-2}$	67.22
2NS-TiO_2	1.309	$3.626x10^{-2}$	96.78

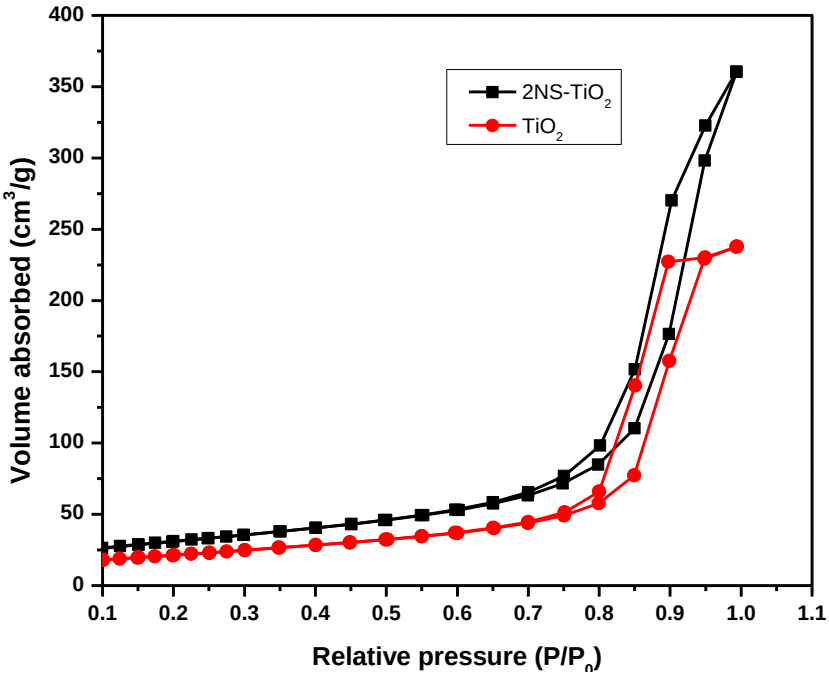

Figure 5. 14: Nitrogen adsorption-desorption isotherms for 2NS-TiO_2 and TiO_2.

5.3.5.5 Morphological studies

The morphologies of the prepared 2NS-TiO_2 and TiO_2 photocatalysts were investigated by FESEM and HRTEM. According to the TEM images of 2NS-TiO_2 and TiO_2 displayed in **Figure 5.15**, both the doped and undoped TiO_2 NPs are spherical in shape, with relatively uniform size. The presence of NPs of sizes ranging from 6 to 18 nm for 2NS-TiO_2 (**Figure 5.15a**) and 18 to 32 nm for TiO_2 NPs (**Figure 5.15b**) is evident. The lattice fringes have an average distance of 0.3589 (**Figure 5.15c**) nm and 0.3491 nm (**Figure 5.15d**) for 1NS-TiO_2 and TiO_2,

respectively. The selected area diffraction (SAED) pattern (**Figure 5.15e** and **f**) for both the doped and undoped TiO_2 indicate a polycrystalline structure. Furthermore, the SAED for 2NS-TiO_2 shows planes (101), (004), (220), (200), (211), and (204). These results are consistent with the XRD analysis (**Figure 5.13)**.

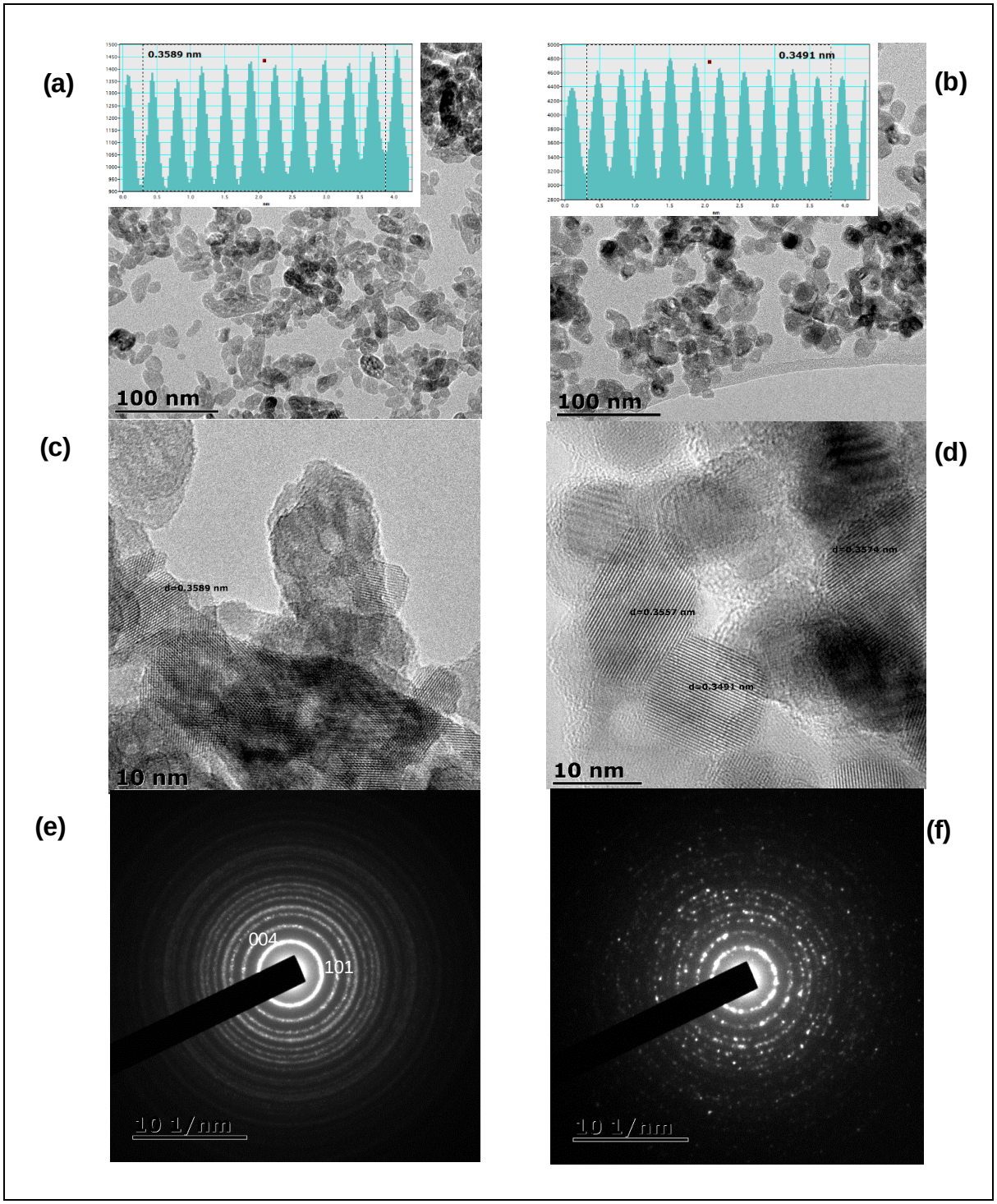

Figure 5. 15: TEM images and particle size distribution curve for (a) 2NS-TiO_2 and b) TEM images and particle distribution curve for TiO_2, HRTEM images of (c) 2NS-TiO_2 and (d) TiO_2, and SAED patterns for (e) 2NS-TiO_2 and (f) TiO_2

The SEM images depicted in **Figure 5.16 a** and **b** show similar spherical structure for both the doped and undoped TiO_2. Furthermore, the particles seem to possess

a uniform size for the doped and undoped TiO_2. The doped and undoped NPs show some level of aggregation because they appear to form lumps of larger sizes. The sizes of the doped TiO_2 NPs appear to be larger than those of the undoped TiO_2 NPs at the same magnification. This concurs with the BET surface area results (**Table 5.3**) and the TEM particle size distribution data (**Figure 5 15a** and **b**) where the presence of NPs of sizes ranging from 6 to 18 nm for 1NS-TiO_2 and 18 to 32 nm for TiO_2 describes this overlap or agreement respectively. The introduction of N and S into the TiO_2 lattice may have inhibited the growth of TiO_2 during calcination [21].

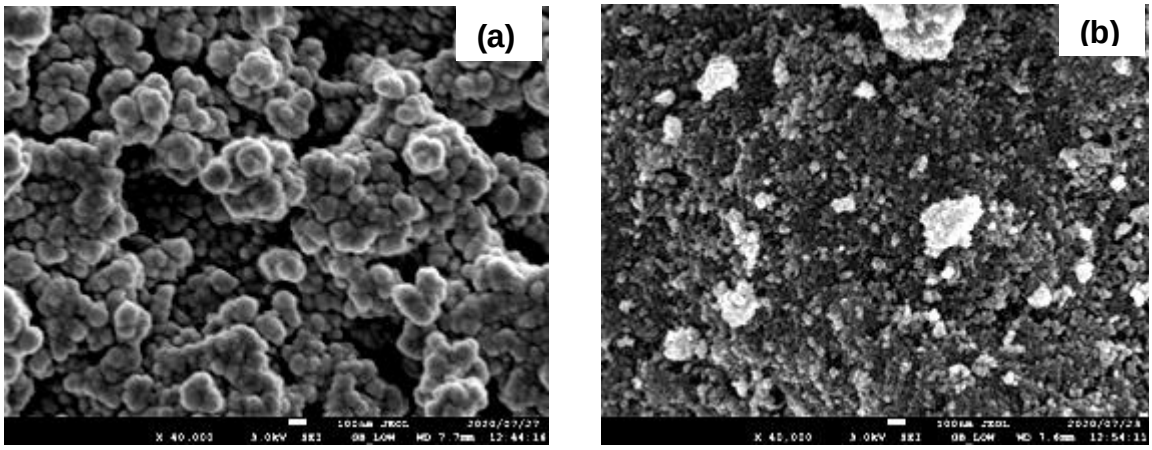

Figure 5. 16: SEM images of (a) 2NS-TiO_2 and (b) TiO_2.

Energy dispersive X-ray analysis was used to provide a qualitative elemental composition of the photocatalysts **Figure 5.17** shows the EDX spectrum of 2NS-TiO_2, which indicates the presence of the elements N, S, O, and Ti. The presence of Cu can be attributed to the copper grid used to mount the sample for analysis. Meanwhile, the emergence of sulphur and nitrogen atoms in the doped sample serves as evidence of their successful incorporation into the TiO_2 matrix. However, as shown in **Table 5.4**, the percentages of S and N are low because they contribute 1.67 wt% and 2.61 wt% of the entire photocatalyst, respectively. The EDX mapping codes show a uniform distribution of all elements throughout the photocatalyst (**Fig 5.18**).

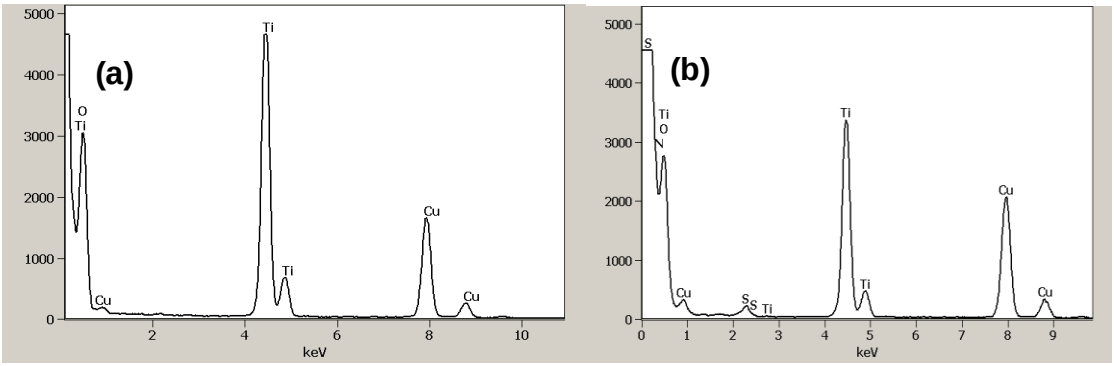

Figure 5. 17: EDX spectra for (a) undoped TiO_2 and (b) 2NS-TiO_2.

Table 5 3: Elemental composition of 2NS-TiO_2

ELEMENT	WEIGHT %	WEIGHT %	ATOM %	ATOM %
N K	2.610	± 0.360	4 51	± 0.620
O K	40.66	± 0.730	61 45	± 1.100
S K	1.670	± 0.050	1 26	± 0.040
Ti K	36.74	± 0.350	18 55	± 0.180

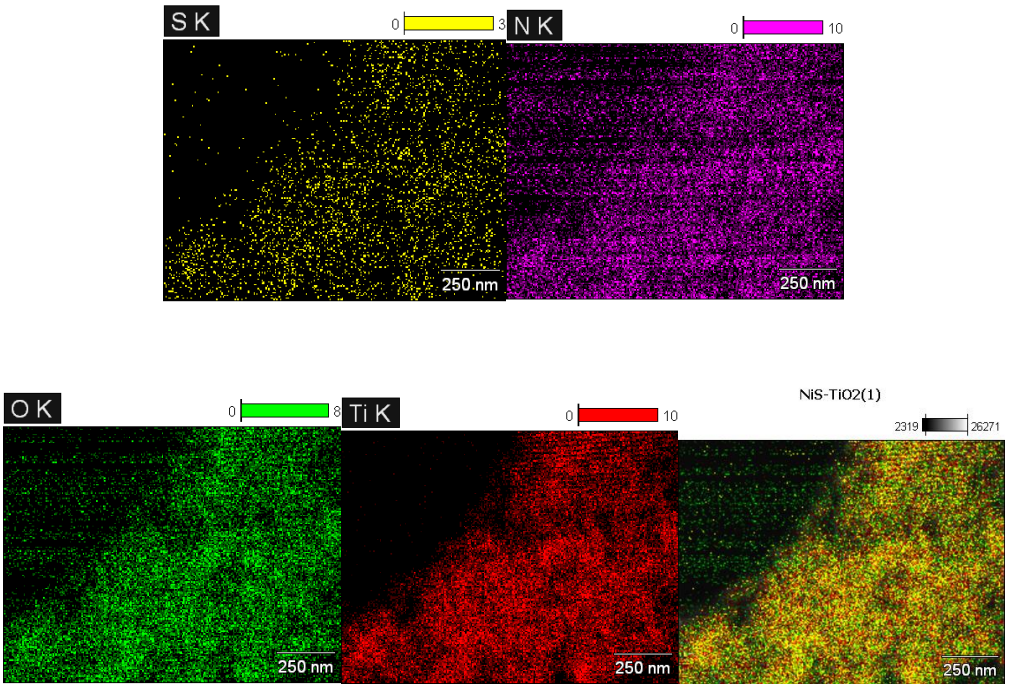

Figure 5. 18: Elemental mapping images for 2NS-TiO_2

5.4 Conclusion

This part of the study was aimed at developing a photocatalysis-coagulation hybrid system for the reduction of humic acid from water using nitrogen and sulphur co-doped TiO_2 nanoparticles. The following conclusions were drawn from the study: 1) Doping TiO_2 with nitrogen and sulphur was successfully used to improve the visible light activity of TiO_2, 2) The recovery of NS-TiO_2 by coagulation with ferric chloride under the optimized conditions was achieved. However, further optimization experiments could lead to improved catalyst recoveries (less than 1 NTU measurement), and 3) The photocatalysis-coagulation combined system showed the highest HA removal compared to when coagulation or photocatalysis were used individually. The combined system was evaluated with photocatalysis and coagulation occurring either sequentially or simultaneously. The photocatalysis-coagulation simultaneous system performed better than the sequential process. Coagulation has a low removal efficiency towards low molecular weight organics, hence post degradation removal of HA by photocatalysis using the sequential process showed low HA removal efficiencies. A proof-of-concept involving the application of photocatalysis-coagulation process in water treatment has been

demonstrated. It is envisaged that existing infrastructure can be retro-fitted to include this treatment step in the treatment train process.

References

[1] M. N. Aziz, S. Alias, F. Assari, “The use of alum, ferric chloride and ferrous sulphate as coagulants in removing suspended solids, colour and COD from semi-aerobic landfill leachate at controlled pH”, *Waste management research*, vol. 25, pp. 556–565, 2005.

[2] B. C. Cao, B. Y. Gao, C. H. Xu, Y. Fu, X. Liu, “Effects of pH on coagulation behaviour and floc properties in Yellow River water treatment using ferric based coagulants”, *Chinese science bulletin*, vol. 55, pp. 1382–1387, 2010.

[3] I. García, “Removal of natural organic matter to reduce the presence of trihalomethanes in drinking water”, Doctoral thesis, School of Chemical Science and Engineering Royal Institute of Technology Stockholm, Sweden 2011.

[4] K. J. Zves, “The scientific basis of flocculation”, Nato advanced study institutes series, *Series E: Applied science*, *Noordhoff International Publishing, Leyden/Niederlande*, pp. 593-593, 1976.

[5] Y. Prisca, A. D. Roberta, L. D. Gone, “Combination of coagulation-flocculation and heterogeneous photocatalysis for improving the removal of humic substances in real treated water from Agbô River (Ivory-Coast)”, *Catalysis today*, vol. 281, pp. 2–13, 2017.

[6] R. J. Honda, V. Keene, L. Daniels, and S. L. Walker, “Removal of TiO_2 Nanoparticles During Primary Water Treatment: Role of Coagulant Type, Dose, and Nanoparticle Concentration”, vol. 31, pp. 127–134, 2014.

[7] F. L. Palmer, B. R. Eggins, and H. M. Coleman, “The effect of operational parameters on the photocatalytic degradation of humic acid”, *Journal of photochemistry and photobiology A: Chemistry*, vol. 148, pp. 137–143, 2002.

[8] V. Etacheri, C. Di Valentin, J. Schneider, D. Bahnemann, and S. C. Pillai, “Visible-light activation of TiO_2 photocatalysts: Advances in theory and experiments”, *Journal of photochemistry and photobiology C: photochemistry reviews*, vol. *25*, pp.1-29, 2015.

[9] H. Khan, I. Khan Swati, M. Younas, and A. Ullah, “Chelated nitrogen-sulphur-Codoped TiO_2: Synthesis, characterization, mechanistic, and UV/Visible photocatalytic studies”, *International journal of photoenergy*, vol. 2017.

[10] C. Di Valentin, G. Pacchioni, “Trends in non-metal doping of anatase TiO_2: B, C, N and F”, *Catalysis today*, vol. 206, pp. 12–18, 2013.

[11] R. Marschall; L. Wang, “Non-metal doping of transition metal oxides for visible-light photocatalysis”, *Catalysis today*, vol. 225, pp. 111–135, 2014.

[12] D. Rajamanickam, and M Shanthi, “Photocatalytic degradation of an organic pollutant by zinc oxide–solar process”, *Arabian journal of chemistry*, vol. 9, pp. 1858–1868, 2016.

[13] K. Polewski, D. Sławińska, J. Sławiński, and A. Pawlak, “The effect of UV and visible light radiation on natural humic acid: EPR spectral and kinetic studies”, *Geoderma*, vol. 126, pp. 291–299, 2005.

[14] M. Sillanpää, M. C. Ncibi, A. Matilainen, and M. Vepsäläinen, “Removal of natural organic matter in drinking water treatment by coagulation: A comprehensive review”, *Chemosphere*, vol. 190, pp. 54–71, 2018.

[15] R. K. Henderson, A. Baker, K. R. Murphy, A. Hambly, R. M. Stuetz, and S. J. Khan, “Fluorescence as a potential monitoring tool for recycled water systems: A review”, *Water research*, vol. 43, pp. 863–881, 2009.

[16] Z. P. C. Li, Z. Zhao, H. S. Lomboleni, H. Huang, “Enhanced visible photocatalytic activity of nitrogen doped single-crystal-like TiO_2 by synergistic treatment with urea and mixed nitrates”, *Journal of materials research*, vol. 32, p. 737, 2017.

[17] M. Castellote, and N. Bengtsson, “Principles of TiO_2 photocatalysis”, *Applications of titanium dioxide photocatalysis to construction materials*, Springer, Dordrecht, 2011, pp. 5–10.

[18] M. Hojamberdiev, G. Zhu, P. Sujaridworakun, S. Jinawath, P. Liu, and J. P Zhou, “Visible-light-driven N–F-codoped TiO_2 powders derived from different ammonium oxofluorotitanate precursors”, *Powder technology*, vol. 218, pp. 140–148, 2012.

[19] A. T Kuvarega, R. W. Krause, and B. B. Mamba, “Comparison between base metals and platinum group metals in nitrogen, M codoped TiO_2 (M= Fe, Cu, Pd, Os) for photocatalytic removal of an organic dye in water”, *Journal of nanomaterials*, 2014.

[20] W. Vallejo, A. Rueda, C. Díaz-Uribe, C. Grande, and P. Quintana,

"Photocatalytic activity of graphene oxide–TiO_2 thin films sensitized by natural dyes extracted from bactris guineensis", *Royal society open science*, vol. 6, pp. 181–824, 2019.

[21] M. Sathish, R. P. Viswanath, and G. S. Gopinath, "N, S-Co-doped TiO_2 nanophotocatalyst: Synthesis, electronic structure and photocatalysis", *Journal of nanoscience and nanotechnology*, vol. 9, pp.423-432, 2009

[22] H. C Wu, S. W. Lin, and J. S. Wu, "Effects of nitrogen concentration on N-doped anatase TiO_2: density functional theory and Hubbard U analysis", *Journal of alloys and compounds*, vol. 522, pp. 46–50, 2012.

[23] O. Autin, J. Hart, P. Jarvis, J. MacAdam, S. A. Parsons and, B. Jefferson, "Comparison of UV/H_2O_2 and UV/TiO_2 for the degradation of metaldehyde: Kinetics and the impact of background organics", *Water research*, vol. 46, pp. 5655–5662, 2012.

[24] R. E. Adam, G. Pozina, M. Willander, and O. Nur, "Synthesis of ZnO nanoparticles by co-precipitation method for solar driven photodegradation of Congo red dye at different pH", *Photonics and nanostructures - Fundamentals and applications*, vol. 32, pp. 11–18, 2018.

CHAPTER 6:
CONCLUSION AND RECOMMENDATIONS

6.1 Introduction

The aim of this work was to: Evaluate an integrated photocatalysis-coagulation system for the removal of a mecoprop over commercial P25 under UVC irradiation. In another part of the study, the aim was to investigate the removal of humic acid by a photocatalytic-coagulation hybrid system under visible light using NS-TiO_2 as the photocatalyst.

This chapter will therefore provide conclusions and recommendations following the findings of this work.

6.2 Part 1: An integrated photocatalysis-coagulation system for the removal of a pesticide (mecoprop) under UVC irradiation

- The removal of NOM from water by coagulation can be affected by the presence of other compounds in the water. Herein the effect of TiO_2 concentration on the removal of UV_{254} absorbing organics was investigated. Results of this investigation have revealed that the presence of TiO_2 has no influence on the extent to which UV_{254} absorbing organics are removed by coagulation with ferric sulphate ($Fe_2(SO_4)_3$) ([Fe^{3+}]= 0.0370 mM and pH= 5. Furthermore, a variation in the concentrations of TiO_2 had no significant change in the UV_{254} readings throughout the coagulation-flocculation process (UV_{254} reduction from 0.13 cm^{-1} to 0.22 cm^{-1} for concentration between 20 mg/L and 100 mg/L of TiO_2).

- Nanoparticles such as TiO_2 contribute as secondary pollution when used for water treatment and recovery thereof is of concern. The recovery of commercial TiO_2 by chemical coagulation was investigated using ferric sulphate ($Fe_2(SO_4)_3$). An 80% removal of commercial TiO_2 was observed at optimal conditions of [Fe^{3+}] = 0.0370 mM and pH = 5. Further removal was not observed for doses above 0.0500 mM of [Fe^{3+}] for TiO_2 concentrations of 60, 80 and 100 mg/L. The photocatalysis-coagulation hybrid system for the

degradation and removal of mecoprop has improved removal rates than the individual processes.

- Synergistic effect was observed between photolysis and the Fe^{3+} processes (contributed by UV in combination with Fe^{3+}), however, the addition of TiO_2 to the system did not make any significant contribution to the combined system (0.0031 $cm^2.mJ^{-1}$ increase).

The removal of mecoprop by the proposed photocatalytic-coagulation hybrid was successful. Moreover, the removal of TiO_2 *via* coagulation could be improved to give turbidity measurements lower than 1 NTU to meet SANS: 241 standards.

6.3 Part 2: The removal of humic acid by a photocatalytic-coagulation hybrid system

- Humic acid degradation was investigated using a photocatalysis-coagulation hybrid system by NS-TiO_2 under visible light irradiation. The photocatalysis-coagulation hybrid system in which both processes were occurring simultaneously gave 98% TOC and 100% UV_{254} removal efficiencies within 48 minutes under optimised conditions (pH = 6, [2NS-TiO_2] = 150 mg/L, [Fe^{3+}] = 0.185 mM). However, 96% humic acid removal efficiency was obtained within 165 minutes when the sequential photocatalysis-coagulation hybrid system was conducted under similar conditions.

- When coagulation was used to evaluate the removal of NS-TiO_2 for post treatment recovery, turbidity removal of 32 NTU to 3.5 NTU was achieved under optimum conditions (pH= 6, [Fe^{3+}] = 0.185 mM). The doping of the TiO_2 matrix with nitrogen and sulphur appears to hinder the aggregation rate of the nanoparticles thus resulting in poor removal of the nanoparticles *via* coagulation and by extension the coagulation-flocculation hybrid process.

- The doping of the TiO_2 matrix by nitrogen and sulphur improves the visible light activity of the photocatalyst and thus the use of carcinogenic UV light

can be avoided. From the investigation of doping nitrogen and sulphur onto the TiO_2 matrix, a clear reduction of the TiO_2 band gap was observed after doping with varying amounts of nitrogen and sulphur (from TiO_2 = 3.20 eV to 3.18 eV for 1NS-TiO_2, 2.55 eV for 2NS-TiO_2, and 2.4 eV for 4NS-TiO_2). Furthermore, the photocatalytic activity of TiO_2 was significantly improved after doping with N and S using 2 g of thiourea compared to higher thiourea loadings.

The removal of humic acid by the photocatalytic-coagulation hybrid system using NS-TiO_2 under visible light was successful. Removal of NS-TiO_2 *via* coagulation was also a success. However, further optimisation is required to achieve turbidity measurements below 1 NTU.

6.4 Recommendations to further the study:

After having successfully achieved the aim and objectives of this study, it would be beneficial to pursue the following:

- Future work is required to evaluate the efficiency of alum and polymer-based coagulants in the recovery of TiO_2 or NS-TiO_2 NPs when using the hybrid coagulation-photocatalysis process.

- Analysis of residual iron using ICP or AA could aid in the optimisation of the coagulant dose in the coagulation tests. Iron has a few negative implications on human health and measures should be put in place to monitor the levels during treatment by coagulation.

- The UV-Fe^{3+} process could be applied at pilot scale for the mitigation of mecoprop since the photolysis equipment could be retrofitted into existing coagulation systems. Retrofitting photocatalysis with existing coagulation equipment will result in immense improvement of mecoprop removal in drinking or wastewater.

- Compilation of risk assessments in this regard to determine the feasibility of the photocatalysis-coagulation hybrid system should be considered.

- Given the successful demonstration of a proof of concept involving the application of photocatalysis-coagulation process in water treatment, proper risk assessment and efficacy evaluation should be conducted at pilot scale.

APPENDIX

A1.1: UV_{254} removal measurements for the effect of NS loadings on NS-TiO_2 performance post treatment of HA by a photocatalytic-coagulation hybrid system

Time	**Absorbance (cm^{-1})**				
	NS-TiO_2 4g	NS-TiO_2 1g	NS-TiO_2 2g	TiO_2	Photolysis
-15	0.7262	0.7146	0.7013	0.7456	0.7459
0	0.7491	0.7491	0.7491	0.7491	0.7432
15	0.4215	0.3128	0.2905	0.7693	0.7453
30	0.3942	0.3103	0.2302	0.7678	0.7445
45	0.3811	0.3091	0.1489	0.7400	0.7444
60	0.3686	0.2535	0.0922	0.7358	0.7423
75	0.3598	0.2239	0.0576	0.7223	0.7422
90	0.3420	0.1921	0.0450	0.6850	0.7422
105	0.3263	0.1797	0.0275	0.6731	0.7419
120	0.2664	0.1418	0.0243	0.6225	0.7414

A1.2: UV_{254} removal measurements for the effect of catalyst dose on the removal of HA post treatment with by a photocatalytic-coagulation hybrid system using NS-TiO_2

Time (min)	**Absorbance (AU)**			
	[2NS-TiO_2]=50 mg/L	**[2NS-TiO_2]=100 mg/L**	**[2NS-TiO_2]=150 mg/L**	**[1NS-TiO_2]=200 mg/L**
	0.5214	0.5021	0.5322	0.1260
0	0.5334	0.5334	0.5334	0.1693
15	0.4601	0.2905	0.0927	0.0775
30	0.3835	0.2302	0.0791	0.0165
45	0.2754	0.1489	0.0634	0.0076
60	0.1487	0.0922	0.0623	0.0020
75	0.0934	0.0576	0.0325	0
90	0.0816	0.0450	0.0275	0
105	0.0765	0.0275	0.0158	0
120	0.0682	0.0243	0.0075	0

A1.3: UV_{254} removal measurements for the effect of pH on the removal of HA post treatment with by a photocatalytic-coagulation hybrid system using 2NS-TiO_2

Time (min)	Absorbance (AU)		
	pH 5	pH 6	pH 7
-15	0.5014	0.5232	0.5262
0	0.5334	0.5334	0.5334
15	0.0927	0.2287	0.4070
30	0.0791	0.1619	0.3711
45	0.0634	0.1171	0.3269
60	0.0323	0.0544	0.3026
75	0.0325	0.0480	0.2840
90	0.0275	0.0418	0.2263
105	0.0158	0.0362	0.1664
120	0.0075	0.0291	0.0963

A1.4: UV_{254} removal measurements for the effect of pollutant concentration ([HA]) on the removal of HA post treatment with by a photocatalytic-coagulation hybrid system using 2NS-TiO_2

Time (min)	**Absorbance (AU)**		
	10 mg/L Humic acid	**20 mg/L Humic acid**	**5 mg/L Humic acid**
-15	0.5334	0.5334	0.5364
0	0.5213	0.5320	0.4362
15	0.0927	0.3494	0.0757
30	0.0791	0.3013	0.0631
45	0.0634	0.2960	0.0544
60	0.0323	0.2571	0.0363
75	0.0325	0.1850	0.0125
90	0.0275	0.1090	0.0076
105	0.0158	0.0924	0.0057
120	0.0075	0.0867	0.0025

A1.5: UV_{254} removal measurements post treatment with by a photocatalytic-coagulation hybrid system using 2NS-TiO_2

Time	Coag+photo pH 5	Coag+photo pH 6	Coag+photo pH 7	Photo ==> Coag	Coag+Vis	Adsorption	pH 5
-15	0.9864	0.29878	0.2987	0.2987	1.2620	0.2462	1
0	0.9621	0.25725	0.2307	0.2615	0.3218	0.2571	1.1614
6	0.8941	0.1511	0.20264	0.2382	0.2987	0.2351	0.5875
12	0.7244	0.1481	0.1688	0.0976	0.2382	0.2473	0.5759
18	0.3218	0.1004	0.11494	0.0826	0.1672	0.2362	0.3904
24	0.1965	0.0465	0.07397	0.0687	0.1350	0.2176	0.1811
30	0.1350	0.0242	0.0657	0.0642	0.0930	0.2164	0.0943
36	0.0473	0.0242	0.02984	0.0642	0.0610	0.2009	0.0942
42	0.0461	0.0166	0.02848	0.0625	0.0473	0.2000	0.0648
48	0.0461	0.0125	0.01863	0.0364	0.0461		0.0489
49				0.0242			
65				0.0188			
95				0.0126			

$[TiO_2]$ = 20 mg/L		$[TiO_2]$ = 40 mg/L		$[TiO_2]$ = 60 mg/L		$[TiO_2]$ = 80 mg/L		$[TiO_2]$ = 1000 mg/L	
Turbidity	**Coag dose**	**Turbidity**	**Coag Dose**	**Turbidity**	**Coag Dose**	**Turbidity**	**Coag dose**	**Turbidity**	**Coag dose**
52.07	0	70	0	123.18	0	177.62	0	231.43	0
6.59	2.5	5.6150	2.5	21.300	2.5	24.500	2.5	27.750	2.5
3.26	5	3.385	5	4.9700	5	11.500	5	19.950	5
4.795	7.5	3.1400	7.5	4.5500	7.5	6.2000	7.5	5.8600	7.5
3.18	10	2.7250	10	3.2050	10	5.3800	10	4.3150	10
3.14	20	2.5900	20	3.4400	20	5.5300	20	3.4600	20
2.14	30	2.4400	30	4.5150	30	3.5200	30	1.5380	30
1.67	40	2.1650	40	4.1600	40	3.0350	40	2.0350	40
Zeta potential	**Coag dose**	**UV_{254}**	**Coag Dose**	**UV_{254}**	**Coag Dose**	**UV_{254}**	**Coag Dose**	**UV_{254}**	**Coag Dose**
-14	0	0.1280	0	0.1250	0	0.1160	0	0.1230	0
-9.6	2.5	0.0540	2.5	0.0465	2.5	0.0450	2.5	0.0420	2.5
-3.06	5	0.0410	5	0.0267	5	0.0310	5	0.0300	5
-2.54	7.5	0.0275	7.5	0.0295	7.5	0.0280	7.5	0.0260	7.5
-4.185	10	0.0230	10	0.0260	10	0.0270	10	0.0260	10

-0.7695	20	0.0260	20	0.0270	20	0.0260	20	0.0270	20
4.17	30	0.0265	30	0.0270	30	0.0260	30	0.0260	30
6.15	40	0.0260	40	0.0260	40	0.0255	40	0.0260	40
UV_{245}	**Coag Dose**	**Zeta potential**	**Coag Dose**	**Zeta potential**	**Coag Dose**	**Zeta Potential**	**Coag Dose**	**Zeta Potential**	**Coag Dose**
0.129	0	-14.300	0	-14	0	-14.000	0	-14.000	0
0.053	2.5	-11.600	2.5	-12.050	2.5	-12.650	2.5	-8.1700	2.5
0.0445	5	-0.4840	5	-2.3200	5	-3.310	5	-3.1050	5
0.027	7.5	-1.7750	7.5	-2.0800	7.5	-1.510	7.5	-2.7650	7.5
0.0255	10	-1.8150	10	-5.8100	10	-9.370	10	-1.1420	10
0.0235	20	1.5400	20	1.3950	20	2.650	20	2.7900	20
0.022	30	3.4600	30	4.1600	30	3.280	30	3.9500	30
0.023	40	3.9200	40	4.5500	40	4.380	40	3.6700	40

A1.6: LCMS quantitative measurements for mecoprop throughout photocatalysis-coagulation hybrid process treatment

Sample Name	Component Name	Actual Concentration	Area	Height	Retention Time	Width at 50%	Used	Calculated Concentration	Accuracy
blank	MCPP 1	N/A	N/A	N/A	N/A	N/A	TRUE	**N/A**	N/A
blank 2	MCPP 1	N/A	N/A	N/A	N/A	N/A	TRUE	**N/A**	N/A
stand 1	MCPP 1	1	7.68E+03	1.2700E+03	1.4000	0.0900	TRUE	**0.8830**	88.250
stand 2	MCPP 1	2	2.110E+04	2.6700E+03	1.3800	0.1000	TRUE	**2.2150**	110.77
stand 5	MCPP 1	5	4.890E+04	6.1300E+03	1.3500	0.1000	TRUE	**4.9830**	99.660
stand 7	MCPP 1	7	7.0700E+04	8.7000E+03	1.3500	0.1000	TRUE	**7.1610**	102.30

stand 10	MCPP 1	10.000	9.9200E+04	1.2100E+04	1.3500	0.1000	TRUE	**9.9960**	99.96
stand 15	MCPP 1	15.000	1.5100E+05	1.8300E+04	1.3500	0.1000	TRUE	**15.145**	100.97
stand 20	MCPP 1	20.000	1.9600E+05	2.3400E+04	1.3500	0.1000	TRUE	**19.617**	98.09
UV+TiO_2 20 mg/L 1 MIN	MCPP 1	4.6544	4.5600E+04	4.7400E+03	1.3500	0.1100	TRUE	**4.6550**	N/A
UV+TIO_2 20 mg/L 3 MIN	MCPP 1	3.3579	3.2500E+04	3.3100E+03	1.3600	0.1100	TRUE	**3.3580**	N/A
UV+TIO_2 20 mg/L 4 MIN	MCPP 1	2.8889	2.7800E+04	2.8200E+03	1.3800	0.1100	TRUE	**2.8890**	N/A
UV+TIO_2 20 mg/L 5 MIN	MCPP 1	2.7465	2.6400E+04	2.7700E+03	1.3300	0.1100	TRUE	**2.7470**	N/A
UV+TIO_2 20 mg/L 7 MIN	MCPP 1	2.0495	1.9400E+04	1.9500E+03	1.3600	0.1100	TRUE	**2.0500**	N/A

UV+TIO$_2$ 20 mg/L 9 MIN	MCPP 1	1.677097069	1.57E+04	1.56E+03	1.36	0.11	TRUE	**1.677**	N/A
UV+TIO$_2$ 40 mg/L 1 MIN	MCPP 1	4.063000817	3.96E+04	3.86E+03	1.37	0.12	TRUE	**4.063**	N/A
blank	MCPP 1	N/A	N/A	N/A	N/A	N/A	TRUE	**N/A**	N/A
blank 2	MCPP 1	N/A	N/A	N/A	N/A	N/A	TRUE	**N/A**	N/A
stand 5	MCPP 1	N/A	3.93E+04	4.41E+03	1.35	0.11	TRUE	**4.03**	N/A
UV+TIO$_2$ 40 mg/L 2 MIN	MCPP 1	3.9186	3.8200E+04	3.8100E+03	1.3700	0.1200	TRUE	**3.9190**	N/A
UV+TIO$_2$ 40 mg/L 3 MIN	MCPP 1	3.1219	3.0200E+04	3.0300E+03	1.3600	0.1200	TRUE	**3.1220**	N/A
UV+TIO$_2$ 40 mg/L 4 MIN	MCPP 1	2.4567	2.3500E+04	2.3300E+03	1.3700	0.1200	TRUE	**2.4570**	N/A

UV-TIO_2 40 mg/L 5 MIN	MCPP 1	2.2855	2.1800E+04	2.1600E+03	1.3700	0.1200	TRUE	**2.2850**	N/A
UV-TIO_2 40 mg/L 7 MIN	MCPP 1	1.7179	1.6100E+04	1.5800E+03	1.3600	0.1300	TRUE	**1.7180**	N/A
UV-TIO_2 40 mg/L 9 MIN	MCPP 1	1.2668	1.1500E+04	1.1800E+03	1.3600	0.1200	TRUE	**1.2670**	N/A
UV-TIO_2 40 mg/L 11 MIN	MCPP 1	0.9830	8.6900E+03	8.2300E+02	1.3800	0.1300	TRUE	**0.9830**	N/A
UV-TIO_2 40 mg/L 15 MIN	MCPP 1	0.5963	4.8100E+03	4.7300E+02	1.3600	0.1200	TRUE	**0.5960**	N/A
UV/TIO_2 40 mg/L 20 MIN	MCPP 1	0.3684	2.5200E+03	2.4200E+02	1.3800	0.1300	TRUE	**0.3680**	N/A
UV/TIO_2 60 mg/L 1 MIN	MCPP 1	4.8875	4.7900E+04	4.5200E+03	1.3900	0.1300	TRUE	**4.8880**	N/A
Blank 1	MCPP 1	N/A	N/A	N/A	N/A	N/A	TRUE	**N/A**	N/A

Blank 2	MCPP 1	N/A	N/A	N/A	N/A	N/A	TRUE	**N/A**	N/A
Stand 2	MCPP 1	N/A	1.7300E+04	1.8800E+03	1.3600	0.1200	TRUE	**1.8370**	N/A
UV+TIO_2 60 mg/L 2 MIN	MCPP 1	4.3995	4.3000E+04	4.2900E+03	1.3600	0.1300	TRUE	**4.4000**	N/A
UV+TIO_2 60 mg/L 3 MIN	MCPP 1	3.6945	3.5900E+04	3.4900E+03	1.3700	0.1300	TRUE	**3.6940**	N/A
UV+TIO_2 60 mg/L 4 MIN	MCPP 1	3.1100	3.0100E+04	2.8900E+03	1.3800	0.1300	TRUE	**3.1100**	N/A
UV+TIO_2 60 mg/L 5 MIN	MCPP 1	2.8491	2.7400E+04	2.6500E+03	1.3600	0.1400	TRUE	**2.8490**	N/A
UV+TIO_2 60 mg/L 7 MIN	MCPP 1	1.8354	1.7300+04	1.5900E+03	1.37	0.14	TRUE	**1.8360**	N/A
UV+TIO_2 60 mg/L 9 MIN	MCPP 1	1.2887	1.1800E+04	1.1000E+03	1.37	0.14	TRUE	**1.2890**	N/A

UV+TIO_2 60 mg/L 11 min	MCPP 1	0.9119	7.98E+03	7.7100E+02	1.3800	0.13	TRUE	**0.9120**	N/A
UV+TiO_2 60 mg/L 15 min	MCPP 1	0.4346	3.18E+03	3.2500E+02	1.3700	0.12	TRUE	**0.4350**	N/A
UV+TiO_2 60 mg/L 20 min	MCPP 1	0.2165	9.93E+02	9.6300E+01	1.3700	0.15	TRUE	**0.2170**	N/A
UV+TiO_2 80 mg/L 1 min	MCPP 1	4.79988	4.70E+04	4.3800E+03	1.3900	0.15	TRUE	**4.8000**	N/A
Blank 1	MCPP 1	N/A	N/A	N/A	N/A	N/A	TRUE	**N/A**	N/A
Blank 2	MCPP 1	N/A	N/A	N/A	N/A	N/A	TRUE	**N/A**	N/A
Stand 1	MCPP 1	N/A	8.7100E+03	9.2000E+02	1.3600	0.1200	TRUE	**0.9850**	N/A
UV+TiO_2 80 mg/L 2 min	MCPP 1	4.3726	4.2700E+04	4.0700E+03	1.3600	0.1600	TRUE	**4.3730**	N/A

UV+TiO_2 80 mg/L 3 min	MCPP 1	3.3490	3.2500E+04	3.0800E+03	1.3800	0.1400	TRUE	**3.3490**	N/A
UV+TiO_2 80 mg/L 4 min	MCPP 1	2.4189	2.3100E+04	2.2200E+03	1.3700	0.1400	TRUE	**2.4190**	N/A
UV+TiO_2 80 mg/L 5 min	MCPP 1	1.9559	1.8500E+04	1.7600E+03	1.3700	0.1400	TRUE	**1.9560**	N/A
UV+TiO_2 80 mg/L 7 min	MCPP 1	1.1463	1.0300E+04	9.8300E+02	1.3700	0.1500	TRUE	**1.1460**	N/A
UV+TiO_2 80 mg/L 9 min	MCPP 1	0.6829	5.6800E+03	5.5500E+02	1.3700	0.1200	TRUE	**0.6830**	N/A
UV+TiO_2 80 mg/L 11 min	MCPP 1	0.3820	2.6600E+03	2.6500E+02	1.3500	0.1300	TRUE	**0.3820**	N/A
UV+TiO_2 80 mg/L 15 min	MCPP 1	0.1922	7.4800E+02	7.5500E+01	1.3700	0.1900	TRUE	**0.1920**	N/A
UV+TiO_2 80 mg/L 20 min	MCPP 1	#VALUE!	N/A	N/A	N/A	N/A	TRUE	**N/A**	N/A

UV/TiO2 100 mg/L 1 min	MCPP 1	4.2034	4.1000E+04	4.0300E+03	1.3500	0.1300	TRUE	**4.203**	N/A
Blank 1	MCPP 1	N/A	N/A	N/A	N/A	N/A	TRUE	**N/A**	N/A
Blank 2	MCPP 1	N/A	N/A	N/A	N/A	N/A	TRUE	**N/A**	N/A
UV+TiO_2 100 mg/L 2 min	MCPP 1	4.7600	4.6600E+04	4.5900E+03	1.3800	0.1400	TRUE	**4.7600**	N/A
UV+TiO_2 100 mg/L 3 min	MCPP 1	2.5802	2.4700E+04	2.3400E+03	1.3700	0.1500	TRUE	**2.5810**	N/A
UV+TiO_2 100 mg/L 4 min	MCPP 1	1.7248	1.6100E+04	1.5500E+03	1.3900	0.1400	TRUE	**1.7250**	N/A
UV+TiO_2 100 mg/L 5 min	MCPP 1	1.2011	1.0900E+04	9.8800E+02	1.3900	0.1800	TRUE	**1.2010**	N/A
UV+TiO_2 100 mg/L 7 min	MCPP 1	0.5020	3.8600E+03	3.5400E+02	1.3800	0.1700	TRUE	**0.5020**	N/A

UV+TiO_2 100 mg/L 9 min	MCPP 1	0.2414	1.2400E+03	1.0300E+02	1.3900	0.1900	TRUE	**0.2410**	N/A
UV+TiO_2 100 mg/L 11 min	MCPP 1	#VALUE!	N/A	N/A	N/A	N/A	TRUE	**N/A**	N/A
UV+TiO_2 100 mg/L 15 min	MCPP 1	#VALUE!	N/A	N/A	N/A	N/A	TRUE	**N/A**	N/A
UV+TiO_2 100 mg/L 20 min	MCPP 1	#VALUE!	N/A	N/A	N/A	N/A	TRUE	**N/A**	N/A
UV 0 min	MCPP 1	4.5041	4.4100E+04	4.0900E+03	1.3800	0.1900	TRUE	**4.5040**	N/A
Blank 1	MCPP 1	N/A	N/A	N/A	N/A	N/A	TRUE	**N/A**	N/A
Blank 2	MCPP 1	N/A	N/A	N/A	N/A	N/A	TRUE	**N/A**	N/A
Stand 5	MCPP 1	4.7192	4.6200E+04	4.9500E+03	1.3300	0.1300	TRUE	**4.7190**	N/A

UV 2 min	MCPP 1	4.1227	4.0200E+04	3.9400E+03	1.3700	0.1400	TRUE	**4.1220**	N/A
UV 3 min	MCPP 1	3.3530	3.2500E+04	3.0800E+03	1.3800	0.1700	TRUE	**3.3530**	N/A
UV 4 min	MCPP 1	2.9288	2.8200E+04	2.6700E+03	1.3600	0.1600	TRUE	**2.9290**	N/A
UV 5 min	MCPP 1	2.4657	2.3600E+04	2.2500E+03	1.3700	0.1700	TRUE	**2.4660**	N/A
UV 7 min	MCPP 1	1.9310	1.8200E+04	1.7400E+03	1.3700	0.1800	TRUE	**1.9310**	N/A
UV 9 min	MCPP 1	1.6213	1.5100E+04	1.4200E+03	1.3600	0.1800	TRUE	**1.6210**	N/A
UV 11 min	MCPP 1	1.3036	1.1900E+04	1.1700E+03	1.3700	0.1500	TRUE	**1.3030**	N/A
UV 15 min	MCPP 1	0.8573	7.4300E+03	6.7300E+02	1.3800	0.1800	TRUE	**0.8570**	N/A

Sample Name	Component Name	Actual Concentration	Area	Height	Retention Time	Width at 50%	Used	Calculated Concentration	Accuracy
blank	MCPP 1	N/A	N/A	N/A	N/A	N/A	TRUE	N/A	N/A
blank 2	MCPP 1	N/A	N/A	N/A	N/A	N/A	TRUE	N/A	N/A
stand 1	MCPP 1	1	1.1300E+04	2.3300E+03	1.2600	0.0700	TRUE	0.9980	99.770
stand 2	MCPP 1	2	2.2800E+04	4.8800E+03	1.2500	0.0600	TRUE	2.0390	101.95
stand 5	MCPP 1	5	5.5600E+04	1.1600E+04	1.2600	0.0600	TRUE	5.0100	100.20
stand 7	MCPP 1	7	7.6500E+04	1.60E+04	1.2600	0.0600	TRUE	6.8990	98.560

stand 10	MCPP 1	10	1.0900E+05	2.3400E+04	1.2600	0.0600	TRUE	9.8680	98.68
stand 15	MCPP 1	15	1.6500E+05	3.4500E+04	1.2500	0.0600	TRUE	14.948	99.66
stand 20	MCPP 1	20	2.2400E+05	4.7900E+04	1.2600	0.0600	TRUE	20.230	101.19
UV+TiO_2 20 mg/L 1 MIN	MCPP 1	N/A	5.5600E+04	1.2000E+04	1.2600	0.0600	TRUE	5.0080	N/A
UV+TiO_2 20 mg/L 2 MIN	MCPP 1	N/A	4.0000E+00		1.2600	0.0600	TRUE	4.2640	N/A
UV+TIO_2 20 mg/L 3 MIN	MCPP 1	N/A	4.1200E+04	9.0000E+03	1.2600	0.0600	TRUE	3.7040	N/A
UV+TIO_2 20 mg/L 4 MIN	MCPP 1	N/A	3.6100E+04	7.8300E+03	1.2600	0.0600	TRUE	3.2400	N/A
UV+TIO_2 20 mg/L 5 MIN	MCPP 1	N/A	3.0600E+04	6.5600E+03	1.2600	0.0600	TRUE	2.7400	N/A

UV+TIO_2 20 mg/L 7 MIN	MCPP 1	N/A	2.4800E+04	5.5000E+03	1.2600	0.0600	TRUE	2.2170	N/A
UV TIO_2 20 mg/L 9 MIN	MCPP 1	N/A	1.9900E+04	4.2500E+03	1.2600	0.0600	TRUE	1.7780	N/A
UV TIO_2 20 mg/L 11 MIN	MCPP 1	N/A	5.3500E+04	1.2000E+04	1.2600	0.0600	TRUE	4.8180	N/A
UV+TIO_2 15 MIN	MCPP 1	N/A	3.5500E+04	7.5000E+03	1.2600	0.0600	TRUE	3.1900	N/A
UV+TIO_2 20 mg/L 20 MIN	MCPP 1	N/A	4.0500E+04	8.8700E+03	1.2600	0.0600	TRUE	3.6370	N/A
UV+TIO_2 40 mg/L 1 MIN	MCPP 1	N/A	5.1700E+04	1.1600E+04	1.2700	0.0600	TRUE	4.6510	N/A
blank	MCPP 1	N/A	N/A	N/A	N/A	N/A	TRUE	N/A	N/A
blank 2	MCPP 1	N/A	N/A	N/A	N/A	N/A	TRUE	N/A	N/A

stand 5	MCPP 1	N/A	5.4000E+04	1.1200E+04	1.2500	0.0600	TRUE	4.8650	N/A
UV+TIO_2 40 mg/L 2 MIN	MCPP 1	N/A	4.9900E+04	1.1400E+04	1.2700	0.0600	TRUE	4.4880	N/A
UV+TIO_2 40 mg/L 3 MIN	MCPP 1	N/A	4.1000E+04	9.1200E+03	1.2600	0.0600	TRUE	3.6840	N/A
UV+TIO_2 40 mg/L 4 MIN	MCPP 1	N/A	3.1800E+04	7.1400E+03	1.2600	0.0600	TRUE	2.8530	N/A
UV+TIO_2 40 mg/L 5 MIN	MCPP 1	N/A	2.7200E+04	6.0700E+03	1.2700	0.0600	TRUE	2.4390	N/A
UV+TIO_2 40 mg/L 7 MIN	MCPP 1	N/A	2.0700E+04	4.6300E+03	1.2600	0.0600	TRUE	1.8510	N/A
UV+TIO_2 40 mg/L 9 MIN	MCPP 1	N/A	1.5500E+04	3.4100E+03	1.2600	0.0600	TRUE	1.3750	N/A
UV+TIO_2 40 mg/L 11 MIN	MCPP 1	N/A	1.2200E+04	2.8600E+03	1.2600	0.0600	TRUE	1.0810	N/A

UV+TIO_2 40 mg/L 15 MIN	MCPP 1	N/A	6.42E+03	1.44E+03	1.26	0.06	TRUE	0.5570	N/A
UV+TIO_2 40 mg/L 20 MIN	MCPP 1	N/A	2.96E+03	6.19E+02	1.26	0.07	TRUE	0.2430	N/A
UV+TIO_2 60 mg/L 1 MIN	MCPP 1	N/A	5.87E+04	1.31E+04	1.26	0.06	TRUE	5.2830	N/A
Blank 1	MCPP 1	N/A	N/A	N/A	N/A	N/A	TRUE	N/A	N/A
Blank 2	MCPP 1	N/A	N/A	N/A	N/A	N/A	TRUE	N/A	N/A
Stand 2	MCPP 1	N/A	2.2100E+04	4.6700E+03	1.2500	0.0600	TRUE	1.9790	N/A
UV+TIO_2 60 mg/L 2 MIN	MCPP 1	N/A	5.4800E+04	1.2100E+04	1.2600	0.0600	TRUE	4.9340	N/A
UV+TIO_2 60 mg/L 3 MIN	MCPP 1	N/A	4.4400E+04	9.9100E+03	1.2500	0.0600	TRUE	3.9890	N/A

UV+TIO_2 60 mg/L 4 MIN	MCPP 1	N/A	3.8300E+04	8.6900E+03	1.2600	0.0600	TRUE	3.4370	N/A
UV+TIO_2 60 mg/L 5 MIN	MCPP 1	N/A	3.1500E+04	7.0900E+03	1.2600	0.0600	TRUE	2.8230	N/A
UV+TIO_2 60 mg/L 7 MIN	MCPP 1	N/A	2.2000E+04	4.8400E+03	1.2600	0.0600	TRUE	1.9690	N/A
UV+TIO_2 60 mg/L 9 MIN	MCPP 1	N/A	1.4600E+04	3.3400E+03	1.2600	0.0600	TRUE	1.3010	N/A
UV+TIO_2 60 mg/L 11 min	MCPP 1	N/A	9.7400E+03	2.0700E+03	1.2600	0.0700	TRUE	0.8570	N/A
UV+TiO_2 60 mg/L 15 min	MCPP 1	N/A	3.8100E+03	8.8500E+02	1.2600	0.0600	TRUE	0.3200	N/A
UV+TiO_2 60 mg/L 20 min	MCPP 1	N/A	9.9200E+02	2.4700E+02	1.2600	0.0500	TRUE	0.0650	N/A
UV+TiO_2 80 mg/L 1 min	MCPP 1	N/A	5.5200E+04	1.2100E+04	1.2600	0.0600	TRUE	4.9700	N/A

Blank 1	MCPP 1	N/A	N/A	N/A	N/A	N/A	TRUE	N/A	N/A
Blank 2	MCPP 1	N/A	N/A	N/A	N/A	N/A	TRUE	N/A	N/A
Stand 1	MCPP 1	N/A	1.1400E+04	2.3100E+03	1.2400	0.0700	TRUE	1.0030	N/A
UV+TiO_2 80 mg/L 2 min	MCPP 1	N/A	4.9400E+04	1.0900E+04	1.2600	0.0600	TRUE	4.4460	N/A
UV+TiO_2 80 mg/L 3 min	MCPP 1	N/A	3.8000E+04	8.4900E+03	1.2600	0.0600	TRUE	3.4160	N/A
UV+TiO_2 80 mg/L 4 min	MCPP 1	N/A	2.87E+04	6.2600E+03	1.2500	0.0600	TRUE	2.5680	N/A
UV+TiO_2 80 mg/L 5 min	MCPP 1	N/A	2.34E+04	5.1000E+03	1.2500	0.0600	TRUE	2.0970	N/A
UV+TiO_2 80 mg/L 7 min	MCPP 1	N/A	1.33E+04	2.9300E+03	1.2600	0.0600	TRUE	1.1760	N/A

UV+TiO_2 80 mg/L 9 min	MCPP 1	N/A	6.72E+03	1.51E+03	1.26	0.06	TRUE	0.5840	N/A
UV+TiO_2 80 mg/L 11 min	MCPP 1	N/A	3.3900E+03	7.16E+02	1.2600	0.0700	TRUE	0.2820	N/A
UV+TiO_2 80 mg/L 15 min	MCPP 1	N/A	8.2200E+02	1.93E+02	1.2600	0.0600	TRUE	0.0500	N/A
UV+TiO_2 80 mg/L 20 min	MCPP 1	N/A	N/A	N/A	N/A	N/A	TRUE	N/A	N/A
UV+TiO_2 100 mg/L 1 min	MCPP 1	N/A	5.0600E+04	1.10E+04	1.2500	0.0600	TRUE	4.5540	N/A
Blank 1	MCPP 1	N/A	N/A	N/A	N/A	N/A	TRUE	N/A	N/A
Blank 2	MCPP 1	N/A	N/A	N/A	N/A	N/A	TRUE	N/A	N/A
Standard 7	MCPP 1	N/A	7.97E+04	1.54E+04	1.2700	0.07	TRUE	7.1830	N/A

UV+TiO_2 100 mg/L 2 min	MCPP 1	N/A	4.4100E+04	9.2700E+03	1.2700	0.0700	TRUE	3.9620	N/A
UV+TiO_2 100 mg/L 3 min	MCPP 1	N/A	3.0000E+04	6.2900E+03	1.2600	0.0600	TRUE	2.6910	N/A
UV+TiO_2 100 mg/L 4 min	MCPP 1	N/A	2.0100E+04	4.2700E+03	1.2500	0.0700	TRUE	1.7960	N/A
UV+TiO2 100 mg/L 5 min	MCPP 2	N/A			1.2600	0.0600	TRUE	1.2300	N/A
UV+TiO_2 100 mg/L 7 min	MCPP 1	N/A	4.4500E+03	9.1100E+02	1.2600	0.0700	TRUE	0.3780	N/A
UV+TiO_2 100 mg/L 9 min	MCPP 1	N/A	1.8200E+03	3.8900E+02	1.2500	0.0600	TRUE	0.1400	N/A
UV+TiO_2 100 mg/L 11 min	MCPP 1	N/A	3.2400E+02	6.4700E+01	1.2500	0.0900	TRUE	0.0050	N/A
UV/TiO2 100 mg/L 15 min	MCPP 1	N/A	N/A	N/A	N/A	N/A	TRUE	N/A	N/A

UV+TiO_2 100 mg/L 20 min	MCPP 1	N/A	N/A	N/A	N/A	N/A	TRUE	N/A	N/A
untreated 0 min	MCPP 1	N/A	6.2800E+05	1.2600E+05	1.23	0.0700	TRUE	56.788	N/A
Blank 1	MCPP 1	N/A	N/A	N/A	N/A	N/A	TRUE	N/A	N/A
Blank 2	MCPP 1	N/A	N/A	N/A	N/A	N/A	TRUE	N/A	N/A
Stand 5	MCPP 1	N/A	5.3600E+04	1.0300E+04	1.2400	0.0700	TRUE	4.8260	N/A
Blank 1	MCPP 1	N/A	N/A	N/A	N/A	N/A	TRUE	N/A	N/A
Blank 2	MCPP 1	N/A	N/A	N/A	N/A	N/A	TRUE	N/A	N/A
Stand 5	MCPP 1	N/A	5.5000E+04	1.2100E+04	1.26	0.0600	TRUE	4.9490	N/A

TiO_2 80 mg/L 3 min	MCPP 1	N/A	73910	16418	1.26568	0.0597	TRUE	6.6641	N/A
TiO_2 80 mg/L 4 min	MCPP 1	N/A	68614	15295	1.2673	0.0598	TRUE	6.1848	N/A
TiO_2 80 mg/L 5 min	MCPP 1	N/A	64598	14216	1.2661	0.0602	TRUE	5.8214	N/A
TiO_2 80 mg/L 7 min	MCPP 1	N/A	73770	16200	1.2650	0.0602	TRUE	6.6514	N/A
TiO_2 80 mg/L 9 min	MCPP 1	N/A	64040	13586	1.2641	0.0625	TRUE	5.7709	N/A
TiO_2 80 mg/L 11 min	MCPP 1	N/A	68205	15196	1.2649	0.0591	TRUE	6.1478	N/A
TiO_2 80 mg/L 15 min	MCPP 1	N/A	67850	15103	1.2636	0.0588	TRUE	6.1157	N/A
TiO_2 80 mg/L 20 min	MCPP 1	N/A	68425	15380	1.2638	0.0579	TRUE	6.1677	N/A

TiO_2 100 mg/L 1 min	MCPP 1	N/A	69795	15946	1.270497	0.05855	TRUE	6.2917	N/A
TiO_2 100 mg/L 2 min	MCPP 1	N/A	70266	15958	1.2696	0.0594	TRUE	6.3343	N/A
Blank 1	MCPP 1	N/A	N/A	N/A	N/A	N/A	TRUE	N/A	N/A
Blank 2	MCPP 1	N/A	N/A	N/A	N/A	N/A	TRUE	N/A	N/A
Stand 5	MCPP 1	N/A	54958	12056	1.2608	0.0603	TRUE	4.9489	N/A
TiO_2 100 mg/L 3 min	MCPP 1	N/A	77440	17850	1.2684	0.0592	TRUE	6.9836	N/A
TiO_2 100 mg/L 4 min	MCPP 1	N/A	78492	18101	1.2681	0.0582	TRUE	7.0788	N/A
TiO_2 100 mg/L 5 min	MCPP 1	N/A	72723	16525	1.2687	0.0594	TRUE	6.5567	N/A

TiO_2 100 mg/L 7 min	MCPP 1	N/A	69456	15775	1.2673	0.0591	TRUE	6.2610	N/A
TiO_2 100 mg/L 9 min	MCPP 1	N/A	71676	16023	1.2675	0.0605	TRUE	6.4619	N/A
TiO_2 100 mg/L 11 min	MCPP 1	N/A	74127	16401	1.2689	0.0610	TRUE	6.6837	N/A
TiO_2 100 mg/L 15 min	MCPP 1	N/A	70692	15758	1.2655	0.0603	TRUE	6.3729	N/A
TiO_2 100 mg/L mg/L 20 min	MCPP 1	N/A	72328	16288	1.2671	0.0601	TRUE	6.5210	N/A
blank 2	MCPP 1	N/A	N/A	N/A	N/A	N/A	TRUE	N/A	N/A
Stand 1	MCPP 1	N/A	1.0800E+04	2.3600E+03	1.2600	0.0600	TRUE	0.9550	N/A
UV 0 min	MCPP 1	4.5041	4.4100E+04	4.0900E+03	1.3800	0.1900	TRUE	4.5040	N/A

UV 2 min	MCPP 1	4.1227	4.0200E+04	3.9400E+03	1.3700	0.1400	TRUE	4.1220	N/A
UV 3 min	MCPP 1	3.3530	3.2500E+04	3.0800E+03	1.3800	0.1700	TRUE	3.3530	N/A
UV 4 min	MCPP 1	2.9288	2.8200E+04	2.6700E+03	1.3600	0.1600	TRUE	2.9290	N/A
UV 5 min	MCPP 1	2.4657	2.3600E+04	2.2500E+03	1.3700	0.1700	TRUE	2.4660	N/A
UV 7 min	MCPP 1	1.9310	1.8200E+04	1.7400E+03	1.3700	0.1800	TRUE	1.9310	N/A
UV 9 min	MCPP 1	1.6213	1.5100E+04	1.4200E+03	1.3600	0.1800	TRUE	1.6210	N/A
UV 11 min	MCPP 1	1.3036	1.1900E+04	1.1700E+03	1.3700	0.1500	TRUE	1.3030	N/A
UV 15 min	MCPP 1	0.8573	7.4300E+03	6.7300E+02	1.3800	0.1800	TRUE	0.8570	N/A

Sample Name	Component Name	Actual Concentration	Area	Height	Retention Time	Width at 50%	Used	Calculated Concentration	Accuracy
blank	MCPP 1	N/A	N/A	N/A	N/A	N/A	TRUE	N/A	N/A
blank 2	MCPP 1	N/A	N/A	N/A	N/A	N/A	TRUE	N/A	N/A
stand 1	MCPP 1	1	11297	2328	1.2576	0.0657	TRUE	0.9977	99.770
stand 2	MCPP 1	2	22803	4875	1.2544	0.0631	TRUE	2.0389	101.94
stand 5	MCPP 1	5	55632	1162	1.2580	0.0636	TRUE	5.0100	100.20
stand 7	MCPP 1	7	76504	1594	1.2559	0.0634	TRUE	6.8991	98.55878

stand 10	MCPP 1	10	10930	23351	1.2554	0.0626	TRUE	9.8676	98.67
stand 15	MCPP 1	15	16544	34479	1.2549	0.0636	TRUE	14.948	99.65
stand 20	MCPP 1	20	22390	47872	1.2562	0.0610	TRUE	20.238	101.19
UV+TiO_2 20 mg/L 1 MIN	MCPP 1	N/A	55610	11966	1.2583	0.0609	TRUE	5.0080	N/A
UV+TIO_2 20 mg/L 3 MIN	MCPP 1	N/A	41200	8996	1.2606	0.0600	TRUE	3.7039	N/A
UV+TIO_2 20 mg/L 4 MIN	MCPP 1	N/A	36075	7826	1.2563	0.0603	TRUE	3.2400	N/A
UV+TIO_2 20 mg/L 5 MIN	MCPP 1	N/A	30554	6562	1.2572	0.0620	TRUE	2.7404	N/A
UV+TIO_2 20 mg/L 7 MIN	MCPP 1	N/A	2477134	5503.69	1.2574	0.0579	TRUE	2.2170	N/A

UV-TiO_2 20 mg/L 9 MIN	MCPP 1	N/A	19925	4253.0	1.2556	0.0618	TRUE	1.7784	N/A
UV-TiO_2 20 mg/L 11 MIN	MCPP 1	N/A	53510	11972	1.2559	0.0585	TRUE	4.8179	N/A
UV-TiO_2 15 MIN	MCPP 1	N/A	35520	7504.0	1.2572	0.0628	TRUE	3.1898	N/A
UV-TiO_2 20 mg/L 20 MIN	MCPP 1	N/A	40462	8867.0	1.2574	0.0597	TRUE	3.6370	N/A
UV-TiO_2 40 mg/L 1 MIN	MCPP 1	N/A	51667	11567	1.2651	0.0593	TRUE	4.6511	N/A
blank	MCPP 1	N/A	N/A	N/A	N/A	N/A	TRUE	N/A	N/A
blank 2	MCPP 1	N/A	N/A	N/A	N/A	N/A	TRUE	N/A	N/A
stand 5	MCPP 1	N/A	54032	1123	1.2498	0.0646	TRUE	4.8651	N/A

UV-TiO_2 40 mg/L 2 MIN	MCPP 1	N/A	49863	11408	1.266341471	0.0591	TRUE	4.4879	N/A
UV-TiO_2 40 mg/L 3 MIN	MCPP 1	N/A	40977	9122	1.26184863	0.0608	TRUE	3.68375	N/A
UV-TiO_2 40 mg/L 4 MIN	MCPP 1	N/A	31802	7141	1.2608	0.0611	TRUE	2.8533	N/A
UV-TiO_2 40 mg/L 5 MIN	MCPP 1	N/A	27224	6070	1.2650	0.0594	TRUE	2.4390	N/A
UV-TiO_2 40 mg/L 7 MIN	MCPP 1	N/A	20721	4632	1.2637	0.0595	TRUE	1.8505	N/A
UV-TiO_2 40 mg/L 9 MIN	MCPP 1	N/A	15471	3412.	1.2635	0.0605	TRUE	1.3754	N/A
UV-TiO_2 40 mg/L 11 MIN	MCPP 1	N/A	12222	2858.	1.2638	0.0552	TRUE	1.0813	N/A
UV-TiO_2 40 mg/L 15 MIN	MCPP 1	N/A	6422	1439	1.2614	0.0604	TRUE	0.5565	N/A

UV-TIO_2 40 mg/L 20 MIN	MCPP 1	N/A	2957	619	1.2615	0.0657	TRUE	0.2429	N/A
UV-TIO_2 60 mg/L 1 MIN	MCPP 1	N/A	58653	13056	1.2590	0.0604	TRUE	5.2834	N/A
Blank 1	MCPP 1	N/A	N/A	N/A	N/A	N/A	TRUE	N/A	N/A
Blank 2	MCPP 1	N/A	N/A	N/A	N/A	N/A	TRUE	N/A	N/A
Stand 2	MCPP 1	N/A	22138	4672	1.2512	0.0630	TRUE	1.9788	N/A
UV-TIO_2 60 mg/L 2 MIN	MCPP 1	N/A	54798	12108	1.2589	0.0611	TRUE	4.9344	N/A
UV-TIO_2 60 mg/L 3 MIN	MCPP 1	N/A	44356	9911	1.2547	0.0613	TRUE	3.9894	N/A
UV-TIO_2 60 mg/L 4 MIN	MCPP 1	N/A	38251	8691	1.2581	0.0589	TRUE	3.4370	N/A

UV-TIO2 60 mg/L 5 MIN	MCPP 1	N/A	31471	7085	1.2576	0.0597	TRUE	2.8234	N/A
UV-TIO2 60 mg/L 7 MIN	MCPP 1	N/A	22035	4841	1.2585	0.0618	TRUE	1.9694	N/A
UV-TIO2 60 mg/L 9 MIN	MCPP 1	N/A	14643	3342	1.2568	0.0594	TRUE	1.3005	N/A
UV-TIO2 60 mg/L 11 min	MCPP 1	N/A	9743	2070	1.2584	0.0653	TRUE	0.8570	N/A
UV-TiO2 60 mg/L 15 min	MCPP 1	N/A	3813	884	1.2564	0.0585	TRUE	0.3204	N/A
UV-TiO2 60 mg/L 20 min	MCPP 1	N/A	992	247	1.2592	0.0477	TRUE	0.0650	N/A
UV-TiO2 80 mg/L 1 min	MCPP 1	N/A	55191	12067	1.2574	0.0627	TRUE	4.9700	N/A
Blank 1	MCPP 1	N/A	N/A	N/A	N/A	N/A	TRUE	N/A	N/A

Blank 2	MCPP 1	N/A	N/A	N/A	N/A	N/A	TRUE	N/A	N/A
Stand 1	MCPP 1	N/A	11353	2305	1.2439	0.0658	TRUE	1.0027	N/A
UV-TiO_2 80 mg/L 2 min	MCPP 1	N/A	49396	10893	1.2566	0.0614	TRUE	4.4456	N/A
UV-TiO_2 80 mg/L 3 min	MCPP 1	N/A	38019	8491	1.2567	0.0597	TRUE	3.4159	N/A
UV-TiO_2 80 mg/L 4 min	MCPP 1	N/A	28651	6259	1.2547	0.0624	TRUE	2.5682	N/A
UV-TiO_2 80 mg/L 5 min	MCPP 1	N/A	23444	5099	1.2549	0.0620	TRUE	2.0969	N/A
UV-TiO_2 80 mg/L 7 min	MCPP 1	N/A	13268	2925	1.2559	0.0630	TRUE	1.1760	N/A
UVTiO_2 80 mg/L 9 min	MCPP 1	N/A	6722	1506	1.2569	0.059676	TRUE	0.5836	N/A

UV-TiO_2 80 mg/L 11 min	MCPP 1	N/A	3392	716	1.2566	0.0650	TRUE	0.2823	N/A
UV-TiO_2 80 mg/L 15 min	MCPP 1	N/A	821	193.	1.2553	0.0609	TRUE	0.0496	N/A
UV-TiO_2 80 mg/L 20 min	MCPP 1	N/A	N/A	N/A	N/A	N/A	TRUE	N/A	N/A
UV-TiO_2 100 mg/L 1 min	MCPP 1	N/A	50590	11000	1.2518	0.0622	TRUE	4.5537	N/A
Blank 1	MCPP 1	N/A	N/A	N/A	N/A	N/A	TRUE	N/A	N/A
Blank 2	MCPP 1	N/A	N/A	N/A	N/A	N/A	TRUE	N/A	N/A
Standard 7	MCPP 1	N/A	76734	15259	1.2430	0.0686	TRUE	6.9197	N/A
UV-TiO_2 100 mg/L 2 min	MCPP 1	N/A	43090	9453	1.25536541	0.0629	TRUE	3.8749	N/A

UV–TiO_2 100 mg/L 3 min	MCPP 1	N/A	29141	6243	1.2552	0.0646	TRUE	2.6125	N/A
UV-TiO_2 100 mg/L 4 min	MCPP 1	N/A	19315	4180	1.2565	0.0646	TRUE	1.7232	N/A
UV-TiO_2 100 mg/L 5 min	MCPP 1	N/A	4766	1022	1.2558	0.0638	TRUE	0.4066	N/A
UV-TiO_2 100 mg/L 7 min	MCPP 1	N/A	1743	384	1.2548	0.0636	TRUE	0.1330	N/A
UV-TiO_2 100 mg/L 9 min	MCPP 1	N/A	198	60	1.2579	0.0481	TRUE	< 0	N/A
UV-TiO_2 100 mg/L 11 min	MCPP 1	N/A	N/A	N/A	N/A	N/A	TRUE	N/A	N/A
UV-TiO_2 100 mg/L 15 min	MCPP 1	N/A	N/A	N/A	N/A	N/A	TRUE	N/A	N/A
UV-TiO_2 100 mg/L 20 min	MCPP 1	N/A	624813	126093	1.2392	0.0656	TRUE	56.5207	N/A

Blank 1	MCPP 1	N/A	N/A	N/A	N/A	N/A	TRUE	N/A	N/A
Blank 2	MCPP 1	N/A	N/A	N/A	N/A	N/A	TRUE	N/A	N/A
Standard 7	MCPP 1	N/A	79645	15438	1.2710	0.0706	TRUE	7.1831	N/A
UV-TiO_2 100 mg/L 2 min	MCPP 1	N/A	44051	9265	1.2680	0.0652	TRUE	3.9619	N/A
UV-TiO_2 100 mg/L 3 min	MCPP 1	N/A	30012	6292	1.2635	0.0642	TRUE	2.6914	N/A
UV-TiO_2 100 mg/L 4 min	MCPP 1	N/A	20117	4265	1.2544	0.0653	TRUE	1.7958	N/A
UV-TiO_2 100 mg/L 7 min	MCPP 1	N/A	4446	910	1.2569	0.0684	TRUE	0.3777	N/A
UV-TiO_2 100 mg/L 9 min	MCPP 1	N/A	1815	389	1.2516	0.0628	TRUE	0.1396	N/A

UV-TiO_2 100 mg/L 11 min	MCPP 1	N/A	324.2012	64.6491	1.252795458	0.091972076	TRUE	0.004605603	N/A
UV-TiO_2 100 mg/L 15 min	MCPP 1	N/A	N/A	N/A	N/A	N/A	TRUE	N/A	N/A
UV-TiO_2 100 mg/L 20 min	MCPP 1	N/A	N/A	N/A	N/A	N/A	TRUE	N/A	N/A
Stand 2	MCPP 1	N/A	N/A	N/A	N/A	N/A	TRUE	N/A	N/A
Blank 1	MCPP 1	N/A	N/A	N/A	N/A	N/A	TRUE	N/A	N/A
Blank 2	MCPP 1	N/A	N/A	N/A	N/A	N/A	TRUE	N/A	N/A
Stand 2	MCPP 1	N/A	24231	5533	1.2672	0.0585	TRUE	2.1682	N/A
TiO_2 80 mg/L 3 min	MCPP 1	N/A	73910	16418	1.2656	0.0597	TRUE	6.6641	N/A

TiO_2 80 mg/L 4 min	MCPP 1	N/A	68614	15295	1.2673	0.0598	TRUE	6.1848	N/A
TiO_2 80 mg/L 5 min	MCPP 1	N/A	64598	14216	1.2661	0.0602	TRUE	5.8214	N/A
TiO_2 80 mg/L 7 min	MCPP 1	N/A	73770	16200	1.26501	0.0602	TRUE	6.6514	N/A
TiO_2 80 mg/L 9 min	MCPP 1	N/A	64040	13586	1.2641	0.0625	TRUE	5.7709	N/A
TiO_2 80 mg/L 11 min	MCPP 1	N/A	68205	15196	1.2649	0.0591	TRUE	6.1478	N/A
TiO_2 80 mg/L 15 min	MCPP 1	N/A	67850	15103	1.2636	0.0588	TRUE	6.1157	N/A
TiO_2 80 mg/L 20 min	MCPP 1	N/A	68425	15380	1.2638	0.0579	TRUE	6.1677	N/A
TiO_2 100 mg/L 1 min	MCPP 1	N/A	69795	15946	1.2704	0.0585	TRUE	6.2913	N/A

TiO_2 100 mg/L 2 min	MCPP 1	N/A	70266	15958	1.2695	0.0594	TRUE	6.3343	N/A
Blank 1	MCPP 1	N/A	N/A	N/A	N/A	N/A	TRUE	N/A	N/A
Blank 2	MCPP 1	N/A	N/A	N/A	N/A	N/A	TRUE	N/A	N/A
Stand 5	MCPP 1	N/A	54958.	12056	1.2608	0.0603	TRUE	4.948	N/A
TiO_2 100 mg/L 3 min	MCPP 1	N/A	77440	17850	1.2684	0.0592	TRUE	6.9836	N/A
TiO_2 100 mg/L 4 min	MCPP 1	N/A	78492	18101	1.2681	0.0582	TRUE	7.0788	N/A
TiO_2 100 mg/L 5 min	MCPP 1	N/A	72723	16525	1.2687	0.0594	TRUE	6.5567	N/A
TiO_2 100 mg/L 7 min	MCPP 1	N/A	69456	15775	1.2673	0.0591	TRUE	6.2610	N/A

TiO_2 100 mg/L 9 min	MCPP 1	N/A	71676	16023	1.2675	0.0605	TRUE	6.4619	N/A
TiO_2 100 mg/L 11 min	MCPP 1	N/A	74127	16401	1.2689	0.0610	TRUE	6.6837	N/A
TiO_2 100 mg/L 15 min	MCPP 1	N/A	70692	15758	1.2655	0.0603	TRUE	6.3729	N/A
TiO_2 100 mg/L 20 min	MCPP 1	N/A	72328	16288	1.2671	0.0601	TRUE	6.5210	N/A
blank 1	MCPP 1	N/A	N/A	N/A	N/A	N/A	TRUE	N/A	N/A
blank 2	MCPP 1	N/A	N/A	N/A	N/A	N/A	TRUE	N/A	N/A
Stand 1	MCPP 1	N/A	10824	2358	1.2603	0.0638	TRUE	0.9548	N/A
blank	MCPP 1	N/A	N/A	N/A	N/A	N/A	TRUE	N/A	N/A

blank 2	MCPP 1	N/A	N/A	N/A	N/A	N/A	TRUE	N/A	N/A
stand 1	MCPP 1	N/A	11012	2410	1.2593	0.0596	TRUE	0.9718	N/A
stand 2	MCPP 1	N/A	23165	4950	1.2604	0.0616	TRUE	2.0717	N/A
stand 5	MCPP 1	N/A	56411	11992	1.2564	0.0629	TRUE	5.0805	N/A
stand 7	MCPP 1	N/A	77427.44	16446	1.2584	0.06227	TRUE	6.9824	N/A
stand 10	MCPP 1	N/A	110907	23094	1.2589	0.0646	TRUE	10.012	N/A
blank	MCPP 1	N/A	N/A	N/A	N/A	N/A	TRUE	N/A	N/A
blank	MCPP 1	N/A	N/A	N/A	N/A	N/A	TRUE	N/A	N/A

stand 1	MCPP 1	1	8.2700E+03	1.5700E+03	1.2500	0.0800	TRUE	1.0120	101.21
stand 2	MCPP 1	2	1.5000E+04	2.9700E+03	1.2500	0.0700	TRUE	1.9460	97.32
stand 5	MCPP 1	5	3.7900E+04	7.3100E+03	1.25	0.0700	TRUE	5.1100	102.21
stand 7	MCPP 1	7	5.2300E+04	1.0100E+04	1.2500	0.0700	TRUE	7.0950	101.36
stand 10	MCPP 1	10	7.1900E+04	1.3800E+04	1.2500	0.0700	TRUE	9.7990	97.99
stand 15	MCPP 1	15	1.0800E+05	2.0300E+04	1.2500	0.0700	TRUE	14.841	98.94
stand 20	MCPP 1	20	1.4700E+05	2.8200E+04	1.2500	0.0700	TRUE	20.196	100.98
raw water 1	MCPP 1	N/A	4.0800E+02	8.8400E+01	1.2400	0.0600	TRUE	< 0	N/A

raw water 2	MCPP 1	N/A	4.0400E+02	9.1000E+01	1.2300	0.0500	TRUE	< 0	N/A
raw water 3	MCPP 1	N/A	4.0900E+02	1.0100E+02	1.2400	0.0500	TRUE	< 0	N/A
raw water 4	MCPP 1	N/A	5.5300E+02	1.1200E+02	1.2400	0.0600	TRUE	< 0	N/A
raw water 5	MCPP 1	N/A	3.8500E+02	8.5700E+01	1.2400	0.0600	TRUE	< 0	N/A
sample r+m 1	MCPP 1	N/A	5.3500E+04	1.0200E+04	1.2300	0.0700	TRUE	7.2580	N/A
sample r+m 2	MCPP 1	N/A	5.4100E+04	1.0100E+04	1.2300	0.0700	TRUE	7.3380	N/A
sample r+m 3	MCPP 1	N/A	5.3100E+04	9.9000E+03	1.2300	0.0700	TRUE	7.2110	N/A
sample r+m 4	MCPP 1	N/A	5.3700E+04	1.0100E+04	1.2300	0.0700	TRUE	7.2940	N/A

sample r+m 5	MCPP 1	N/A	5.3500E+04	1.0100E+04	1.2300	0.0700	TRUE	7.2600	N/A
standard 40	MCPP 1	N/A	2.5800E+05	4.9100E+04	1.2800	0.0700	FALSE	35.480	N/A
								7.2722	